Univerzita Karlova v Praze

1. lékařská fakulta

Studijní program: Doktorské studium biomedicíny

Studijní obor: Biologie a patologie buňky

Mgr. Klára Zacharovová

Diagnostický příspěvek k hodnocení intervenčních modelů léčby diabetu mellitu 1. typu

Diagnostic contribution to the evaluation of intervention models in the treatment of type 1 diabetes mellitus

Disertační práce

Školitel:

prof. MUDr. František Saudek, DrSc.

Praha, 2012

Děkuji svému školiteli prof. MUDr. Františkovi Saudkovi, DrSc. za umožnění podílet se na výzkumných i klinických projektech Laboratoře Langerhansových ostrůvků v IKEM. Děkuji za jeho podněty, konzultace, motivaci a pomoc při řešení výzkumných problémů a za odborné vedení při přípravě této práce. Děkuji za jeho srdečný a velmi lidský přístup, kterým vytvořil příjemnou atmosféru na pracovišti i mimo něj. Poděkování patří také všem kolegům z Laboratoře Langerhansových ostrůvků za podporu a pomoc při řešení pracovních úkolů. Děkuji za vytvoření příjemného a přátelského prostředí. Dále děkuji Ing. Danielovi Jirákovi, Ph.D. a Mgr. Vítovi Herynkovi, Ph.D. za jejich ochotnou pomoc v otázkách magnetické rezonance. Děkuji celému týmu Laboratoře elektronové mikroskopie Biologického centra AVČR, předně pak RNDr. Marii Vancové, Ph.D. za pomoc v oblasti elektronové mikroskopie. Děkuji pracovní skupině doc. MUDr. Kateřiny Štechové z Pediatrické kliniky 2. lékařské fakulty UK a pracovní skupině prof. RNDr. Ivana Lukeše, CSc. z katedry anorganické chemie Přírodovědecké fakulty UK, za pomoc a spolupráci na dílčích projektech této práce.

V neposlední řadě děkuji své rodině za vytrvalou podporu, předně svému manželovi Petrovi za jeho trpělivost a motivaci k dokončení této práce.

Dílčí projekty této disertační práce byly podpořeny grantovými projekty řešitelského pracoviště a to grantem MŠMT ČR č. 2B06175, grantem IGA MZ ČR č. NR/8127-3, projektem (Ministerstva zdravotnictví) rozvoje výzkumné organizace 00023001 (IKEM) – Institucionální podpora, grantem GAČR č. P304/10/0762,
a grantem Univerzity Karlovy v Praze č. SVV-2012-264514.

Prohlášení:

Prohlašuji, že jsem závěrečnou práci zpracovala samostatně a že jsem řádně uvedla a citovala všechny použité prameny a literaturu. Současně prohlašuji, že práce nebyla využita k získání jiného nebo stejného titulu.

Souhlasím s trvalým uložením elektronické verze mé práce v databázi systému meziuniverzitního projektu Theses.cz za účelem soustavné kontroly podobnosti kvalifikačních prací.

V Praze, 18.6. 2012

Klára Zacharovová

Identifikační záznam:

ZACHAROVOVÁ, Klára. *Diagnostický příspěvek k hodnocení intervenčních modelů léčby diabetu mellitu 1. typu. [Diagnostic contribution to the evaluation of intervention models in the treatment of type 1 diabetes mellitus]*. Praha, 2012. Počet stran 102, počet příloh 7. Disertační práce. Univerzita Karlova v Praze, 1. lékařská fakulta, Institut klinické a experimentální medicíny. Vedoucí závěrečné práce prof. MUDr. František Saudek, DrSc.

OBSAH

ABSTRAKT 2
ABSTRACT 3
CÍLE DISERTAČNÍ PRÁCE 4
ÚVOD 5
VÝSLEDKY 17
PODÍL PRÁCE NA JEDNOTLIVÝCH PUBLIKACÍCH 18
KOMENTÁŘ K VÝSLEDKŮM A DISKUZE 19
ČÁST 1 19
ČÁST 2 24
ZÁVĚRY 28
LITERATURA 30
PUBLIKAČNÍ AKTIVITY AUTORKY 36
PUBLIKACE 36
PREZENTACE NA KONGRESECH A SYMPOZIÍCH 39
PŘÍLOHY 47

ABSTRAKT

Při imunointervenční či transplantační léčbě diabetu je nutné monitorovat ukazatele imunitní nebo rejekční destrukce přežívající inzulín produkující tkáně. Disertační práce si klade za cíl zlepšit možnosti sledování průběhu autoimunitního procesu a in vivo průkazu přežívání transplantovaných Langerhansových ostrůvků.

Dílčí úkoly zahrnovaly průkaz vitality izolovaných ostrůvků určených k transplantaci měřením respirační aktivity, objasnění průběhu in vitro značení izolovaných ostrůvků superparamagnetickou kontrastní látkou pro následné zobrazení pomocí magnetické rezonance a sledování transportu této látky po transplantaci. Pro identifikaci kontrastních částic v histologickém materiálu jsme studovali nově připravenou paramagnetickou kontranstní látku s navázaným fluoresceinem. Dále jsme se zaměřili na hodnocení autoimunitního procesu pomocí sledování cytokinové odpovědi na specifickou stimulaci autoantigenem. Autoimunitní poškození beta buněk v experimentu u myší jsme se snažili ovlivnit polyklonálními anti-thymocytárními protilátkami.

Nová metoda testování respirační aktivity ostrůvků dobře korelovala s ostatními metodami testování kvality ostrůvků a byla navržena do diagnostického schématu před klinickou transplantací. Při studiu intercelulárního transportu železitých kontrastních látek jsme získali důležité výsledky, které ukázaly, že se nanočástice železa během značení dostávají endocytózou do všech typů ostrůvkových buněk. Po transplantaci ostrůvků jsou částice přemístěny do tkáňových makrofágů, kde v případě tolerance zůstávají, ale při rejekci jsou z jater eliminovány. Prokázali jsme, že nová bimodální kontrastní látka dovoluje zobrazení ostrůvků pomocí magnetické rezonance i ověření jejich lokalizace fluorescenční mikroskopií. Při vyšetření profilů cytokinové reakce lymfocytů po stimulaci potenciálními autoantigeny in vitro u nově zjištěných diabetiků a jejich zdravých příbuzných jsme zjistili rozdíly svědčící o aktivaci zánětlivého procesu ve skupině pacientů. Pomocí průtokové cytometrie jsme zjistili zvýšení populace regulačních T-lymfocytů po léčbě antithymocytární globulinem.

Nové nálezy přispěly k řešení dlouhodobých projektů na řešitelském pracovišti a byly publikovány v časopisech s faktorem impaktu.

Klíčová slova: diabetes mellitus 1. typu, Langerhansovy ostrůvky, transplantace, magnetická rezonance, autoreaktivní lymfocyty, imunointervenční terapie, anti-thymocytární globulin

ABSTRACT

During treatment of diabetes mellitus by immunointervention or transplantation, it is necessary to monitor the markers of immune destruction or rejection of surviving insulin producing cells. An aim of this thesis is to improve the possibilities of following autoimmunity and to detect the survival of transplanted pancreatic islet in vivo.

Partial aims included vitality testing of isolated islets for transplantation by measurement of respiration activity, observing the process of in vitro labeling of isolated islets with superparamagnetic iron oxide (SPIO) contrast agent for subsequent magnetic resonance imaging (MRI) of islets and observing SPIO particles transport after transplantation. We also studied a new dual paramagnetic contrast agent combined with fluorescein intended for identification of the MRI contrast agent in samples for histology. Further, we assessed autoimmune reaction by evaluation of cytokine response to specific stimulation with auto-antigens. We tried to affect beta-cells destruction by polyclonal anti-thymocyte antibodies in a mouse experimental model.

A new method of the islet respiration measurement correlated with other methods of islet quality testing and it was suggested as a diagnostic test before clinical transplantation. Results obtained studying the intercellular transport of SPIO particles showed that the particles are incorporated into all islet cell types during islet labeling. After transplantation, the particles were translocated into tissue macrophages, they persisted there in the case of immune tolerance but they were eliminated from the liver during rejection. We showed that a new dual contrast agent enables both islet imaging by MRI and localization by fluorescence microscopy. We found differences in cytokine reaction profiles after stimulation of lymphocytes with specific auto-antigens in groups of recent onset diabetic patients and their healthy relatives. This pointed to activation of inflammatory reaction in this group of patients. By flow cytometry we found an increase of regulatory T-lymphocytes population after the anti-thymocyte globulin treatment.

The new findings helped to solve long-term projects of the working group and were published in impacted journals.

KEYWORDS: type 1 diabetes mellitus, islets of Langerhans, transplantation, magnetic resonance imaging, auto-reactive lymphocytes, immunointervention therapy, anti-thymocyte globulin

CÍLE DISERTAČNÍ PRÁCE

Diabetes mellitus 1. typu je způsoben autoimunitní destrukcí beta buněk pankreatu. Zastavení této autoimunitní reakce nebo náhrada zničených buněk transplantací představují perspektivní přístupy v jeho léčbě. Cílem předkládané disertační práce bylo vyvinout metody, které by umožnily diagnostikovat efektivitu dvou modelových léčebných postupů, a sice: 1) transplantace izolovaných Langerhansových ostrůvků u již rozvinutého onemocnění a 2) imunitní intervence v časném stádiu onemocnění.

Část 1

Při hodnocení efektu transplantace Langerhansových ostrůvků jsme se zaměřili nejprve na vypracování nové testovací metody pro kontrolu kvality ostrůvků založené na měření spotřeby kyslíku. Hlavní výstup tohoto úkolu představuje příloha I.

Druhým cílem bylo navázat na prioritní výsledky naší pracovní skupiny v oblasti vizualizace transplantovaných Langerhansových ostrůvků a objasnit ultrastrukturní lokalizaci superparamagnetických částic oxidů železa (SPIO částic) - kontrastní látka pro zobrazování magnetickou rezonancí - v buňkách Langerhansových ostrůvků po jejich in vitro značení touto kontrastní látkou nejprve in vitro a pak in vivo. Hlavními výstupy tohoto úkolu jsou přílohy II a III.

Třetím cílem bylo ověřit efektivitu značení izolovaných ostrůvků pomocí nové bimodální kontrastní látky pro současnou detekci magnetickou rezonanci a fluorescenční mikroskopií. Tato nová kontrastní látka se skládá z perovskitu manganu s vázaným fluoresceinem (příloha IV).

Část 2

Pro monitorování autoimunitního procesu byly stanoveny následující cíle:

Zavedení metody pro testování reaktivity imunitních buněk pacientů s diabetem 1.typu, která by umožnila sledovat aktivitu specifických T-lymfocytů na základě produkce vybraných cytokinů po stimulaci diabetogenními antigeny (příloha V a VI).

Dalším cílem v této části bylo sledování efektu imunointervenční léčby anti-thymocytárním globulinem na populace imunitních buněk a na progresi diabetu u modelu NOD (non-obese diabetic) myší (příloha VII).

ÚVOD

Diabetes mellitus je metabolický syndrom, jehož nejnápadnějším znakem je zvýšená hladina krevního cukru. Je způsoben absolutním nebo relativním nedostatkem životně důležitého hormonu inzulínu. Dlouhodobě zvýšená hladina krevního cukru je hlavní příčinou vzniku tzv. pozdních komplikací diabetu, které postihují drobné i velké cévy v organismu a vedou k poškození mnoha orgánů. Diabetes dnes patří k nejvíce rozšířeným chorobám a proto má jeho prevence i léčba velký společenský i ekonomický dopad. Jednotlivé úkoly předkládané disertační práce byly řešeny na základě aktuální potřeby pracoviště, které se systematicky zabývá transplantačními a imunointervenčními metodami léčby diabetu 1. typu a usiluje o jejich přenos do klinické praxe.

Langerhansovy ostrůvky

Langerhansovy ostrůvky tvoří endokrinní část slinivky břišní. Jedná se o shluky buněk produkujících několik typů hormonů. V pankreatu dospělého člověka je rozmístěn asi 1 milion ostrůvků a tvoří tak asi 1 - 2 % celkového objemu pankreatu (Korc 1993). Ostrůvky obsahují čtyři hlavní typy endokrinních buněk: beta buňky produkují inzulín a amylin, alfa-buňky tvoří glukagon, delta-buňky uvolňují somatostation a PP-buňky neboli gamma-buňky produkují pankreatický polypeptid (Nussey and Whitehead 2001). Později identifikované epsilon-buňky tvoří peptid ghrelin (Wierup, Svensson et al. 2002). Ostrůvky dále obsahují nervové buňky a hustou síť krevních a lymfatických cév.

V Langerhasových ostrůvcích jsou nejvíce zastoupené beta buňky. V lidských ostrůvcích je jejich zastoupení značně variabilní, v průměru představují 54 % endokrinních buněk. Oproti tomu u myší zastupují beta buňky kolem 75 % všech buněk ostrůvku (Brissova, Fowler et al. 2005). Hormon beta buněk inzulín je syntetizován jako neaktivní prohormon preproinzulín. Pomocí signálního peptidu je preproinzulín transportován do endoplazmatického retikula. Odštěpením 24 aminokyselin signálního peptidu vzniká proinzulín, který prochází přes Golgiho aparát do sekrečních váčků. Zde je enzymy prohormonkonvertázami odštěpena střední část peptidu, která je označována jako c-peptid. Další dvě aminokyseliny jsou zde odštěpeny karboxypeptidázou E. Tím vzniká aktivní forma inzulínu, která se skládá ze dvou řetězců (Steiner 1998). V beta buňkách jsou molekuly inzulínu skladovány jako dimery, které jsou agregovány spolu s Zn^{2+} a Ca^{2+} ionty do

hexamerů. V krvi, kde je koncentrace nižší, se však inzulín vyskytuje jako monomer, který je biologicky aktivní (Dunn 2005).

Beta buňky uvolňují inzulín jako odpověď na zvýšený metabolismus glukózy, která je přenášena do buňky pomocí specifických membránových transportérů glukózy – GLUT2. Z buněk se inzulín uvolňuje splynutím sekrečních granul s buněčnou mebránou. V první fázi je rychle uvolněn inzulín, který je již v granulech připravený, ve druhé fázi dochází během dvou hodin k postupnému nárůstu sekrece, kdy je uvolňován nově syntetizovaný inzulín (Straub and Sharp 2002).

Inzulín působí na buňky pomocí vazby na inzulínový receptor, což je tyrosin kinázový receptor vyskytující se na buňkách ve dvou splicingových formách (Moller, Yokota et al. 1989; Seino and Bell 1989).

Z aktivovaného receptoru je signál přenášen aktivací několika různých drah. Hlavním účinkem inzulínu je stimulace transportu glukózy do buněk, která je umožněna translokací glukózového kanálu GLUT4 na buněčnou membránu. Inzulín také stimuluje syntézu bílkovin, glykogenezi a lipogenezi. Naopak tlumí glykogenolýzu a glukoneogenezi. Inzulín dále ovlivňuje růst a diferenciaci buněk a působí anti-apoptoticky. Celkově způsobuje snížení hladiny glukózy v krvi, ukládání živin a jejich přeměnu ve vysokoenergetické produkty (Shepherd and Kahn 1999).

Beta buňky kromě inzulínu produkují také ostrůvkový amyloidový polypeptid (IAPP, amylin). Tento peptid je skladován i uvolňován spolu s inzulínem v granulech beta buněk. Amylin způsobuje mimo jiné zpomalením trávení potravy a inhibuje sekreci glukagonu, čímž snižuje koncentraci glukózy v krvi. Agregáty amylinu však působí na beta buňky toxicky a jsou spojovány s vývojem diabetu 2. typu (Lukinius, Wilander et al. 1989).

Diabetes mellitus

Diabetes mellitus je endokrinní porucha způsobená relativním nebo absolutním nedostatkem inzulínu, který vede k vysokým koncentracím glukózy v krvi. Zvýšené koncentrace glukózy pak způsobují pozdní komplikace jako poškození očí, ledvin, nervů nebo kardiovaskulárního ústrojí. Klasifikuje se několik typů diabetu mellitu; diabetes mellitus I. typu, diabetes mellitus II. typu, ostatní specifické typy diabetu a gestační diabetes mellitus (Škrha and et.al 2009).

Diabetes I. typu

Diabetes I. typu (T1D) je charakterizován velmi nízkou produkcí inzulínu. Ve většině případů se objevuje u dětí či během dospívání. Je způsoben autoimunitním procesem, kdy imunitní buňky reagují proti beta buňkám Langerhansových ostrůvků, což vede k jejich destrukci a nutnosti dodávat inzulín z vnějšku. Spouštěcí mechanizmus T1D je závislý na mnoha faktorech a podílí se na něm genetická predispozice a faktory vnějšího prostředí.

Existuje několik genů, jejichž některé alely jsou považovány za rizikové. Silná asociace T1D byla prokázána s výskytem některých haplotypů HLA II. třídy, DR a DQ (Pociot and McDermott 2002). Slabší genetická predispozice je vázána na polymorfní varianty promotorové oblasti genu pro inzulín (Bell, Horita et al. 1984), na alelické varianty genu pro IL-2 receptoru alfa (Lowe, Cooper et al. 2007), genu pro CTLA-4 (cytotoxic T lymphocyte-associated protein 4) (Nistico, Buzzetti et al. 1996) nebo genu PTPN22 pro tyrosin fosfatázu lymfocytů (LYP) (Bottini, Musumeci et al. 2004; Smyth, Cooper et al. 2004), která je negativním regulátorem aktivace T-lymfocytů. Nedávná široká genomová asociační studie pak ukázala dalších více než 40 genových oblastí, jejichž varianty jsou rizikové pro výskyt T1D (Barrett, Clayton et al. 2009). Většina genových oblastí asociovaných s T1D je ale současně asociována i s jinými autoimunitními onemocněními.

Jako faktory prostředí spouštějící diabetes se z experimentálních studií ukazují různé patogeny, toxiny, léky nebo potravní složky (Knip and Akerblom 1999).

Na základě zkoumání patogeneze T1D u modelových zvířat jako jsou NOD myši nebo BB potkani, byly navrženy modely imunitní reakce, které vysvětlují mechanizmus autoimunitní destrukce beta buněk. Přímých informací o patogenezi diabetu u člověka je však velmi málo. Autoimunitní proces začíná měsíce možná i roky před klinickým projevem diabetu a obecně se má za to, že beta buňky exprimující HLA I ve spojení s některým z autoantigenů slouží jako cíl pro destrukci specifickými cytotoxickými T-lymfocyty. Zánětlivá reakce je spojena s produkcí řady cytokinů a vede k produkci protilátek proti autoantigenům (Notkins and Lernmark 2001) (Obr. 1).

Autoprotilátky rozpoznávají čtyři hlavní autoantigeny ostrůvkových buněk – IA2 (insulinoma-associated antigen-2), inzulín, glutamát dekarboxylázu 65 (GAD65) a zinkový transportér 8 (ZnT8) (Pihoker, Gilliam et al. 2005; Wenzlau, Juhl et al. 2007). Autoprotilátky se v krvi pacientů vyskytují ještě před záchytem hyperglykemií. Případná detekce těchto protilátek a zvlášť jejich kombinace je silně spojena s rizikem vývoje T1D, ne však stoprocentním.

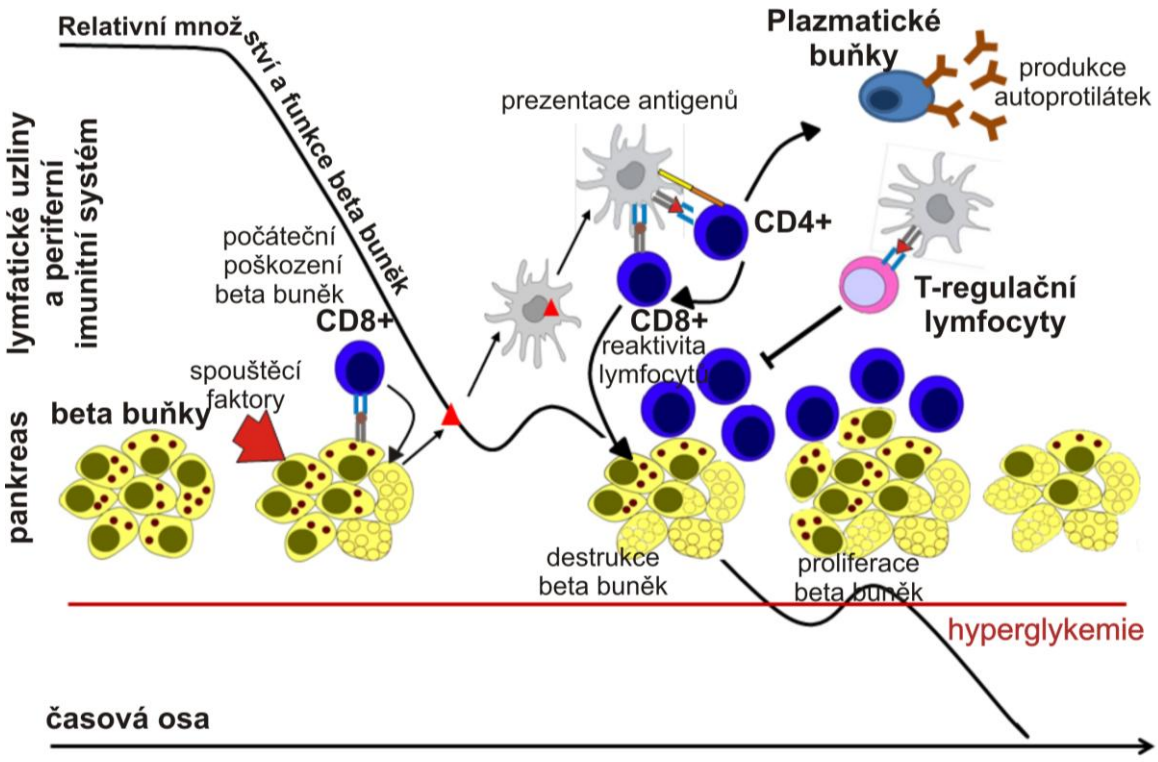

Obr. 1: Model vývoje T1D. Diagram ukazuje množství nebo funkci beta buněk v jednotlivých imunologických fázích, které se odehrávají v pankreatu nebo v periferii (popis vlevo). Schéma vytvořeno podle Eisenbarth et al. 1986 a van Belle et al. 2011 (Eisenbarth 1986; van Belle, Coppieters et al. 2011).

Samotná destrukce beta buněk cytotoxickými CD8+ T-lymfocyty je pravděpodobně způsobena běžnými mechanizmy těchto buněk, uvolněním cytolytických granul nebo přes interakci s Fas-recetorem, která spouští apoptózu cílové buňky. Pomocné CD4+ T-lymfocyty, které se také akumulují v ostrůvcích, produkují prozánětlivé cytokiny a podporují tak funkci cytotoxických T- i B-lymfocytů. B-lymfocyty napomáhají v destrukčním procesu nejen produkcí specifických protilátek, ale také jako antigen prezentující buňky. Epitopů, které autoreaktivní buňky rozpoznávají, byla identifikována celá řada. Epitopy rozpoznávané CD4+ T-lymfocyty jsou odvozeny hlavně z GAD65, IA-2, proinzulín, HSP 60 (heat shock protein 60), HSP 70 nebo IGRP (islet-specific glucose-6-phosphatase catalytic subunit-related protein). Autoreaktivní CD8+ T-lymfocyty rozpoznávají epitopy odvozené z preproinzulínu, IA2, IAPP (human islet amyloid polypeptide), IGRP, ZnT8 nebo GAD65 (Di Lorenzo, Peakman et al. 2007).

V důsledku autoimunitního procesu ubývá beta buněk v pankreatu. V době, kdy se diabetes projeví hyperglykemií je již zničeno 60 – 90% beta buněk. Současně ale

nedostatečná produkce inzulínu stimuluje proliferaci beta buněk a autoimunitní proces je regulován specifickými regulačními lymfocyty (Treg lymfocyty) (van Belle, Coppieters et al. 2011).

Intervenční studie u T1D

Snahou potlačit vývoj T1D se zabývá mnoho intervenčních studií. Studie, které jsou založené na podávání konkrétních antigenů odvozených z inzulínu nebo GAD 65, mají za cíl potlačit specifickou autoimunitní reakci indukcí specifických T regulačních lymfocytů nebo potlačením autoreaktivních buněk. Další studie byly založeny na nespecifickém ovlivnění imunity. Testovány byly imunosupresivní látky jako cyklosporin A (Bougneres, Landais et al. 1990), ATG (anti-thymocytární globulin) (Lopez, Clarkson et al. 2006; Simon, Parker et al. 2008) nebo ALS (anti-lymfocytární sérum) (Maki, Ichikawa et al. 1992). Asi nejlepších výsledků v zachování produkce c-peptidu, snížení potřeby vnějšího inzulínu nebo indukce Treg lymfocytů bylo dosaženo po podávání protilátek proti CD3 antigenu T-lymfocytů (Chatenoud, Thervet et al. 1994; Herold, Gitelman et al. 2005). Pro imunomodulaci byly dále použity protilátky proti dalším lymfocytárním znakům jako CD20 nebo kostimulačním molekulám jako CTLA-4 (Tooley, Waldron-Lynch et al. 2012). Další intervenční studie mají za cíl stimulovat produkci inzulínu nebo regeneraci beta buněk. Uplatňují se zde různá analoga GLP-1 (glucagon-like peptide-1) (Li, Hansotia et al. 2003), která se pro stimulaci sekrece inzulínu používají u diabetu 2. typu. Obdobný mechanizmus účinku má inhibitor degradace GLP-1 - inhibitor dipeptidyl peptidázy IV (Sitagliptin) (Kim, Nian et al. 2009). Aby se uplatnilo potlačení autoimunitní reakce, navození tolerance i podpora regenerace beta buněk, podává se v kombinačních studiích několik účinných látek současně. Ačkoliv u většiny intervenčních přístupů byl prokázaný pozitivní vliv na vývoj T1D u experimentálních modelů, klinické studie mají výsledky stále velmi neuspokojivé s pouze částečným omezením progrese T1D a částečným zachováním vlastní sekrece inzulínu (Ludvigsson 2009; Michels and von Herrath 2011).

Léčba diabetu

Prevalence diabetu je vysoká a stále stoupá. V roce 2010 bylo v ČR evidováno více než 806 tisíc pacientů, což je o 23 tisíc více než v roce 2009. Rovněž stále vzrůstá výskyt chronických diabetických komplikací. Náchylnější k těmto komplikacím jsou pacienti s diabetem I. typu, kteří představují asi 7 % z celkového počtu diabetiků (Ústav zdravotnických informací a statistiky ČR 2011). K rozvoji komplikací diabetu dochází

v důsledku nedostatečnosti léčby a přetrvávajících výkyvů glykémií. Standardem pro léčbu je tzv. intenzifikovaná inzulínová terapie, která spočívá ve snaze co nejvíce napodobit přirozenou sekreci podkožním podáváním inzulínu na základě samostatného monitorování glykémií a náležitého poučení pacienta. Dosáhnout dostatečné kompenzace diabetu se ale i při velkém úsilí daří jen asi u 5 % pacientů (Reichard, Nilsson et al. 1993).

Zlepšování technologií by snad mohlo v budoucnu vést k vytvoření uzavřeného okruhu, kdy bude kontinuálně permanentním senzorem měřena koncentrace krevního cukru a na její hodnoty bude pružně reagovat dávkování inzulínu inzulínovou pumpou. Problém tohoto systému je však zpoždění detekce reálné koncentrace glukózy, které je dáno jejím měřením v mezibuněčném prostoru namísto v krvi (Renard 2004).

Zatím jedinou léčebnou metodou, která dokáže navodit dlouhodobou normoglykémii a bránit tak rozvoji dlouhodobých diabetických komplikací, je transplantace pankreatu, případně Langerhansových ostrůvků (Adamec and Saudek 2005).

Transplantační léčba diabetu

V současné době se klinicky nejvíce uplatňuje orgánová transplantace pankreatu. Pokud je transplantace úspěšná, zajišťuje udržení normoglykémie a nezávislost na zevním inzulínu. V důsledku toho se zpomalí rozvoj komplikací diabetu a případně může dojít k jejich regresi. Transplantace pankreatu je však i přes značné zlepšení techniky život ohrožující zákrok. Riziko přináší i potřeba užívat imunosupresivní léčbu. U pacientů je proto třeba zvážit rizika diabetu a transplantace, takže se transplantace pankreatu provádí u příjemců s již pokročilými stádii orgánových komplikací diabetu (Saudek 2010).

Alternativou k celoorgánové transplantaci pankreatu je transplantace izolovaných Langerhansových ostrůvků. Podobně jako transplantace pankreatu zlepšuje kontrolu glukózového metabolizmu a snižuje riziko hypoglykémií (Tufveson 2009). Transplantací ostrůvků ale není vždy dosaženo nezávislosti na inzulínu, funkce transplantovaných ostrůvků postupem času klesá v důsledku jejich poškození a ztrát a post-transplantační léčba vystavuje pacienta efektům imunosuprese. Výrazně menší invazivita transplantace ostrůvků však umožňuje využití u pacientů v časnějších fázích diabetu. Současnými postupy izolace se sice získávají ostrůvky, jejichž transplantace vede k častějšímu a dlouhodobějšímu dosažení nezávislosti na inzulínu, nicméně další zlepšení životnosti a funkce izolovaných ostrůvků je pro dlouhodobé udržení normoglykémie nezbytné.

Další možností léčby diabetu by mohla být transplantace inzulín produkujících buněk získaných z alternativních zdrojů. Tyto snahy jsou ale zatím realizovány pouze

v experimentu. Buňky exprimující inzulín byly získány kultivací embryonálních kmenových buněk (Segev, Fishman et al. 2004), pankreatických neendokrinních buněk (Bonner-Weir, Taneja et al. 2000) nebo změnou vývoje kmenových buněk například z kostní dřeně (Oh, Muzzonigro et al. 2004).

Izolace a transplantace ostrůvků

Pankreatické ostrůvky jsou izolovány z pankreatů kadaverózních dárců, které jsou většinou získány v rámci multiorgánového odběru. Orgány včetně pankreatu jsou během odběru perfundovány vhodným konzervačním roztokem, ve kterém jsou rovněž transportovány. Čas studené ischemie pankreatu do počátku izolace ostrůvků by neměl přesáhnout 8 hodin.

Lidské ostrůvky jsou z pankreatu získávány automatizovanou metodou izolace (Ricordi, Finke et al. 1988), která byla postupem času zčásti modifikována (Ricordi, Gray et al. 1990) a uzpůsobena pro konkrétní izolační laboratoře.

Základní kroky izolace jsou tyto. Pankreatickým duktem je pankreas naplněn roztokem enzymu kolagenázy. Plnění je prováděno pomocí automatické pumpy a tlak roztoku je v průběhu regulován. Enzymatické natrávení kolagenázou uvolní ostrůvky z jejich okolní tkáně, aniž by byly mechanicky poškozeny. Pankreas s kolagenázou se umístí do digesční komory, která je napojena na cirkulační okruh. V systému je regulována teplota (optimálně 37°C) a průtok. Během recirkulační fáze je sledován průběh trávení pankreatické tkáně a míra uvolnění ostrůvků. Po dostatečném uvolnění ostrůvků se natrávená tkáň ze systému postupně vymývá a koncentruje. Ostrůvky jsou pak od exokrinní tkáně odděleny na základě rozdílných hustot pomocí hustotního gradientu. Pro centrifugaci gradientu je používán buněčný separátor COBE 2991 (Caridian BCT, Terumo BTC, USA). Ostrůvky z jednotlivých frakcí gradientu jsou resuspendovány v médiu, kde se stanovuje jejich počet, procentuální zastoupení ve tkáňové suspenzi (čistota) a objem tkáně. Počet ostrůvků se vztahuje na tzv. ostrůvkové ekvivalenty (IEQ, islet equivalent), kde 1 IEQ odpovídá ostrůvku o průměru 150 μm. Přispění ostrůvků různých velikostí do celkového počtu ostrůvkových ekvivalentů je pak dáno jejich objemem. Izolované ostrůvky jsou až do transplantace uloženy do kultivačních nádob v buněčném inkubátoru. Transplantace se provádí, jen pokud je při izolaci získán dostatečný počet ostrůvků (více než 4000 IEQ / kg váhy příjemce).

Transplantace pankreatických ostrůvků se klinicky rozšířila po publikaci edmontonské skupiny v roce 2000 (Shapiro, Lakey et al. 2000). Tato skupina provedla transplantace u 7

pacientů a u všech bylo dosaženo nezávislosti na inzulínu. Všem byly transplantovány ostrůvky od 2 dárců a byla použita imunosuprese bez glukokortikoidů.

Ostrůvky jsou transplantovány příjemci se shodnou krevní skupinou. Suspenze ostrůvků je nejčastěji transplantována transkutánně katetrem do vena porte, který je zavedený pomocí rentgenu. Infuze ostrůvků probíhá samovolně, aby nedošlo k výraznému zvýšení portálního tlaku.

Transplantace pankreatických ostrůvků je určena hlavně pro pacienty s diabetem 1. typu, kteří trpí hypoglykemickými stavy, metabolickou nestabilitou nebo časnými sekundárními komplikacemi diabetu (Ryan, Bigam et al. 2006).

Faktory ovlivňující funkci ostrůvků po transplantaci

Funkci a uchycení ostrůvků ovlivňuje mnoho faktorů. Pro dostatečnou funkci je kritický počet implantovaných ostrůvků. Ten závisí na stavu orgánu, jeho prezervaci a na procesu izolace. Transplantované ostrůvky se zachytí v drobných cévách krevního řečiště jater, což představuje zcela nové mikroprostředí bez inervace, vnitřní vaskularizace a bez vlastní extracelulární matrix. Přímý kontakt ostrůvků s krví navíc vede k rozvoji akutní reakce (instant blood-mediated inflammatory reaction - IBMIR) (Bennet, Groth et al. 2000). Její součástí je aktivace koagulační i komplementové kaskády a na ně navazující zánětlivá reakce, která může vést k destrukci ostrůvků. Po transplantaci jsou dále ostrůvky vystaveny aloimunitní reakci, která může vést k jejich rejekci. Ostrůvky mohou být ztraceny také díky autoimunitní reakci, která přetrvává i v pozdních fázích diabetu (Pileggi, Ricordi et al. 2001). Nové imunosupresivní režimy sice snižují riziko rejekce a potlačují autoimunitu, v případě transplantace ostrůvků ale chybí specifický marker, který by umožňoval jejich monitorování. Proto je velmi těžké nastavit vhodný imunosupresivní režim, který by přežití ostrůvků prodloužil.

Sledování ostrůvků po transplantaci

Rozložení transplantovaných ostrůvků neumožňuje sledování jejich rejekce pomocí biopsie nebo běžných zobrazovacích metod. Sledování transplantovaných ostrůvků je tak založeno pouze na monitorování jejich funkce. Sleduje se sekrece c-peptidu, glykémie, koncentrace glykovaného hemoglobinu nebo množství potřebného exogenního inzulínu. Zhoršená funkce ostrůvků je zjištěna výskytem hyperglykemií, snížením sekrece c-peptidu nebo vyšší spotřebou inzulínu. Tyto ukazatele jsou ale zachyceny až v době, kdy už došlo ke ztrátě většiny ostrůvků. Pro zlepšení přežívání transplantovaných ostrůvků je zapotřebí

metoda, která by umožnila včas detekovat, kdy dochází k jejich poškození a jakým mechanizmem jsou poškozeny (Berney and Toso 2006).

Možnosti zobrazení transplantovaných ostrůvků

Nejslibnějšími přístupy sledování transplantovaných ostrůvků jsou neinvazivní metody zobrazování. Jednou z možných metod pro zobrazení transplantovaných ostrůvků je pozitronová emisní tomografie (PET). PET- kompatibilní částice mohou být použity pro označení ostrůvků ex vivo před transplantací. Takto byly ostrůvky pro experimentální i klinickou transplantaci označeny pomocí 2-[18F]fluoro-2deoxy-D-glukózy a následně zobrazeny (Eich, Eriksson et al. 2007). Nevýhodou této metody je její nízké prostorové rozlišení. Signál navíc přetrvává pouze několik hodin. Metoda tak neumožňuje následné sledování ostrůvků. Na druhou stranu detekce signálu je velmi citlivá a signál je dobře kvantifikovatelný.

V experimentu je pro zobrazení transplantovaných ostrůvků používaná také metoda detekce bioluminiscence, která využívá světlo generující enzym, např. luciferázu, a světelný (bioluminiscenční) signál je nad povrchem tkáně snímán velmi citlivou kamerou. U myší byly takto zobrazeny transplantované ostrůvky, jejichž buňky po transfekci tento enzym produkovaly. Trvalá exprese enzymu umožnila zobrazit ostrůvky i dlouho po transplantaci (Fowler, Virostko et al. 2005) (Chen, Zhang et al. 2006). Nevýhodou této metody je ale snížení bioluminiscenčního signálu při průchodu tkání a v současné době není aplikovatelná v klinické praxi.

Nejvíce používanou metodou pro detekci transplantovaných ostrůvků je zobrazování pomocí magnetické rezonance (MRI - magnetic resonace imaging). Pro odlišení ostrůvků od okolní tkáně využívají MRI studie běžně dostupné kontrastní látky vyvinuté pro MRI (Saudek, Brogren et al. 2008).

Magnetické působení MRI skeneru vyvolává změnu spinu jader některých atomů a jejich následný návrat do původního stavu (relaxace). Energie, která se při relaxaci uvolní je detekována a převedena do formy obrazu. MRI kontrastní látky mění tzv. relaxační časy jader ve své blízkosti, hlavně protonů vody, a zvětšují tak kontrast mezi zobrazovanými tkáněmi. Vliv kontrastní látky na MRI je charakterizován jejími účinky na T1-relaxační čas (doba trvání změny způsobené v podélném magnetickém poli) a T2-relaxační čas (doba trvání změny vyvolané působením příčného magnetického pole). Látky, které zkracují T1 relaxační čas, jsou zobrazeny jako intenzivnější, světlé body a označují se jako T1-kontrastní látky (pozitivní) a látky, které zkracují T2 relaxační čas, dávají obraz se sníženou intenzitou signálu

a označují se jako T2-kontrastní látky (negativní). Kontrastní látky mohou být dále klasifikovány na základě jejich rozložení ve tkáni, chemického složení, magnetických vlastností nebo vlivu na MRI (Na, Song et al. 2009).

Stále nejčastěji používanými kontrastní látkami jsou cheláty gadolinia. Tyto komplexy Gd^{3+} jsou velmi stabilní, což brání toxicitě gadolinia. Tyto kontrastní látky jsou paramagnetické a zkracují T1-relaxační časy. V závislosti na chemické struktuře jsou některé gadoliniové kontrastní látky po intravenózní aplikaci distribuovány nespecificky extracelulárně, jiné vstupují do buněk specifické tkáně nebo zůstávají vázány na krevní bílkoviny.

Kontrastní látky na bázi manganu mají paramagnetické vlastnosti. Cheláty manganu jsou specificky rozpoznávány transportním systémem hepatocytů a slouží tak jako kontrastní látky pro zobrazení jaterní tkáně.

Další skupinou kontrastních látek jsou superparamagnetické částice oxidů železa - SPIO částice (superparamagentic iron oxide particles). Jsou tvořeny magnetickým jádrem z oxidů železa a obalem z dextranu nebo carboxydextranu. Silná magnetizace superparamagnetických částic způsobuje mikroskopické nehomogenity v magnetickém poli ve svém okolí. SPIO částice tak zkracují T2-relaxační časy i v přilehlé oblasti a v MRI značně snižují intenzitu signálu. Obal částic brání toxicitě železa a umožňuje jejich biologickou distribuci. SPIO částice jsou specificky zachycovány buňkami retikuloendoteliálního systému převážně v játrech a slezině. Dostupné jsou dvě formy, ferumoxidy a ferucarbotrany.V průměru větší ferumoxidy (kolem 150 nm) jsou přednostně vychytávány Kupfferovými buňkami v játrech, kdežto menší ferucarbotrany cirkulují v krvi déle a mohou být vychytány makrofágy v lymfatických uzlinách, játrech nebo slezině. SPIO částice jsou metabolizovány a uvolněné neparamagnetické železo je začleněno do feritinu, hemoglobinu nebo hemosiderinu.

Značení ostrůvků pomocí SPIO částic

V roce 2004, naše skupina (IKEM, Praha) jako první zobrazila transplantované ostrůvky pomocí MRI v experimentálním modelu (Jirak, Kriz et al. 2004). Izolované ostrůvky byly před transplantací in vitro označeny SPIO kontrastní látkou. Pro značení byla použita komerčně dostupná kontrastní látka Resovist® (ferucarbotran, Schering AG, Berlin, Germany). Po intraportální transplantaci jsou ferucarbotranem značené ostrůvky v játrech zobrazeny jako hypointensní body na T2*-vážených snímcích MRI (Obr. 2).

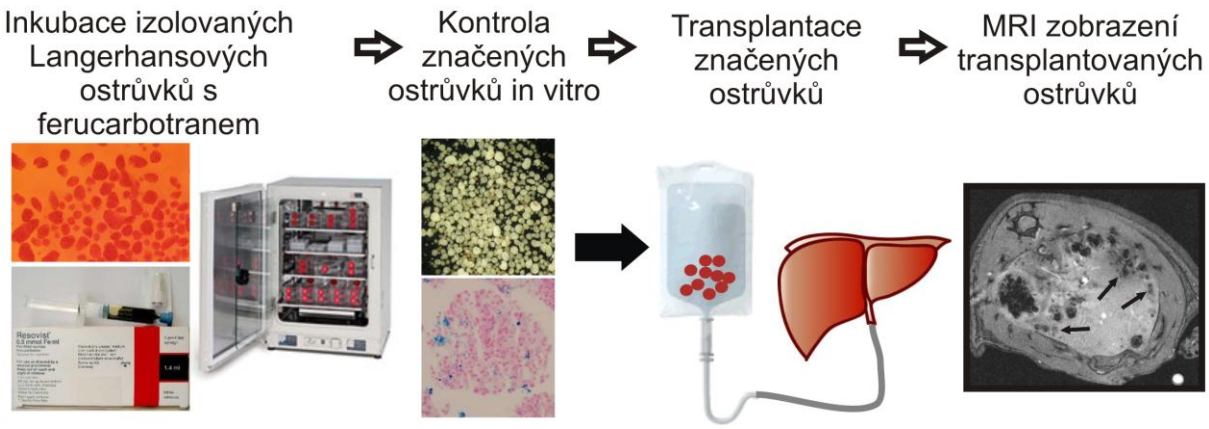

Obr. 2: Schéma postupu značení Langerhansových ostrůvků pomocí SPIO částic a jejich zobrazení

Obdobně byly transplantované ostrůvky zobrazeny po označení kontrastními látkami ferumoxidy (Feridex®, ferumoxide; Advanced Magnetics, Cambridge, MA nebo Endorem®, Guerbet, Paris, France) (Evgenov, Medarova et al. 2006; Tai, Foster et al. 2006; Ris, Lepetit-Coiffe et al. 2010). Diky SPIO kontrastním látkám schváleným pro klinické MRI bylo možné přenést tuto metodu zobrazování do klinické praxe (Toso, Vallee et al. 2008; Saudek, Jirak et al. 2010). Produkce klinicky používané kontrastní látky Resovist® byla ale bohužel v současné době zastavena.

Kvantifikace hypointenzních spotů ostrůvků na MRI byla z počátku prováděna manuálním počítáním na několika vybraných optických řezech. V dnešní době bylo vyvinuto několik způsobů automatizované kvantifikace, které vychází z různých režimů MRI snímání a analýzy obrazu (Jirak, Kriz et al. 2009; Medarova, Vallabhajosyula et al. 2009; Crowe, Ris et al. 2011). Počet spotů dobře koreluje s počtem transplantovaných ostrůvků, i když jednotlivé signály odpovídají spíše skupině několika ostrůvků. Spoty jsou dobře rozpoznatelné díky superparamagnetickým vlastnostem SPIO částic, které způsobují hypointenzní signál v oblasti větší než je skutečná velikost ostrůvků.

Velkou výhodou značení pomocí SPIO částic je to, že značené ostrůvky lze zobrazit i 6 měsíců po transplantaci (Jirak, Kriz et al. 2004; Toso, Vallee et al. 2008; Saudek, Jirak et al. 2010). Citlivost MRI navíc umožňuje zachytit pokles počtu hypointenzních spotů, ke kterému dochází během rejekce značených ostrůvků (Kriz, Jirak et al. 2005; Evgenov, Medarova et al. 2006; Kriz, Jirak et al. 2012).

Bimodální kontrastní látky

Značení pomocí MRI kontrastní látek se využívá pro sledování mnoha typů transplantovaných buněk. Běžné MRI kontrastní látky umožňují zobrazení s vysokým rozlišením, ale nelze je přímo zobrazit jinými, například mikroskopickými metodami. Nově vyvíjené kontrastní látky, tzv. bimodální kontrastní látky, proto využívají nanostrukturní materiály, ve kterých jsou paramagnetické částice imobilizovány v liposomechy, perfluorocarbonových nebo silikonových částicích. Na tyto strukturní části může být navázán luminiscenční nebo fluorescenční marker. Komplexy navíc obsahují větší počet paramagnetických částic a mají tak intenzivnější vliv na MRI (Na and Hyeon 2009). Kontrasty tohoto typu byly několikrát použity i pro značení a detekci izolovaných ostrůvků (Barnett, Ruiz-Cabello et al. 2011).

VÝSLEDKY

Vlastní výsledky práce jsou v rozšířené verzi obsaženy v přiložených pracích.
Část 1, která je zaměřena na diagnostiku transplantace izolovaných Langerhansových ostrůvků, je založena na výsledcích, které byly součástí následujících publikací:

Příloha I. **Zacharovova, K.**, Z. Berkova, T. Spacek, J. Kriz, E. Dovolilova, P. Girman, T. Koblas, P. Jezek, and F. Saudek, In vitro assessment of pancreatic islet vitality by oxymetry. Transplant Proc, 2005. 37(8): p. 3454-6. (IF = 0,799)

Příloha II. Berkova, Z., D. Jirak, **K. Zacharovova**, J. Kriz, A. Lodererova, P. Girman, T. Koblas, E. Dovolilova, M. Vancova, M. Hajek, and F. Saudek, Labeling of pancreatic islets with iron oxide nanoparticles for in vivo detection with magnetic resonance. Transplantation, 2008. 85(1): p. 155-9. (IF = 3,816)

Příloha III. **Zacharovová, K.**, Z. Berková, D. Jirák, V. Herynek, M. Vancová, E. Dovolilová, and F. Saudek, Processing of superparamagnetic iron contrast agent ferucarbotran in transplanted pancreatic islets. Contrast Media & Molecular Imaging. Manuskript přijat k publikaci 8. května 2012. (IF = 4,020 z roku 2010)

Příloha IV. Kacenka, M., O. Kaman, J. Kotek, L. Falteisek, J. Cerny, D. Jirak, V. Herynek, **K. Zacharovova**, Z. Berkova, P. Jendelova, J. Kupcik, E. Pollert, P. Veverka, and I. Lukes, Dual imaging probes for magnetic resonance imaging and fluorescence microscopy based on perovskite manganite nanoparticles. Journal of Materials Chemistry, 2011. 21(1): p. 157-164. (IF z roku 2010 = 5,101)

Část 2, která je zaměřena na diagnostiku imunitní intervence v časném stádiu diabetu 1. typu, je založena na publikacích:

Příloha V. Vrabelova, Z., S. Kolouskova, K. Bohmova, M.K. Faresjo, Z. Sumnik, M. Pechova, M. Kverka, D. Chudoba, **K. Zacharovova**, G. Stadlerova, P. Pithova, M. Hladikova, and K. Stechova, Protein microarray analysis as a tool for monitoring cellular autoreactivity in type 1 diabetes patients and their relatives. Pediatr Diabetes, 2007. 8(5): p. 252-60. (IF = 2,314)

Příloha VI. Stechova, K., K. Bohmova, Z. Vrabelova, A. Sepa, G. Stadlerova, **K. Zacharovova**, and M. Faresjo, High T-helper-1 cytokines but low T-helper-3 cytokines, inflammatory cytokines and chemokines in children with high risk of developing type 1 diabetes. Diabetes Metab Res Rev, 2007. 23(6): p. 462-71. (IF = 3,087)

Příloha VII. Vargova, L., **K. Zacharovova**, E. Dovolilova, L. Vojtova, and F. Saudek, Immunoregulatory effect of anti-thymocyte globulin monotherapy on peripheral lymphoid tissues of non-obese diabetic mice. Transplant Proc, 2011. 43(9): p. 3277-80. (IF z roku 2010 = 0,993)

PODÍL PRÁCE NA JEDNOTLIVÝCH PUBLIKACÍCH

Příloha I. *In vitro assessment of pancreatic islet vitality by oxymetry. Transplant Proc, 2005.*
Spolu se školitelem jsem se podílela na návrhu studie. Provedla jsem izolace ostrůvků a testování jejich kvality metodami statické inkubace a fluorescenčního barvení živých a mrtvých buněk. Respirační aktivitu ostrůvků jsem měřila ve spolupráci s pracovištěm Akademie věd ČR. Výsledky jsem zpracovala a připravila text publikace.

Příloha II. *Labeling of pancreatic islets with iron oxide nanoparticles for in vivo detection with magnetic resonance. Transplantation, 2008.*
Pro tuto publikaci jsem zpracovala vzorky pro analýzu pomocí transmisní elektronové mikroskopie. Vzorky jsem vyšetřila a z morfologického obrazu jsem vyhodnotila postupný proces pronikání SPIO partikulí do buněk ostrůvků. Fotodokumentaci spolu s metodickou částí a popisem jsem předala k vytvoření publikace hlavní autorce.

Příloha III. *Processing of superparamagnetic iron contrast agent ferucarbotran in transplanted pancreatic islets. Contrast Media & Molecular Imaging. Manuskript přijat k publikaci 8. května 2012.*
V tomto projektu jsem se podílela na přípravě konceptu studie a na experimentálních postupech jako je izolace ostrůvků, jejich značení ferucarbotranem a následné značení pomocí CMFDA Cell Tracker^{TM}Green. Provedla jsem imunofluorescenční i histologická barvení, zpracovala jsem vzorky pro elektronovou mikroskopii a vzorky jsem vyhodnotila. Výsledky jsem zpracovala formou publikace jako hlavní autor.

Příloha IV. *Dual imaging probes for magnetic resonance imaging and fluorescence microscopy based on perovskite manganite nanoparticles. Journal of Materials Chemistry, 2011.*
Pro tuto publikaci jsem zpracovala histologické vzorky značených ostrůvků a vyhodnotila efekt značení pomocí fluorescenční mikroskopie.

Příloha V. *Protein microarray analysis as a tool for monitoring cellular autoreactivity in type 1 diabetes patients and their relatives. Pediatr Diabetes, 2007.*
a příloha VI. *High T-helper-1 cytokines but low T-helper-3 cytokines, inflammatory cytokines and chemokines in children with high risk of developing type 1 diabetes. Diabetes Metab Res Rev, 2007.*
V rámci tohoto projektu jsem prováděla sběr vzorků krve, jejich zpracování, izolace mononukleárních buněk a jejich stimulace. Vzorky jsem analyzovala pomocí proteinové cytokinové array.

Příloha VII. *Immunoregulatory effect of anti-thymocyte globulin monotherapy on peripheral lymphoid tissues of non-obese diabetic mice. Transplant Proc, 2011.*
Navrhla jsem postup a způsob realizace tohoto projektu. Pracovala jsem na všech využitých postupech. Na sledovaných myších jsem prováděla testování glukózového metabolismu a v terminální fázi odběr a zpracování krve, sleziny, pankreatických uzlin a pankreatu. Značila jsem izolované buňky sleziny a uzlin a provedla jejich analýzu pomocí průtokové cytometrie. Podílela jsem se na vyhodnocení výsledků a přípravě publikace.

KOMENTÁŘ K VÝSLEDKŮM A DISKUZE

ČÁST 1

I. Stanovení životnosti izolovaných ostrůvků pomocí oxymetrie (příloha I.)

Úspěšnost transplantace pankreatických ostrůvků je do značné míry závislá na kvalitě podaných ostrůvků. Životnost ostrůvků může být ovlivněna již dobou ischemie odebraného orgánu, během izolačního procesu i při kultivaci ostrůvků před transplantací. K posouzení kvality ostrůvků jsou potřeba rychlé a spolehlivé metody testování.

V předkládané práci bylo testováno měření respirační aktivity izolovaných ostrůvků jako případná alternativní metoda sledování jejich kvality. V experimentu byla pomocí respirometru Oxygraph K2 měřena spotřeba kyslíku izolovaných Langerhansových ostrůvků potkanů kmene Wistar. Respirační aktivita dobře korelovala s výsledky standardního testování ostrůvků metodou statické inkubace a rychlost spotřeby kyslíku byla úměrná počtu testovaných ostrůvků.

Rychlost spotřeby kyslíku ostrůvky byla následně testována i dalšími autory. Výsledky ukazují, že je přímo úměrná počtu živých buněk a koreluje s integritou membrány buněk ostrůvků (Sweet, Khalil et al. 2002). Metabolická aktivita beta buněk je navíc zvýšená při glukózou stimulované sekreci inzulínu. Měření proto bylo rozšířeno o sledování zvýšení rychlosti spotřeby kyslíku po aplikaci glukózy. Vyšší stimulační index spotřeby kyslíku byl zaznamenán u ostrůvků s vyšší životností (Wang, Upshaw et al. 2005). Velkou výhodou je to, že stimulovaná spotřeba kyslíku je glukózou zvýšena téměř výhradně v beta buňkách. Je tedy velmi specifickým markerem kvality beta buněk a není významně ovlivněna přítomností neendokrinních buněk (Sweet, Gilbert et al. 2008). Pro měření respirační aktivity byly použity různé metody měření koncentrace kyslíku, například pomocí kyslíkové elektrody nebo detekcí signálu z fluoroforů zhášených kyslíkem. Pro sledování respirační aktivity ostrůvků byla také vyvinuta speciální komerční sestava komůrek s integrovaným fluorescenčním senzorem (Instech Lab) (Papas, Pisania et al. 2007). Měření spotřeby kyslíku se tak ukazuje jako jednoduchá a rychlá metoda, která dobře vypovídá o kvalitě testovaných ostrůvků a jejich vhodnosti pro transplantaci (Papas, Colton et al. 2010). Po zavedení metody se oxymetrické vyšetření v naší laboratoři stalo rutinním způsobem testování vitality ostrůvků.

II. Značení pankreatických ostrůvků SPIO nanočásticemi pro jejich in vivo zobrazení pomocí MRI (příloha II.)

Zobrazování transplantovaných ostrůvků může být využito pro jejich sledování během transplantace, vaskularizace, autoimunitního nebo aloimunitního zánětu. Dlouhodobé sledování, dostatečné rozlišení a využitelnost v klinické praxi umožňuje v současné době stále jen jediná metoda: značení ostrůvků SPIO částicemi před transplantací a jejich následné zobrazení pomocí MRI (Borot, Crowe et al. 2011). V předkládané práci bylo cílem podrobně poznat proces značení ostrůvků SPIO částicemi, sledovat časový vývoj značení, akumulaci železa v jednotlivých typech buněk ostrůvků a na základě toho optimalizovat značení ostrůvků a ověřit bezpečnost této metody.

Pomocí transmisní elektronové mikroskopie (TEM) jsme sledovali ultrastrukturní lokalizaci SPIO částic ferucarbotranu a průběh jejich vstupu do buněk ostrůvků. Ostrůvky byly značeny po dobu 1, 4, 8, 12 a 24 hodin. SPIO částice byly v TEM zobrazeny jako silně elektrodenzní krystaly, které byly snadno rozpoznatelné zvlášť na nekontrastovaných řezech. V endozómech makrofágů byly SPIO částice detekovány již po jedné hodině značení. U endokrinních buněk byly SPIO částice nejdříve detekovány jen adherované na povrchu, ale po čtyřech hodinách značení byly lokalizovány i v malých vezikulech v cytoplazmě. S délkou času značení přibývalo množství částic začleněných do buněk ostrůvků. Částice byly detekovány ve větších endozómech a postupně byly akumulovány do elektrodenzních klastrů. Ferucarbotran byl zachycen ve všech typech buněk ostrůvků, ale největší množství SPIO částic bylo nahromaděno v makrofázích. In vitro značení neovlivnilo strukturu endokrinních buněk ani funkci ostrůvků.

Ferucarbotran byl vyvinut jako kontrastní látka pro MRI pro zobrazení jaterních lézí (Reimer and Tombach 1998; Vogl, Schwarz et al. 2003). Oxidy železa v jádře částic jsou obaleny karboxydextranem, který podporuje fagocytózu těchto částic Kupferovými buňkami v játrech (Reimer and Tombach 1998; Wang, Hussain et al. 2001). Karboxydextran je pravděpodobně důvodem, proč jsou částice intenzivně fagocytovány i makrofágy ostrůvků.

SPIO částice byly lokalizovány v makrofázích i endokrinních buňkách jak naší skupinou v předcházejících pracích (Jirak, Kriz et al. 2004; Kriz, Jirak et al. 2005), tak dalšími autory, kteří používaly ke značení ostrůvků ferucarbotran (Kim, Choi et al. 2009) nebo jiné typy SPIO částic (Evgenov, Medarova et al. 2006; Tai, Foster et al. 2006). Pro značení lidských ostrůvků se pak jeví jako vhodnější právě ferucarbotranové SPIO částice (Ris, Lepetit-Coiffe et al. 2010).

Pomocí MRI byly značené ostrůvky viditelné na T2*- vážených snímcích jako silně hypointenzní spoty již po jedné hodině značení, ale superparamgnetický efekt byl v této fázi způsoben hlavně částicemi zachycenými na povrchu buněk ostrůvků. Množství železa začleněného do ostrůvků se zvyšovalo s dobou značení.

Sekrece inzulínu jako reakce na stimulaci glukózou nebyla značením ostrůvků ovlivněna a značené ostrůvky normalizovaly glykemie diabetických zvířat. Obdobně byla ověřena bezpečnost značení SPIO částicemi i dalšími autory (Tai, Foster et al. 2006; Evgenov, Pratt et al. 2008; Kim, Choi et al. 2009). U lidských ostrůvků také nebyla značením ovlivněna životnost, funkce ani exprese genů pro proteiny sekrečních granul a transkribčních faktorů beta buněk (Malosio, Esposito et al. 2009).

Z našich výsledků vyplynula jako nejvhodnější 24 hodinová doba značení, kdy je dosaženo dostatečné intenzity značení bez zjevných nežádoucích efektů na životnost a morfologii ostrůvků.

III. Sledování SPIO nanočástic po transplantaci značených ostrůvků (příloha III.)

Metoda značení Langerhansových ostrůvků pro jejich zobrazení pomocí MRI byla použita i v publikaci v příloze III. Cílem této části práce bylo sledování výskytu magnetických částic in vivo po transplantaci značených ostrůvků. Abychom objasnili vztah výskytu magnetických partikulí a transplantovaných ostrůvků, sledovali jsme morfologii značených ostrůvků po transplantaci. Jako model transplantace jsme použili transplantaci do jaterní žíly a transplantaci pod renální kapsulu.

V syngenním modelu bylo MRI hypointenzních spotů vyvolaných značenými ostrůvky bez výrazných změn po dobu 3 měsíčního sledování po transplantaci. Podobně jako popisovali ostatní autoři (Evgenov, Medarova et al. 2006; Tai, Foster et al. 2006), tak i v naší studii byly na MRI v játrech detekovány jednotlivé spoty, kdežto při transplantaci pod renální kapsulu byla zobrazena souvislá hypointenzní oblast na okraji ledviny. Pro MRI ostrůvků není jejich umístění pod pouzdro ledviny příliš vhodné. Jednak překrývající superparamagnetický signál neumožňuje jejich kvantifikaci a navíc na rozhraní ledviny vzniká takzvaný ”chemical shift artifact“, kdy odlišné rezonanční frekvence různých tkání mají za následek tmavou linii na jejich rozhraní v MRI (Weinreb, Brateman et al. 1985). Na okraji ledviny tak může tento artefakt zastírat místo transplantovaných ostrůvků.

V naší studii jsme se zaměřili na lokalizaci SPIO částic ve značených ostrůvcích po jejich transplantaci. Oproti situaci in vitro, kdy se částice po značení ostrůvků nachází v cytoplasmě buněk ostrůvků, jsme po transplantaci pozorovali výrazné změny, které byly

u syngenního modelu srovnatelné jak po transplantaci do jater tak pod renální kapsulu. Metodami imunofluorescence, histochemie a transmisní elektronové mikroskopie jsme prokázali, že SPIO částice byly po transplantaci ostrůvků postupně eliminovány z endokrinních buněk a byly akumulovány v makrofázích v těsné blízkosti ostrůvků. Fibroblasty a myofibroblasty, které byly v okolí ostrůvků také četné, obsahovaly jen malé množství SPIO částic. Železné částice byly takto lokalizovány i po 3 měsících po transplantaci. Přítomnost SPIO částic v buňkách v okolí ostrůvků již byla popsána v několika studiích (Tai, Foster et al. 2006; Jiao, Peng et al. 2008; Kim, Kim et al. 2010). Část partikulí uvolněných z buněk ostrůvků mohlo být také zmetabolizováno (Weissleder, Stark et al. 1989; Arbab, Wilson et al. 2005). Nicméně v našem syngenním modelu většina SPIO částic uvolněných z ostrůvků zůstávala v těsné blízkosti funkčních ostrůvků po dlouhou dobu a to na obou místech transplantace.

Přetrvávání železných částic v blízkosti ostrůvků v četných makrofázích nás vedlo k průkazu původu těchto buněk. Ostrůvky značené ferucarbotranem jsme proto následně značili fluorescenční barvou CellTracker™ Green CMFDA (5-chloromethylfluorescein diacetate) (Invitrogen, OR, USA). CMFDA tvoří v cytoplasmě živých buněk nerozpustný fluorescenční konjugát, který umožňuje identifikaci označených buněk v kratším období po transplantaci. Sekundární značení ostrůvků pomocí CMFDA neovlivnilo lokalizaci SPIO částic po syngenní transplantaci ostrůvků. Histologické sledování ukázalo, že buňky, ve kterých se po transplantaci nacházely SPIO částice, byly téměř výhradně původem příjemcovy. Předpokládáme, že makrofágy migrující na místo transplantace pohltily uvolněné železo nebo přímo značené buňky. Podobný mechanizmus byl pozorován i po transplantaci SPIO značených buněk kostní dřeně (Pawelczyk, Jordan et al. 2009), neurálních prekurzorů (Lepore, Walczak et al. 2006) nebo mezenchymálních kmenových buněk (Terrovitis, Stuber et al. 2008).

V alogenním modelu byly transplantované ostrůvky zcela odhojeny během několika dnů a to jak po transplantaci do jater tak pod renální kapsulu. Osud SPIO částic na těchto dvou transplantačních místech se však významně lišil. Při transplantaci pod renální kapsulu překvapivě nedošlo ke změně MRI po rejekci ostrůvků ani po dvou měsících po transplantaci a obraz byl stejný jako při transplantaci ostrůvků syngenních. Histologicky byly železné částice detekovány v makrofázích v místě transplantace, i když endokrinní buňky již nebyly přítomné. Výsledky tak ukazují, že MRI značených ostrůvků transplantovaných pod renální kapsulu nevypovídá o jejich přítomnosti a funkčnosti. Podobný model alogenní transplantace

značených ostrůvků pod pouzdro ledviny u imunokompetentních zvířat nebyl dosud publikován.

Naopak u alogenního modelu transplantace ostrůvků do jater byl zaznamenán postupný pokles hypointenzních spotů v souvislosti s rejekcí ostrůvků, stejně jako byl pozorován dalšími autory již dříve (Kriz, Jirak et al. 2005; Evgenov, Medarova et al. 2006). Devátý den po transplantaci byly sice na histologických řezech železné částice stále detekovány v místě po rejekci ostrůvků, ale čtrnáctý den bylo železo detekováno jen velmi ojediněle. Poněkud protichůdné výsledky publikace Marzola et al. (Marzola, Longoni et al. 2009), kde je popisována přítomnost SPIO částic v játrech i 42 dnů po transplantaci ostrůvků, by mohly být vysvětleny nižší intezitou aloimunitní reakce a tím i pomalejšího odstranění železných částic. V popisovaném modelu (transplantace mezi potkany kmenů Wistar a Sprague–Dawley) totiž byly endokrinní buňky detekovány ještě 29 den po transplantaci. Obdobně Kříž et al. (Kriz, Jirak et al. 2012) ukazují přetrvávající MRI signál u modelu rejekce zmírněné antirejekční léčbou. V našem modelu transplantace (transplantace mezi potkany kmenů Brown Norway a Lewis) snižující se hypointenzní MRI signál korespondoval s odstraněním železných částic z odhojených ostrůvků.

IV. Značení a zobrazení transplantovaných ostrůvků pomocí nové duální kontrastní látky na bázi nanočástic Perovskite Manganite pro MRI a fluorescenční mikroskopii (příloha IV.)

Nové bimodální (neboli duální) kontrastní látky umožňují současně detekci pomocí MRI i další citlivější zobrazovací metodou jako luminiscence nebo fluorescence. Ve spolupráci s Oddělením anorganické chemie, Přírodovědecké fakulty UK, Ústavem anorganické chemie, AVČR a Institutem experimentální medicíny, AVČR jsme testovali nové duální kontrastní látky. Nanočástice byly syntetizovány dvěma postupy a to s použitím molekul „perovskite manganite“ La0.75Sr0.25MnO3 (LSMO), který má paramagnetické vlastnosti T2-kontrastních látek a byl připraven ve spolupracující laboratoři Přírodovědecké fakulty UK. LSMO je dvojitě potažen silikonem a ve vnitřní vrstvě je kovalentně vázaný fluorescein. Tyto nové kontrastní látky jsou tak detekovatelné pomocí MRI jako hypointenzní signály a pomocí fluorescenční mikroskopie jako zelená fluorescence s emisním maximem o vlnové délce 514 nm.

Fyzikální a MRI vlastnosti kontrastních látek byly testovány na pracovištích Oddělení anorganické chemie, Přírodovědecké fakulty UK a Ústavu anorganické chemie, AVČR, kde

byla látka syntetizována. Testy biologických vlastností na buněčných kulturách byly prováděny pracovištěm Institutu experimentální medicíny, AVČR.

Na našem pracovišti jsme provedli 24 hodinovou inkubaci izolovaných ostrůvků s těmito kontrastními látkami. Životnost ostrůvků po značení byla minimálně 75 % a produkce inzulínu in vitro nebyla značením ovlivněna. Mikroskopické pozorování ukázalo přítomnost kontrastní látky v okrajových buňkách ostrůvků. Částice byly detekovány v endokrinních buňkách i makrofázích a rozložení ukazovalo na uložení v endozomálních váčcích. Hypointenzní signál takto značených ostrůvků byl dostatečně silný, takže in vitro byly pomocí MRI rozlišitelné jednotlivé ostrůvky již po jedné akvizici signálu.

Ke zpřesnění lokalizace kontrastní látky ve značených ostrůvcích, byla již v minulosti použita SPIO kontrastní látka s navázaným fluoroforem Cy5.5 (Evgenov, Medarova et al. 2006). Obdobně jako v naší práci, byla tato kontrastní látka detekována také v endokrinních buňkách ostrůvků. Nověji byly zobrazeny také ostrůvky značené bimodální fluorescenční/MRI kontrastní látkou na bázi Gadolinia ve spojení s fluoresceninem (Kotkova, Kotek et al. 2010). V tomto případě se však jednalo o T1 kontrastní látku a detekovaný signál byl hyperintenzní.

Z výsledků naší práce vyplývá, že testované duální kontrastní látky jsou vhodné pro in vitro značení izolovaných pankreatických ostrůvků a neovlivňují jejich kvalitu.

ČÁST 2

V. Sledování buněčné autoreaktivity u pacientů s diabetem 1. typu a jejich příbuzných (přílohy V. a VI.)

Pro komplexnější sledování autoreaktivních T-lymfocytů u pacientů s diabetem 1. typu lze v poslední době využít multiparametrové genomické nebo proteomické metody. V naší studii jsme pro sledování cytokinové odpovědi lymfocytů na specifickou stimulaci diabetogenními antigeny použili semikvantitativní proteinovou microarray.

První studie, jejíž výsledky jsou v publikaci v příloze V., sledovala menší skupinu diabetiků, jejich příbuzných a zdravé kontrolní jedince. Izolované mononukleární buňky periferní krve byly stimulovány in vitro směsí peptidů odvozených od známých diabetogenních autoantigenů GAD 65, IA-2 a proinzulínu. Produkce cytokinů po stimulaci byla srovnávána s produkcí nestimulovaných buněk (bazální). Překvapivě, rozdíly v sekreci cytokinů mezi skupinami byly pozorovány spíše v kultivaci bez stimulace, ačkoliv jsme předpokládali rozdíly spíše v sekreci po stimulaci. Vyšší koncentrace cytokinů byly zaznamenané hlavně v kontrolní skupině. Naopak nižší produkce cytokinů byla pozorována

ve skupině příbuzných diabetiků. Stimulace autoantigeny vedla k významnému snížení tvorby IL-2, IL-13, GCSF a IFN-gamma u kontrolní skupiny. Produkce cytokinů u skupiny diabetiků byla velmi různorodá, jen po stimulaci buněk pacientů 12 měsíců po záchytu diabetu bylo zaznamenáno významné snížení produkce cytokinů IL-2, IL-6, Th1 cytokinů INF-gamma a TNF-beta, Th2 cytokinu IL-4 a Th3 cytokinu TGF-beta. Snížení tvorby prozánětlivých cytokinů po stimulaci bylo popsáno také u příbuzných osob s rizikem vývoje diabetu skupinou Karlsson et al. (Karlsson, Lawesson et al. 2000). Stejná skupina dále ukázala, že v době záchytu diabetu je bazální i stimulovaná tvorba cytokinů velmi nízká, ale po jednom měsíci vyvolala stimulace peptidem GAD65 zvýšení tvorby INF-gamma (Karlsson Faresjo, Ernerudh et al. 2004). Pfleger et al. (Pfleger, Meierhoff et al. 2010) obdobně pozorovali mírný nárůst produkce INF-gamma čtyři týdny po zahájení sledování, ale následně došlo k poklesu reaktivity vůči peptidu GAD65 (sledováno pomocí metody ELISPOT). Tyto i naše výsledky ukazují na významný vliv doby, kdy je po nástupu diabetu autoimunitní reaktivita sledována.

Druhá studie, jejíž výsledky jsou součástí přílohy VI., sledovala sekreci cytokinů bazální a po stimulaci peptidem GAD65 a.a. 247-279. Sledované skupiny byli diabetičtí pacienti dětského věku, osoby s vysokým rizikem vývoje diabetu a zdraví jedinci. Testované mononukleární buňky byly izolovány z periferní krve pacientů čtyři dny po záchytu diabetu. Osoby zařazené do ostatních skupin byly vybírány tak, aby odpovídali věkem skupině diabetiků. Všechny sledované osoby nesly některé z rizikových alel genů pro HLA II. třídy.

Obdobně jako v první studii jsme pozorovali rozdíly v nestimulované produkci cytokinů. Vyšší bazální tvorba cytokinů INF-gamma a TNF-beta ukazovala na převládající Th1 profil u dětí s vysokým rizikem vzniku diabetu. U rizikových osob byla podobná Th1 reaktivita pozorována již dříve (Karlsson, Lawesson et al. 2000). Karlsson Faresjo et al. následně sledovali rizikové pacienty v porovnání s kontrolními osobami, které byly vybrány tak, aby věkově i zastoupením HLA antigenů odpovídala přesně skupině rizikových pacientů (Karlsson Faresjo and Ludvigsson 2005). Výsledky ukázaly snížení Th1 reaktivity již v preklinické fázi diabetu.

U dětí s projeveným diabetem 1. typu byla námi zachycena vyšší produkce zánětlivých cytokinů, některých chemokinů a regulačních cytokinů Th3 odpovědi. Výsledky ukázaly vztah vyšší tvorby Th1 cytokinů a nižší produkce zánětlivých cytokinů u rizikové skupiny a inverzně nižší produkce Th1 cytokinů a vyšší produkce zánětlivých cytokinů u skupiny diabetiků. Z toho lze usuzovat, že Th1 reaktivita předchází klinické manifestaci diabetu a je následována zánětlivou reakcí způsobující destrukci zbývajících beta buněk pankreatu.

V jiné studii, bylo ale naopak pozorováno výrazné zvýšení tvorby INF-gamma po stimulaci buněk diabetiků in vitro (Arif, Tree et al. 2004). Ke stimulaci zde byly použity sekvence peptidů, které byly získány přímo elucí z MHC molekul. Stimulační peptidy tak zcela odpovídali MHC sledovaných osob a měly tak pravděpodobně vyšší efektivitu při stimulaci imunitních buněk. Jediným dalším sledovaným cytokinem v této studii byl IL-10, jehož sekrece byla více stimulována u kontrolních osob.

Cytokinová array použitá v našich studiích umožnila komplexnější zhodnocení imunitní odpovědi na stimulaci diabetogenními autoantigeny. Dříve používaná metoda ELISPOT sice umožňuje dobrou kvantifikaci odpovědi, ale sledování je omezeno jen na několik málo cytokinů.

Jedním z limitujících faktorů stimulačních testů je jistě výběr vhodného stimulačního antigenu a forma jeho prezentace imunitním buňkám. V současné době proto v podobných studiích již převládá stimulace buněk pomocí MHC molekul, případně tetramerů MHC s vázaným konkrétním stimulačním peptidem (Reijonen, Novak et al. 2002; Reijonen, Mallone et al. 2004; Cernea and Herold 2010; Kronenberg, Knight et al. 2012). Zatím asi nejuspokojivějších výsledků dosáhli Velthuis et al. (Velthuis, Unger et al. 2010), kteří sestavili assay pro identifikaci autoreaktivních buněk. Metoda využívá značení autoreaktivních CD8+ lymfocytů pomocí několika různě specifických molekul MHC I tetramerů současně a jejich identifikaci pomocí mnohobarevné průtokové cytometrie. Metoda je velmi senzitivní s minimální detekcí pozitivních buněk u zdravých kontrol. Velkou nevýhodou značení pomocí tetramerů je ale to, že její využití je možné jen u osob se shodným typem MHC.

Obecně lze říci, že ve studiích, které sledují reaktivitu buněk proti diabetogenním autoantigenům, je nutný pečlivý výběr skupin sledovaných osob, stimulačních antigenů i metodiky k identifikaci autoreaktivních buněk.

VI. Imunoregulační efekt monoterapie anti-thymocytárním glubulinem na diabetické myši kmene NOD (non-obese diabetic) (příloha VII.)

Experimentální i klinické studie ukazují, že autoimunitní proces, který způsobuje destrukci beta buněk ostrůvků, může být zastaven vhodnou imunitní intervencí. Pozitivní efekt ovlivnění časného vývoje autoimunitního diabetu byl popsán u anti-thymocytárního globulinu (ATG) (Simon, Parker et al. 2008), anti-lymfocytárního séra (Maki, Ichikawa et al. 1992) nebo protilátek proti CD3 (Chatenoud, Primo et al. 1997).

Naše studie sledovala vliv podávání mATG (anti-mouse ATG) NOD myším po manifestaci diabetu. Ačkoliv terapie mATG nebyla dostatečná k léčbě diabetu, zaznamenali jsme vliv na metabolizmus i na imunitní systém sledovaných myší. Terapie vedla jen k malému zvýšení počtu zachycených remisí oproti kontrolní skupině bez terapie. K remisi navíc došlo jen u jedinců, u kterých byla glykemie v době zahájení terapie nižší než 15,6 mmol/l. To potvrzuje významný vliv stavu jedinců v době zahájení terapie na její úspěšnost (Mottram, Murray-Segal et al. 2002; Keymeulen, Vandemeulebroucke et al. 2005). Většina studií, které popisují zlepšení nebo zabránění vzniku diabetu, byla prováděna na pre-diabetických myších. Ze 463 testovaných intervenčních postupů v diabetu bylo jen 23 zahájeno po nástupu hyperglykemií a jen u 16 z nich byl zaznamenán pozitivní efekt terapie (Shoda, Young et al. 2005).

Hlavní efekt terapie mATG jsme zaznamenali v populacích T-lymfocytů. Podávání mATG vedlo ke snížení poměru CD8+/CD4+ T-lymfocytů a to jak mezi splenocyty tak v populacích buněk pankreatických lymfatických uzlin. Ve studiích, které sledovali populace T-lymfocytů v periferní krvi, byl sice popsán pokles poměru CD4+/CD8+ (Saudek, Havrdova et al. 2004; Herold, Gitelman et al. 2005), ale tato neshoda může být dána funkčním rozdílem mezi populacemi T-lymfocytů v periferii a v orgánech lymfatického systému.

Terapie mATG dále vedla ke zvýšení populace regulačních lymfocytů FoxP3+ (Tregs) a to ve slezině i pankreatických lymfatických uzlinách. Podobný efekt byl popsán v experimentálních i klinických studiích s anti-lymfocytární léčbou (Lopez, Clarkson et al. 2006; Feng, Kajigaya et al. 2008). V naší studii však populace Tregs postupně klesala v čase od podání mATG. Lepšího efektu léčby by tak mohlo být dosaženo dlouhodobějším podáváním ATG, podobně jako ve studii Vergani et al. (Vergani, D'Addio et al. 2010).

Jako slibný směr intervenčních studií se v poslední době jeví použití více účinných látek v kombinaci. Mohou tak být ovlivněny různé větve autoreaktivního imunitního systému (Vergani, D'Addio et al. 2010) a současně indukována regenerace beta buněk v pankreatu (Fan, Kang et al. 2011). Naše studie na NOD myších v současné době také pokračuje sledováním vlivu kombinační léčby. Včasné zahájení intervence a vhodná kombinace terapií dává naději i pro klinické použití (Bach and Chatenoud 2011; Tooley, Waldron-Lynch et al. 2012). V kombinační terapii nyní testujeme efekt inhibitoru DPP-IV sitagliptin a molekuly s imunosupresivním účinkem deoxyspergualinu.

ZÁVĚRY

V předkládané disertační práci jsou shrnuty výsledky studií provedených v laboratoři Langerhansových ostrůvků Centra experimentální medicíny IKEM. Zabývali jsme se sledováním izolovaných Langerhansových ostrůvků, jejich zobrazením po transplantaci a imunologickými aspekty diabetu 1. typu. Všechny tyto studie byly součástí širších projektů, které jsou na pracovišti školitele systematicky řešeny. Shrnujeme hlavní dílčí výsledky těchto prací, jež se staly součástí předkládané disertační práce.

Prokázali jsme, že měření spotřeby kyslíku vysoce citlivou metodou oxymetrie dobře koreluje s ostatními metodami testování kvality ostrůvků. V porovnání s ostatními metodami se jedná o jednodušší, rychlejší a reprodukovatelnější metodu. Po doplnění standardizace u lidských ostrůvků bude oxymetrie využita pro testování kvality ostrůvků určených pro klinickou transplantaci.

Značení ostrůvků pomocí superparamagnetických nanočástic oxidů železa (SPIO) je závislé na době značení. Ostrůvky je možné pomocí magnetické rezonance (MRI) zobrazit již po jedné hodině značení. Železné partikule jsou nejintenzivněji akumulovány v makrofázích, ale s prodlužující se dobou značení jsou částice začleněny i do endokrinních buněk ostrůvků. Akumulace SPIO partikulí v cytoplazmatických váčcích neovlivňuje morfologii endokrinních buněk. Sekrece inzulínu a schopnost normalizovat glykémie po transplantaci také není značením ovlivněna. Pro in vivo zobrazení ostrůvků je zcela dostatečná doba značení 24 hodin. Publikovaná práce navázala na naše předchozí výsledky a nalezla již poměrně velkou odezvu ve vědecké veřejnosti.

Po transplantaci značených ostrůvků dochází k translokaci SPIO nanočástic z buněk ostrůvků. Partikule však dlouhodobě zůstávají v těsné blízkosti transplantovaných ostrůvků, většina v makrofázích příjemce. Při transplantaci pod pouzdro ledviny zůstávají partikule v místě transplantace i po odhojení ostrůvků a MRI obraz tak nevypovídá o přežívání ostrůvků. Oproti tomu při transplantaci do jater po odhojení ostrůvků postupně vymizí i makrofágy obsahující SPIO částice. Pomocí MRI by tak bylo možné včas diagnostikovat rejekci ostrůvků transplantovaných do jater. Práce přinesla nové poznatky potřebné k interpretaci MRI nálezů používaných k in vivo zobrazení ostrůvků.

Pomocí nové duální MRI kontrastní látky, která se skládá z perovskitu manganu a fluoresceinu, je možné značit izolované ostrůvky. Značení neovlivňuje kvalitu ostrůvků. Kontrastní látka umožňuje zobrazit ostrůvky pomocí fluorescenční mikroskopie a současně dává dostatečný MRI signál.

Pomocí víceparametrové analýzy sekrece cytokinů in vitro je možné sledovat charakter a intenzitu autoimunitní odpovědi pacientů s diabetem 1. typu nebo rizikových skupin. U dětí s vysokým rizikem vývoje diabetu má cytokinová odpověď charakter Th1 imunitní reakce. Izolované lymfocyty pacientů záhy po záchytu diabetu produkují spíše cytokiny prozánětlivé a odpovídající Th3 imunitní reakci.

Terapie autoimunitního diabetu u NOD myší pomocí mATG není dostatečná k vyléčení již rozvinutého diabetu, ale vede k nárůstu populace regulačních lymfocytů a k poměrnému snížení populace CD8+ lymfocytů. Lepších výsledků by pravděpodobně mohlo být dosaženo u pre-diabetického modelu nebo při dlouhodobější terapii.

Souhrnné výsledky této práce odpovídají původní anotaci a přispívají k hodnocení intervenčních přístupů v léčbě diabetu mellitu 1. typu.

LITERATURA

Adamec, M. and F. Saudek (2005). Transplantace slinivky břišní a diabetes mellitus. Praha, Karolinum.

Arbab, A. S., L. B. Wilson, et al. (2005). "A model of lysosomal metabolism of dextran coated superparamagnetic iron oxide (SPIO) nanoparticles: implications for cellular magnetic resonance imaging." NMR. Biomed. 18(6): 383-389.

Arif, S., T. I. Tree, et al. (2004). "Autoreactive T cell responses show proinflammatory polarization in diabetes but a regulatory phenotype in health." J Clin Invest 113(3): 451-463.

Bach, J. F. and L. Chatenoud (2011). "A historical view from thirty eventful years of immunotherapy in autoimmune diabetes." Semin Immunol 23(3): 174-181.

Barnett, B. P., J. Ruiz-Cabello, et al. (2011). "Use of perfluorocarbon nanoparticles for non-invasive multimodal cell tracking of human pancreatic islets." Contrast Media Mol Imaging 6(4): 251-259.

Barrett, J. C., D. G. Clayton, et al. (2009). "Genome-wide association study and meta-analysis find that over 40 loci affect risk of type 1 diabetes." Nat Genet 41(6): 703-707.

Bell, G. I., S. Horita, et al. (1984). "A polymorphic locus near the human insulin gene is associated with insulin-dependent diabetes mellitus." Diabetes 33(2): 176-183.

Bennet, W., C. G. Groth, et al. (2000). "Isolated human islets trigger an instant blood mediated inflammatory reaction: implications for intraportal islet transplantation as a treatment for patients with type 1 diabetes." Ups J Med Sci 105(2): 125-133.

Berney, T. and C. Toso (2006). "Monitoring of the islet graft." Diabetes Metab 32(5 Pt 2): 503-512.

Bonner-Weir, S., M. Taneja, et al. (2000). "In vitro cultivation of human islets from expanded ductal tissue." Proc Natl Acad Sci U S A 97(14): 7999-8004.

Borot, S., L. A. Crowe, et al. (2011). "Noninvasive imaging techniques in islet transplantation." Curr Diab Rep 11(5): 375-383.

Bottini, N., L. Musumeci, et al. (2004). "A functional variant of lymphoid tyrosine phosphatase is associated with type I diabetes." Nat Genet 36(4): 337-338.

Bougneres, P. F., P. Landais, et al. (1990). "Limited duration of remission of insulin dependency in children with recent overt type I diabetes treated with low-dose cyclosporin." Diabetes 39(10): 1264-1272.

Brissova, M., M. J. Fowler, et al. (2005). "Assessment of human pancreatic islet architecture and composition by laser scanning confocal microscopy." J Histochem Cytochem 53(9): 1087-1097.

Cernea, S. and K. C. Herold (2010). "Monitoring of antigen-specific CD8 T cells in patients with type 1 diabetes treated with antiCD3 monoclonal antibodies." Clin Immunol 134(2): 121-129.

Crowe, L. A., F. Ris, et al. (2011). "A novel method for quantitative monitoring of transplanted islets of langerhans by positive contrast magnetic resonance imaging." Am. J. Transplant. 11(6): 1158-1168.

Di Lorenzo, T. P., M. Peakman, et al. (2007). "Translational mini-review series on type 1 diabetes: Systematic analysis of T cell epitopes in autoimmune diabetes." Clin Exp Immunol 148(1): 1-16.

Dunn, M. F. (2005). "Zinc-ligand interactions modulate assembly and stability of the insulin hexamer -- a review." Biometals 18(4): 295-303.

Eich, T., O. Eriksson, et al. (2007). "Positron emission tomography: a real-time tool to quantify early islet engraftment in a preclinical large animal model." Transplantation 84(7): 893-898.

Eisenbarth, G. S. (1986). "Type I diabetes mellitus. A chronic autoimmune disease." N Engl J Med 314(21): 1360-1368.

Evgenov, N. V., Z. Medarova, et al. (2006). "In vivo imaging of islet transplantation." Nat. Med. 12(1): 144-148.

Evgenov, N. V., Z. Medarova, et al. (2006). "In vivo imaging of immune rejection in transplanted pancreatic islets." Diabetes 55(9): 2419-2428.

Evgenov, N. V., J. Pratt, et al. (2008). "Effects of glucose toxicity and islet purity on in vivo magnetic resonance imaging of transplanted pancreatic islets." Transplantation 85(8): 1091-1098.

Fan, R., Z. Kang, et al. (2011). "Exendin-4 improves blood glucose control in both young and aging normal non-diabetic mice, possible contribution of beta cell independent effects." PLoS One 6(5): e20443.

Feng, X., S. Kajigaya, et al. (2008). "Rabbit ATG but not horse ATG promotes expansion of functional CD4+CD25highFOXP3+ regulatory T cells in vitro." Blood 111(7): 3675-3683.

Fowler, M., J. Virostko, et al. (2005). "Assessment of pancreatic islet mass after islet transplantation using in vivo bioluminescence imaging." Transplantation 79(7): 768-776.

Herold, K. C., S. E. Gitelman, et al. (2005). "A single course of anti-CD3 monoclonal antibody hOKT3gamma1(Ala-Ala) results in improvement in C-peptide responses and clinical parameters for at least 2 years after onset of type 1 diabetes." Diabetes 54(6): 1763-1769.

Chatenoud, L., J. Primo, et al. (1997). "CD3 antibody-induced dominant self tolerance in overtly diabetic NOD mice." J Immunol 158(6): 2947-2954.

Chatenoud, L., E. Thervet, et al. (1994). "Anti-CD3 antibody induces long-term remission of overt autoimmunity in nonobese diabetic mice." Proc Natl Acad Sci U S A 91(1): 123-127.

Chen, X., X. Zhang, et al. (2006). "In vivo bioluminescence imaging of transplanted islets and early detection of graft rejection." Transplantation 81(10): 1421-1427.

Jiao, Y., Z. H. Peng, et al. (2008). "Assessment of islet graft survival using a 3.0-Tesla magnetic resonance scanner." Anat. Rec. (Hoboken) 291(12): 1684-1692.

Jirak, D., J. Kriz, et al. (2004). "MRI of transplanted pancreatic islets." Magn Reson Med 52(6): 1228-1233.

Jirak, D., J. Kriz, et al. (2009). "Monitoring the survival of islet transplants by MRI using a novel technique for their automated detection and quantification." MAGMA 22(4): 257-265.

Karlsson Faresjo, M. G., J. Ernerudh, et al. (2004). "Cytokine profile in children during the first 3 months after the diagnosis of type 1 diabetes." Scand J Immunol 59(5): 517-526.

Karlsson Faresjo, M. G. and J. Ludvigsson (2005). "Diminished Th1-like response to autoantigens in children with a high risk of developing type 1 diabetes." Scand J Immunol 61(2): 173-179.

Karlsson, M. G., S. S. Lawesson, et al. (2000). "Th1-like dominance in high-risk first-degree relatives of type I diabetic patients." Diabetologia 43(6): 742-749.

Keymeulen, B., E. Vandemeulebroucke, et al. (2005). "Insulin needs after CD3-antibody therapy in new-onset type 1 diabetes." N Engl J Med 352(25): 2598-2608.

Kim, H. S., Y. Choi, et al. (2009). "Magnetic resonance imaging and biological properties of pancreatic islets labeled with iron oxide nanoparticles." NMR Biomed 22(8): 852-856.

Kim, H. S., H. Kim, et al. (2010). "Evaluation of porcine pancreatic islets transplanted in the kidney capsules of diabetic mice using a clinically approved superparamagnetic iron oxide (SPIO) and a 1.5T MR scanner." Korean J. Radiol. 11(6): 673-682.

Kim, S. J., C. Nian, et al. (2009). "Dipeptidyl peptidase IV inhibition with MK0431 improves islet graft survival in diabetic NOD mice partially via T-cell modulation." Diabetes 58(3): 641-651.

Knip, M. and H. K. Akerblom (1999). "Environmental factors in the pathogenesis of type 1 diabetes mellitus." Exp Clin Endocrinol Diabetes 107 Suppl 3: S93-100.

Korc, M. (1993). Normal Function of the Endocrine Pancreas. The pancreas Biology, Pathology, and Disease V. L. W. Go, E. P. DiMagno, J. D. Gardneret al. New York, Raven Press, Ltd.: 751 - 758.

Kotkova, Z., J. Kotek, et al. (2010). "Cyclodextrin-based bimodal fluorescence/MRI contrast agents: an efficient approach to cellular imaging." Chemistry 16(33): 10094-10102.

Kriz, J., D. Jirak, et al. (2012). "Detection of pancreatic islet allograft impairment in advance of functional failure using magnetic resonance imaging." Transpl Int 25(2): 250-260.

Kriz, J., D. Jirak, et al. (2005). "Magnetic resonance imaging of pancreatic islets in tolerance and rejection." Transplantation 80(11): 1596-1603.

Kronenberg, D., R. R. Knight, et al. (2012). "Circulating, Preproinsulin Signal Peptide-Specific CD8 T Cells Restricted by the Susceptibility Molecule HLA-A24 Are Expanded at Onset of Type 1 Diabetes and Kill beta-Cells." Diabetes.

Lepore, A. C., P. Walczak, et al. (2006). "MR imaging of lineage-restricted neural precursors following transplantation into the adult spinal cord." Exp Neurol 201(1): 49-59.

Li, Y., T. Hansotia, et al. (2003). "Glucagon-like peptide-1 receptor signaling modulates beta cell apoptosis." J Biol Chem 278(1): 471-478.

Lopez, M., M. R. Clarkson, et al. (2006). "A novel mechanism of action for anti-thymocyte globulin: induction of CD4+CD25+Foxp3+ regulatory T cells." J Am Soc Nephrol 17(10): 2844-2853.

Lowe, C. E., J. D. Cooper, et al. (2007). "Large-scale genetic fine mapping and genotype-phenotype associations implicate polymorphism in the IL2RA region in type 1 diabetes." Nat Genet 39(9): 1074-1082.

Ludvigsson, J. (2009). "The role of immunomodulation therapy in autoimmune diabetes." J Diabetes Sci Technol 3(2): 320-330.

Lukinius, A., E. Wilander, et al. (1989). "Co-localization of islet amyloid polypeptide and insulin in the B cell secretory granules of the human pancreatic islets." Diabetologia 32(4): 240-244.

Maki, T., T. Ichikawa, et al. (1992). "Long-term abrogation of autoimmune diabetes in nonobese diabetic mice by immunotherapy with anti-lymphocyte serum." Proc Natl Acad Sci U S A 89(8): 3434-3438.

Malosio, M. L., A. Esposito, et al. (2009). "Improving the procedure for detection of intrahepatic transplanted islets by magnetic resonance imaging." Am J Transplant 9(10): 2372-2382.

Marzola, P., B. Longoni, et al. (2009). "In vivo visualization of transplanted pancreatic islets by MRI: comparison between in vivo, histological and electron microscopy findings." Contrast Media Mol Imaging 4(3): 135-142.

Medarova, Z., P. Vallabhajosyula, et al. (2009). "In vivo imaging of autologous islet grafts in the liver and under the kidney capsule in non-human primates." Transplantation 87(11): 1659-1666.

Michels, A. W. and M. von Herrath (2011). "2011 Update: antigen-specific therapy in type 1 diabetes." Curr Opin Endocrinol Diabetes Obes 18(4): 235-240.

Moller, D. E., A. Yokota, et al. (1989). "Tissue-specific expression of two alternatively spliced insulin receptor mRNAs in man." Mol Endocrinol 3(8): 1263-1269.

Mottram, P. L., L. J. Murray-Segal, et al. (2002). "Remission and pancreas isograft survival in recent onset diabetic NOD mice after treatment with low-dose anti-CD3 monoclonal antibodies." Transpl Immunol 10(1): 63-72.

Na, H. B. and T. Hyeon (2009). "Nanostructured T1 MRI contrast agents." Journal of Materials Chemistry 19(35): 6267-6273.

Na, H. B., I. C. Song, et al. (2009). "Inorganic Nanoparticles for MRI Contrast Agents." Advanced Materials 21(21): 2133-2148.

Nistico, L., R. Buzzetti, et al. (1996). "The CTLA-4 gene region of chromosome 2q33 is linked to, and associated with, type 1 diabetes. Belgian Diabetes Registry." Hum Mol Genet 5(7): 1075-1080.

Notkins, A. L. and A. Lernmark (2001). "Autoimmune type 1 diabetes: resolved and unresolved issues." J Clin Invest 108(9): 1247-1252.

Nussey, S. and S. Whitehead, Eds. (2001). Endocrinology: An Integrated Approach. Oxford, BIOS Scientific Publishers.

Oh, S. H., T. M. Muzzonigro, et al. (2004). "Adult bone marrow-derived cells trans-differentiating into insulin-producing cells for the treatment of type I diabetes." Lab Invest 84(5): 607-617.

Papas, K. K., C. K. Colton, et al. (2010). "Prediction of marginal mass required for successful islet transplantation." J Invest Surg 23(1): 28-34.

Papas, K. K., A. Pisania, et al. (2007). "A stirred microchamber for oxygen consumption rate measurements with pancreatic islets." Biotechnol Bioeng 98(5): 1071-1082.

Pawelczyk, E., E. K. Jordan, et al. (2009). "In vivo transfer of intracellular labels from locally implanted bone marrow stromal cells to resident tissue macrophages." PLoS One 4(8): e6712.

Pfleger, C., G. Meierhoff, et al. (2010). "Association of T-cell reactivity with beta-cell function in recent onset type 1 diabetes patients." J Autoimmun 34(2): 127-135.

Pihoker, C., L. K. Gilliam, et al. (2005). "Autoantibodies in diabetes." Diabetes 54 Suppl 2: S52-61.

Pileggi, A., C. Ricordi, et al. (2001). "Factors influencing Islet of Langerhans graft function and monitoring." Clin Chim Acta 310(1): 3-16.

Pociot, F. and M. F. McDermott (2002). "Genetics of type 1 diabetes mellitus." Genes Immun 3(5): 235-249.

Reichard, P., B. Y. Nilsson, et al. (1993). "The effect of long-term intensified insulin treatment on the development of microvascular complications of diabetes mellitus." N Engl J Med 329(5): 304-309.

Reijonen, H., R. Mallone, et al. (2004). "GAD65-specific CD4+ T-cells with high antigen avidity are prevalent in peripheral blood of patients with type 1 diabetes." Diabetes 53(8): 1987-1994.

Reijonen, H., E. J. Novak, et al. (2002). "Detection of GAD65-specific T-cells by major histocompatibility complex class II tetramers in type 1 diabetic patients and at-risk subjects." Diabetes 51(5): 1375-1382.

Reimer, P. and B. Tombach (1998). "Hepatic MRI with SPIO: detection and characterization of focal liver lesions." Eur Radiol 8(7): 1198-1204.

Renard (2004). "Implantable glucose sensors for diabetes monitoring." Minim Invasive Ther Allied Technol 13(2): 78-86.

Ricordi, C., E. H. Finke, et al. (1988). "Automated isolation of mouse pancreatic islets." Transplantation 46(3): 455-457.
Ricordi, C., D. W. Gray, et al. (1990). "Islet isolation assessment in man and large animals." Acta Diabetol Lat 27(3): 185-195.
Ris, F., M. Lepetit-Coiffe, et al. (2010). "Assessment of human islet labeling with clinical grade iron nanoparticles prior to transplantation for graft monitoring by MRI." Cell Transplant 19(12): 1573-1585.
Ryan, E. A., D. Bigam, et al. (2006). "Current indications for pancreas or islet transplant." Diabetes Obes Metab 8(1): 1-7.
Saudek, F. (2010). Transplantační léčba diabetu. Praha, Maxdorf.
Saudek, F., C. H. Brogren, et al. (2008). "Imaging the Beta-cell mass: why and how." Rev Diabet Stud 5(1): 6-12.
Saudek, F., T. Havrdova, et al. (2004). "Polyclonal anti-T-cell therapy for type 1 diabetes mellitus of recent onset." Rev Diabet Stud 1(2): 80-88.
Saudek, F., D. Jirak, et al. (2010). "Magnetic resonance imaging of pancreatic islets transplanted into the liver in humans." Transplantation 90(12): 1602-1606.
Segev, H., B. Fishman, et al. (2004). "Differentiation of human embryonic stem cells into insulin-producing clusters." Stem Cells 22(3): 265-274.
Seino, S. and G. I. Bell (1989). "Alternative splicing of human insulin receptor messenger RNA." Biochem Biophys Res Commun 159(1): 312-316.
Shapiro, A. M., J. R. Lakey, et al. (2000). "Islet transplantation in seven patients with type 1 diabetes mellitus using a glucocorticoid-free immunosuppressive regimen." N Engl J Med 343(4): 230-238.
Shepherd, P. R. and B. B. Kahn (1999). "Glucose transporters and insulin action--implications for insulin resistance and diabetes mellitus." N Engl J Med 341(4): 248-257.
Shoda, L. K., D. L. Young, et al. (2005). "A comprehensive review of interventions in the NOD mouse and implications for translation." Immunity 23(2): 115-126.
Simon, G., M. Parker, et al. (2008). "Murine antithymocyte globulin therapy alters disease progression in NOD mice by a time-dependent induction of immunoregulation." Diabetes 57(2): 405-414.
Smyth, D., J. D. Cooper, et al. (2004). "Replication of an association between the lymphoid tyrosine phosphatase locus (LYP/PTPN22) with type 1 diabetes, and evidence for its role as a general autoimmunity locus." Diabetes 53(11): 3020-3023.
Steiner, D. F. (1998). "The proprotein convertases." Curr Opin Chem Biol 2(1): 31-39.
Straub, S. G. and G. W. Sharp (2002). "Glucose-stimulated signaling pathways in biphasic insulin secretion." Diabetes Metab Res Rev 18(6): 451-463.
Sweet, I. R., M. Gilbert, et al. (2008). "Glucose-stimulated increment in oxygen consumption rate as a standardized test of human islet quality." Am J Transplant 8(1): 183-192.
Sweet, I. R., G. Khalil, et al. (2002). "Continuous measurement of oxygen consumption by pancreatic islets." Diabetes Technol Ther 4(5): 661-672.
Škrha, J. and et.al (2009). Diabetologie. Praha, Galén.
Tai, J. H., P. Foster, et al. (2006). "Imaging islets labeled with magnetic nanoparticles at 1.5 Tesla." Diabetes 55(11): 2931-2938.
Terrovitis, J., M. Stuber, et al. (2008). "Magnetic resonance imaging overestimates ferumoxide-labeled stem cell survival after transplantation in the heart." Circulation 117(12): 1555-1562.
Tooley, J. E., F. Waldron-Lynch, et al. (2012). "New and future immunomodulatory therapy in type 1 diabetes." Trends Mol Med 18(3): 173-181.
Toso, C., J. P. Vallee, et al. (2008). "Clinical magnetic resonance imaging of pancreatic islet grafts after iron nanoparticle labeling." Am J Transplant 8(3): 701-706.

Tufveson, G. (2009). "An experience of pancreas and islet transplantation in patients with end stage renal failure due to diabetes type I." Curr Opin Organ Transplant 14(1): 95-102.

Ústav zdravotnických informací a statistiky ČR (2011). "Aktuální informace č. 26/2011." http://www.uzis.cz/system/files/26_11.pdf.

van Belle, T. L., K. T. Coppieters, et al. (2011). "Type 1 diabetes: etiology, immunology, and therapeutic strategies." Physiol Rev 91(1): 79-118.

Velthuis, J. H., W. W. Unger, et al. (2010). "Simultaneous detection of circulating autoreactive CD8+ T-cells specific for different islet cell-associated epitopes using combinatorial MHC multimers." Diabetes 59(7): 1721-1730.

Vergani, A., F. D'Addio, et al. (2010). "A novel clinically relevant strategy to abrogate autoimmunity and regulate alloimmunity in NOD mice." Diabetes 59(9): 2253-2264.

Vogl, T. J., W. Schwarz, et al. (2003). "Preoperative evaluation of malignant liver tumors: comparison of unenhanced and SPIO (Resovist)-enhanced MR imaging with biphasic CTAP and intraoperative US." Eur Radiol 13(2): 262-272.

Wang, W., L. Upshaw, et al. (2005). "Increased oxygen consumption rates in response to high glucose detected by a novel oxygen biosensor system in non-human primate and human islets." J Endocrinol 185(3): 445-455.

Wang, Y. X., S. M. Hussain, et al. (2001). "Superparamagnetic iron oxide contrast agents: physicochemical characteristics and applications in MR imaging." Eur Radiol 11(11): 2319-2331.

Weinreb, J. C., L. Brateman, et al. (1985). "Chemical shift artifact in clinical magnetic resonance images at 0.35 T." AJR Am J Roentgenol 145(1): 183-185.

Weissleder, R., D. D. Stark, et al. (1989). "Superparamagnetic iron oxide: pharmacokinetics and toxicity." AJR Am J Roentgenol 152(1): 167-173.

Wenzlau, J. M., K. Juhl, et al. (2007). "The cation efflux transporter ZnT8 (Slc30A8) is a major autoantigen in human type 1 diabetes." Proc Natl Acad Sci U S A 104(43): 17040-17045.

Wierup, N., H. Svensson, et al. (2002). "The ghrelin cell: a novel developmentally regulated islet cell in the human pancreas." Regul Pept 107(1-3): 63-69.

PUBLIKAČNÍ AKTIVITY AUTORKY

PUBLIKACE

1. **Zacharovová, K**., Z. Berková, D. Jirák, V. Herynek, M. Vancová, E. Dovolilová, and F. Saudek, Processing of superparamagnetic iron contrast agent ferucarbotran in transplanted pancreatic islets. Contrast Media & Molecular Imaging, Manuskript přijat k publikaci 8. května 2012. IF 4,020 z roku 2010
2. Vargova, L., **K. Zacharovova**, E. Dovolilova, L. Vojtova, and F. Saudek, Immunoregulatory effect of anti-thymocyte globulin monotherapy on peripheral lymphoid tissues of non-obese diabetic mice. Transplant Proc, 2011. 43(9): p. 3277-80. IF 0,993 z roku 2010
3. Leontovyc, I., T. Koblas, L. Pektorova, **K. Zacharovova**, Z. Berkova, and F. Saudek, The Effect of Epigenetic Factors on Differentiation of Pancreatic Progenitor Cells Into Insulin-Producing Cells. Transplantation Proceedings, 2011. 43(9): p. 3212-3216. IF 0,993 z roku 2010
4. Kacenka, M., O. Kaman, J. Kotek, L. Falteisek, J. Cerny, D. Jirak, V. Herynek, **K. Zacharovova**, Z. Berkova, P. Jendelova, J. Kupcik, E. Pollert, P. Veverka, and I. Lukes, Dual imaging probes for magnetic resonance imaging and fluorescence microscopy based on perovskite manganite nanoparticles. Journal of Materials Chemistry, 2011. 21(1): p. 157-164. IF 5,101 z roku 2010
5. Alan, L., T. Spacek, J. Zelenka, J. Tauber, Z. Berkova, **K. Zacharovova**, F. Saudek, and P. Jezek, Assessment of Mitochondrial DNA as an Indicator of Islet Quality: An Example in Goto Kakizaki Rats. Transplantation Proceedings, 2011. 43(9): p. 3281-3284. IF 0,993 z roku 2010
6. Marada, T., **K. Zacharovova,** and F. Saudek, Perfluorocarbon Improves Post-Transplant Survival and Early Kidney Function following Prolonged Cold Ischemia. European Surgical Research, 2010. 44(3-4): p. 170-178. IF 1,214
7. Koblas, T., **K. Zacharovova**, Z. Berkova, P. Girman, and F. Saudek, An Acidic pH and Activation of Phosphoinositide 3-Kinase Stimulate Differentiation of Pancreatic Progenitors Into Insulin-Producing Cells. Transplantation Proceedings, 2010. 42(6): p. 2075-2080. IF 0,993

8. Koblas, T., **K. Zacharovova**, Z. Berkova, I. Leontovic, E. Dovolilova, L. Zamecnik, and F. Saudek, In Vivo Differentiation of Human Umbilical Cord Blood-Derived Cells into Insulin-Producing beta Cells. Folia Biologica, 2009. 55(6): p. 224-232. IF 0,924

9. Spacek, T., J. Santorova, **K. Zacharovova**, Z. Berkova, L. Hlavata, F. Saudek, and P. Jezek, Glucose-stimulated insulin secretion of insulinoma INS-1E cells is associated with elevation of both respiration and mitochondrial membrane potential. International Journal of Biochemistry & Cell Biology, 2008. 40(8): p. 1522-1535. IF 4,178

10. Koblas, T., L. Pektorova, **K. Zacharovova**, Z. Berkova, P. Girman, E. Dovolilova, L. Karasova, and F. Saudek, Differentiation of CD133-positive pancreatic cells into insulin-producing islet-like cell clusters. Transplantation Proceedings, 2008. 40(2): p. 415-418. IF 1,055

11. Berkova, Z., D. Jirak, **K. Zacharovova**, J. Kriz, A. Lodererova, P. Girman, T. Koblas, E. Dovolilova, M. Vancova, M. Hajek, and F. Saudek, Labeling of pancreatic islets with iron oxide nanoparticles for in vivo detection with magnetic resonance. Transplantation, 2008. 85(1): p. 155-159. IF 3,816

12. Vrabelova, Z., S. Kolouskova, K. Bohmova, M.K. Faresjo, Z. Sumnik, M. Pechova, M. Kverka, D. Chudoba, **K. Zacharovova**, G. Stadlerova, P. Pithova, M. Hladikova, and K. Stechova, Protein microarray analysis as a tool for monitoring cellular autoreactivity in type 1 diabetes patients and their relatives. Pediatric Diabetes, 2007. 8(5): p. 252-260. IF 2,314

13. Stechova, K., K. Bohmova, Z. Vrabelova, A. Sepa, G. Stadlerova, **K. Zacharovova**, and M. Faresjo, High T-helper-1 cytokines but low T-helper-3 cytokines, inflammatory cytokines and chemokines in children with high risk of developing type1 diabeties. Diabetes-Metabolism Research and Reviews, 2007. 23(6): p. 462-471. IF 3,087

14. Koblas, T., **K. Zacharovova**, Z. Berkova, M. Mindlova, P. Girman, E. Dovolilova, L. Karasova, and F. Saudek, Isolation and characterization of human CXCR4-positive pancreatic cells. Folia Biologica, 2007. 53(1): p. 13-22. IF 0,596

15. Vancova, M., **K. Zacharovova**, L. Grubhoffer, and J. Nebesarova, Ultrastructure and lectin characterization of granular salivary cells from Ixodes ricinus females. Journal of Parasitology, 2006. 92(3): p. 431-438. IF 1,300

16. **Zacharovova, K.**, Z. Berkova, T. Spacek, J. Kriz, E. Dovolilova, P. Girman, T. Koblas, P. Jezek, and F. Saudek, In vitro assessment of pancreatic islet vitality by oxymetry. Transplantation Proceedings, 2005. 37(8): p. 3454-3456. IF 0,799

17. Kriz, J., D. Jirak, P. Girman, Z. Berkova, **K. Zacharovova**, E. Honsova, A. Lodererova, M. Hajek, and F. Saudek, Magnetic resonance imaging of pancreatic islets in tolerance and rejection. Transplantation, 2005. 80(11): p. 1596-1603. IF 3,879

18. Koblas, T., P. Girman, Z. Berkova, D. Jirak, J. Kriz, E. Dovolilova, **K. Zacharovova**, M. Hajek, and F. Saudek, Magnetic resonance imaging of intrahepatically transplanted islets using paramagnetic beads. Transplantation Proceedings, 2005. 37(8): p. 3493-3495. IF 0,799

19. Berkova, Z., J. Kriz, P. Girman, **K. Zacharovova**, T. Koblas, E. Dovolilova, and F. Saudek, Vitality of pancreatic islets labeled for magnetic resonance imaging with iron particles. Transplantation Proceedings, 2005. 37(8): p. 3496-3498. IF 0,799

PREZENTACE NA KONGRESECH A SYMPOZIÍCH

1. Berková Z., **Zacharovová K.**, Špaček T., Kříž J., Girman P., Koblas T., Dovolilová E., Saudek F.: In vitro assessment of pancreatic islets vitality: relevance of cellular oxymetry; 24th workshop of the AIDPIT study group, Igls – Innsbruck, Austria, 23.-25.1.2005. Poster
2. Kříž J., Jirák D., Honsová E., Girman P., Berková Z., Lodererová A., Koblas T., **Zacharovová K.**, Hájek M., Saudek F. Magnetic resonance imaging pancreatic islets rejection; 24th workshop of the AIDPIT study group, Igls – Innsbruck, Austria, 23.-25.1. 2005. Přednáška s abstraktem mezinárodní
3. Štechová, K., Vrábelová, Z., Šumník, Z., Dovolilová, E., Chudoba, D., Cinek, O., Piťhová, P., Janeček, L., **Zacharovová, K.**, Saudek, F., Vavřinec, J.: Postavení buněčných testů v diagnostice časných stádií inzulitidy. 41.diabetologické dny. Luhačovice, CZ, 21.-23.4.2005. In: Diabetologie Metabolismus Endokrinologie Výživa. 2005, roč. 8, č. suppl. 1, s. 47-48. Přednáška s abstraktem domácí
4. Berková Z., Špaček T., Kříž J., Dovolilová E., Girman P., **Zacharovová K.**, Koblas T., Ježek P., Saudek F.: In vitro assessment of pancreatic islets vitality by oxymetry; 10th world congress of IPITA, Geneva, Switzerland, 4.-7.5.2005. Poster
5. Berková Z., **Zacharovová K.**, Kříž J., Jirák D., Girman P., Dovolilová E., Koblas T., Hájek M., Saudek F.: The impact of islet labeling with superparamagnetic nanoparticles for magnetic resonance imaging on islet vitality; 10th world congress of IPITA, Geneva, Switzerland, 4.-7.5.2005. Poster
6. Kříž J., Jirák D., Honsová E., Girman P., Berková Z., Lodererová A., Koblas T., **Zacharovová K.**, Hájek M., Saudek F.: Magnetic resonance imaging of transplanted pancreatic islets in tolerance and rejection; 10th world congress of IPITA, Geneva, Switzerland, 4.-7.5.2005. Poster
7. Girman P., Berková Z., Jirák D., Kříž J., Dovolilová E., Koblas T., **Zacharovová K.**, Hájek M., Saudek F.: Magnetic resonance imaging of intrahepatically transplanted islets using superparamagnetic beads; 10th world congress of IPITA, Geneva, Switzerland, 4.-7.5.2005. Přednáška s abstraktem mezinárodní
8. Havrdová, T., **Zacharovová, K**. 10th World Congress of the International Pancreas and Islet Transplant Association 4.-7. květen 2005, Ženeva. Journal of Diabetes and its Complications (CZ), 2005, roč. 3, č. 3, s. 184-185. Dopis.
9. Štechová K., Karlsson Faresjo M., Kolousková S., Böhmová K., Vrábelová Z., Kverka M., Cinek O., Chudoba D., Pechová M., **Zacharovová K.**, Saudek F., Vavřinec J.: Study of complex cytokine response after specific diabetogenic stimulation by array techniques. The 8th Meeting of the Immunology of Diabetes Society, 6.-9.10. 2005. In: Endocrine journal 2005, vol. 52, p.89. Poster

10. Berková Z., Jirak D., Kříž J., Girman P., Dovolilová E., **Zacharovová K.**, Koblas T., Hájek M., Saudek F.: The effect of islet labeling with SPIO particles on islet function in vivo; 25th workshop of the AIDPIT study group, Pisa, Italy, 5.-7.2.2006 Poster

11. **Zacharovová K.**, Berková Z., Koblas T., Kříž J., Girman P., Dovolilová E., Vrábelová Z., Böhmová K., Kverka M., Štechová K., Saudek F.: Cytokine protein array as a tool for monitoring of cellular response in autoimmune type 1 diabetes; 25th workshop of the AIDPIT study group, Pisa, Italy, 5.-7.2.2006. Poster

12. Saudek F., Havrdová T., Bouček P. , Novota P., Karasova L., Lanska V., **Zacharovova K.**: Polyclonal anti-T-cell therapy in type 1 diabetes of recent onset. 7th international konference on new trends in immunosuppression and immunotherapy, Berlin, German, February 16-19, 2006. Přednáška s abstraktem mezinárodní

13. Kříž J., Jirák D., Girman P., Berková Z., **Zacharovová K.**, Koblas T., Hájek M., Saudek F.: Diagnosis of islet rejection using magnetic resonance – preliminary results; 3rd workshop of Imaging the pancreatic beta cell in health and disease, Washington, USA, 24.-25.4. 2006. Poster

14. Girman P., Kříž J., Jirák D., Berková Z., **Zacharovová K.**, Koblas T., Hájek M., Saudek F.: The role of paramagnetic beads in islet imaging; 3rd workshop of Imaging the pancreatic beta cell in health and disease, Washington, USA, 24.-25.4. 2006. Poster

15. Štechová K., Koloušková S., Böhmová K., Štádlerová G., Šumník Z., Vrábelová Z., **Zacharovová K.**, Chudoba D., Cinek O., Piťhová P., Saudek F., Vavřinec J., Faresjo M.: Nové možnosti predikce diabetu 1. typu. 7. český pediatrický kongres. Praha, Česká Republika, 8.-11.6.2006 In. Časopis české a slovenské pediatrické společnosti 2006, vol. 61, p.320. Poster

16. **K Zacharovová**, K Štechová, K Böhmová, Z Vrábelová, G Štádlerová, S Koloušková, Z Šumník, O Cinek, M Pechová, D Chudoba, P Piťhová, M Kverka, E Dovolilová, F Saudek: Buněčné testy v predikci a prevenci 1. typu diabetu se zaměřením na proteinovou microarray. P-93. XXIII. Sjezd českých a slovenských alergologů a klinických imunologů, XI. Kongres českých a slovenských imunologů, Hradec Králové, 25. – 28. 10. 2006. In *Alergie, Supplementum,* 2/2006. Poster

17. **Zacharovova K**, Berkova Z, Koblas T, Girman P, Mindlova M, Kriz J, Dovolilova E, Vancova M, Nebesarova J, Saudek F: Ultrastrukturní Analýza značení potkaních Langerhansových ostrůvků superparamagnetickými partikulemi. I. československý transplantační kongres, Brno, 16. – 18. 11. 2006. U 31 Přednáška

18. Saudek F, Girman P, Kříž J, Peregrin J, Bouček P, Kožnarová R, Berková Z, **Zacharovová K**, Koblas T, Dovolilová E, Číhalová E, Adamec M: První klinická transplantace pankreatických ostrůvků v ČR. I. československý transplantační kongres, Brno, 16. – 18. 11. 2006. U 13 Přednáška

19. Kříž J, Jirák D, Berková Z, Girman P, Dovolilová E, **Zacharovová K**, Koblas T, Honsová E, Lodererová A, Hájek M, Saudek F: Časná detekce rejekce allaogenních ostrůvků

pomocí magnetické rezonance. I. československý transplantační kongres, Brno, 16. – 18. 11. 2006. U 29. Přednáška

20. Berková Z, Jirák D, **Zacharovová K**, Kříž J, Girman P, Dovolilová E, Koblas T, Honsová E, Hájek M, Saudek F: Dynamika značení Langerhansových ostrůvků nanopartikulemi železa. I. československý transplantační kongres, Brno, 16. – 18. 11. 2006. P6. Poster

21. Koblas T, **Zacharovová K**, Girman P, Berková Z, Mindlová M, Kříž J, Dovolilová E, Saudek F: Izolace a charakteristika CXCR-4 pozitivních pankreatických buněk. I. československý transplantační kongres, Brno, 16. – 18. 11. 2006. P7. Poster

22. **K Zacharovova,** K Stechova, S Kolouskova, K Böhmova, G Stadlerova, Z Sumnik, Z Vrabelova, D Chudoba, P Pithova, F Saudek: Cytokine and Chemokine spectrum of Periferal blood Mononuclear Cells in Type 1 Diabetes (T1D) Patients and Their Relatives. 5th International congress on Autoimmunity, Sorrento, Italy, November 29 – December 3, 2006. In Autoimmunity Reviews, p 368. Poster

23. **K Zacharovova**, Z Berkova, T Koblas, L Pektorova, M Mindlova, P Girman, J Kriz, E Dovolilova, M Vancova, J Nebesarova, F Saudek**:** Ultrastructural analysis of islets labelling with superparamagnetic particles. 26th Workshop of the AIDPIT Study group, 1st European Diabetes Technology and Transplantation Meeting, Montpellier, France, February 4-6, 2007. PS-23 Poster

24. Z Berkova, D Jirak, A Lodererova, **K Zacharovova**, J Kriz, P Girman, E Dovolilova, T Koblas, E Honsova, M Hajek, F Saudek:The Mechanism of Islet Labeling with Iron Nanoparticules for Magnetic Resonance Imaging. 26th Workshop of the AIDPIT Study group, 1st European Diabetes Technology and Transplantation Meeting, Montpellier, France, February 4-6, 2007. PS-26 Poster

25. **Zacharovova K**, Berkova Z, Girman P, Koblas T, Pektorova L, Dovolilova E, Vancova M, Nebesarova J, Saudek F: Transmission electron microscopy of islets labeled with iron nanoparticles for magnetis resonance imaging. The Joint Meeting of IXA, IPITA and CTS, Minneapolis, USA, September 15 – 20 2007. PL1217. In *Xenotransplantation*, Vol 14, N. 5, 2007. Poster

26. Berkova Z, Jirak D, **Zacharovova K**, Lodererova A, Girman P, Dovolilova E, Koblas T, Hajek M, Saudek F: Labeling of pancreatic ilstes with iron nanoparticles for magnetic resonance imaging. The Joint Meeting of IXA, IPITA and CTS, Minneapolis, USA, September 15 – 20 2007. PL1216. In *Xenotransplantation*, Vol 14, N. 5, 2007. Poster

27. Koblas T, **Zacharovova K**, Pektorova L, Berkova Z, Girman P, Dovolilova E, Saudek F: Differentiation of CD133 positive pancreatic cells into insuliln producing islet-like cell clusters. The Joint Meeting of IXA, IPITA and CTS, Minneapolis, USA, September 15 – 20 2007. PM1312. In *Xenotransplantation*, Vol 14, N. 5, 2007. Poster

28. Girman P, Berkova Z, Dovolilova E, **Zacharovova K**, Koblas T, Saudek F: Computer-assisted method for counting of non-purified pancreatic islets. The Joint Meeting of

IXA, IPITA and CTS, Minneapolis, USA, September 15 – 20 2007. PL1203. In *Xenotransplantation*, Vol 14, N. 5, 2007. Poster

29. **Zacharovova K**, Berkova Z, Herynek V, Girman P, Koblas T, Pektorova L, Dovolilova E, Vancova M, Nebesarova J, Saudek F: Ultrastructural localization of magnetic resonance contrast iron nanoparticles in transplanted rat pancreatic islet. 27th Workshop of the AIDPIT Study group, 2nd European Diabetes Technology and Transplantation Meeting, Innsbruck-Igls, Austria, January 27 – 29, 2008. IE 12 Poster

30. Pektorova L, Koblas T, **Zacharovova K**, Berkova Z, Girman P, Dovolilova E, Saudek F: Differentiation of human pancreatic non-endocrine cells into insulin producing islet-like cell clusters. 27th Workshop of the AIDPIT Study group, 2nd European Diabetes Technology and Transplantation Meeting, Innsbruck-Igls, Austria, January 27 – 29, 2008. OP-20 přednáška

31. Girman P, Mindlova M, Berkova Z, Koblas T, **Zacharovova K,** Dovolilova E, Pektorova L, Vavrova E, Bobek V, Koznarova R, Lipar K, Adamec M, Saudek F: Islet and pancreas transplantation alone: one centre short-term results. 27th Workshop of the AIDPIT Study group, 2nd European Diabetes Technology and Transplantation Meeting, Innsbruck-Igls, Austria, January 27 – 29, 2008. OP-13 přednáška

32. **Zacharovová K**, Berková Z, Herynek V, Girman P, Koblas T, Pektorová L, Vávrová E, Mindlová M, Dovolilová E, Bobek V, Vancová M, Nebesáøová J, Saudek F: Ultrastrukturní sledování transplantovaných Langerhansových ostrůvků značených paramagnetickými partikulemi. 2. Československý transplantační kongres, Starý Smokovec, Slovensko, 10.-12.9. 2008. P.46 Poster

33. Dovolilová E, Girman P, Berková Z, **Zacharovová K**, Koblas T, Pektorová L, Mindlová M, Vávrová E, Bobek V, Saudek F: Transplantace Langerhansových ostrůvků v IKEM - technika izolace. 2. Československý transplantační kongres, Starý Smokovec, Slovensko, 10.-12.9. 2008. S.7 přednáška

34. Bobek V, Girman P, **Zacharovová K**, Koblas T, Berková Z, Pektorová L, Dovolilová E, Vávrová E, Mindlová M, Saudek F: Transplantace Langerhansových ostrůvků.
2. Československý transplantační kongres, Starý Smokovec, Slovensko, 10.-12.9. 2008. S.8 přednáška

35. Marada T, **Zacharovová K**, Vávrová E, Saudek F: Konzervace ledviny pomocí TLM (Two Layer Method) v experimentu na laboratorních potkanech. 2. Československý transplantační kongres, Starý Smokovec, Slovensko, 10.-12.9. 2008. L.56 přednáška

36. Pektorová L, Girman P, Mindlová M, Berková Z, **Zacharovová K**, Bobek V, Vávrová E, Koblas T, Dovolilová E, Saudek F: Klinický program transplantací Langerhansových ostrůvků v IKEM. 2. Československý transplantační kongres, Starý Smokovec, Slovensko, 10.-12.9. 2008. L.65 přednáška

37. Koblas T, **Zacharovová K**, Girman P, Berková Z, Pektorová L, Mindlová M, Dovolilová E, Saudek F: Diferenciace pankreatických duktálních progenitorů na inzulín

produkující beta buňky. . 2. Československý transplantační kongres, Starý Smokovec, Slovensko, 10.-12.9. 2008. L.66 přednáška

38. **Zacharovova K**, Berkova Z, Herynek V, Girman P, Koblas T, Pektorova L, Dovolilova E, Vancova M, Nebesarova J, Saudek F: Magnetic iron nanoparticles in rat pancreatic islets: post-transplantation tracking. 44th Annual Meeting of the European Association for the Study of Diabetes, Roma, Italy, September 7 – 11, 2008. 604 Poster

39. Girman P, Mindlova M, Berkova Z, Koblas T, **Zacharovova K**, Pektorova L, Dovolilova E, Vavrova E, Koznarova R, Bobek V, Adamec M, Lipar K, Saudek F: Islet and pancreas transplantation alone: one center short-term results. 44th Annual Meeting of the European Association for the Study of Diabetes, Roma, Italy, September 7 – 11, 2008. 596 Poster

40. Saudek F, Havrdova T, Boucek P, Hirsch HH, **Zacharovova K**, Lanska V: Polyclonal anti-T-lymphocyte globulin preserves C-peptide production in type 1 diabetes of recent onset. 44th Annual Meeting of the European Association for the Study of Diabetes, Roma, Italy, September 7 – 11, 2008. 577 Poster

41. Koblas T, Pektorova L, **Zacharovova K**, Berkova Z, Girman P, Dovolilova E, Saudek F: Differentiation of pancreatic non-endocrine progenitor cells into the insulin producing cells. 28th Workshop of the AIDPIT Study Group, 3rd European Diabetes Technology and Transplantation Meeting (EuDTT), Igls / Austria, Jan 25-27, 2009. IE 14 přednáška

42. **Zacharovova K**, Berkova Z, Herynek V, Girman P, Koblas T, Pektorova L, Dovolilova E, Vancova M, Nebesarova J, SaudekF: Post-transplantation processing of magnetic iron nanoparticles in rat pancreatic islets. 28th Workshop of the AIDPIT Study Group, 3rd European Diabetes Technology and Transplantation Meeting (EuDTT), Igls / Austria, Jan 25-27, 2009. IE 17 poster

43. Z Berková, **K Zacharovová**, V Herynek, I Lukeš, M Hájek, F Saudek: New Gd contrast agents for islet labeling. 28th Workshop of the AIDPIT Study Group, 3rd European Diabetes Technology and Transplantation Meeting (EuDTT), Igls / Austria, Jan 25-27, 2009. IE 20 poster

44. T Koblas, L Pektorova, **K Zacharovova**, Z Berkova, P Girman, E Dovolilova, F Saudek: Differentiation of pancreatic progenitors into the insulin producing cells. BetaCellTherapy Fourth Training Course, Ghent, Belgium, 25-27 May 2009. poster

45. **K Zacharovova**, Z Berkova, V Herynek, P Girman, T Koblas, L Pektorova, M Mindlova, E Vavrova, M Vancova, J Nebesarova, E Dovololova, V Bobek, F Saudek: Post-transplant processing of superparamagnetic iron nanoparticles used for islet labeling and MR detection. 2009 IPITA-IXA Joint Meeting, Venice, Italy, 12-18 October 2009, P-15.10 poster.

46. Z Berkova, **K Zacharovova**, D Jirak, V Herynek, I Lukes, M Hajek, F Saudek: Labeling of the pancreatic islets with Gd contrast agent for magnetic resonance imaging and fluorescence microscopy. 2009 IPITA-IXA Joint Meeting, Venice, Italy, 12-18 October 2009, O -8.10 přednáška.

47. T. Koblas, **K. Zacharovova**, Z. Berkova, P. Girman, J. Kriz, F. Saudek: An acid pH and stimulation of phosphoinoisitide 3-kinase stimulate the differentiation of pancreatic progenitors into the insulin producing cells. 2009 IPITA-IXA Joint Meeting, Venice, Italy, 12-18 October 2009, O-10.9 přednáška.

48. **K Zacharovová**, Z Berková, E Dovolilová, V Herynek, F Saudek: Transplantation of double labeled rat islets – superparamagnetic iron (SPIO) nanoparticles in combination with CellTracker™ Green CMFDA. 29th Workshop of the AIDPIT Study Group. Innsbruck-Igls, Austria, January 24-26, 2010. G poster.

49. Z Berkova, **K Zacharovova**, D Jirak, I Lukes, M Hajek, F Saudek: New gadolinium based contrast agent designed for magnetic resonance imaging and fluorescence microscopy. 29th Workshop of the AIDPIT Study Group. Innsbruck-Igls, Austria, January 24-26, 2010. 14 přednáška.

50. T Koblas, I Leontovyc, **K Zacharovova**, Z Berkova, P Girman, E Dovolilova, F Saudek: Leukaemia inhibitory factor and noggin stimulate differentiation of pancreatic non-endocrine cells into insulin producing cells. 29th Workshop of the AIDPIT Study Group. Innsbruck-Igls, Austria, January 24-26, 2010. 24 přednáška.

51. Dovolilová E., Bobek V., Girman P., Berková Z., **Zacharovová K**., Koblas T.[1], Pektorová L., Mindlová M., Vávrová E., Saudek F.: Human pancreatic islets isolation and transplantation at the Institute for Clinical and Experimental Medicine (IKEM). 29th Workshop of the AIDPIT Study Group. Innsbruck-Igls, Austria, January 24-26, 2010. B poster.

52. Saudek F., Jirák D., Girman P., Herynek V., Dezortová M., Peregrin J., Berkova Z., **Zacharovová K.**, Hájek M.: Klinické zobrazení transplantovaných langerhansových ostrůvků (LO) u člověka pomocí magnetické rezonance (MR). III. Česko-Slovenský transplantační kongres, Špindlerův Mlýn, 16.-18.9. 2010. O-6 přednáška.

53. Koblas T., Leontovyč I., **Zacharovová K.,** Girman P., Berková Z., Kříž J., Dovolilová E., Saudek F.: Příprava izulín produkujících buněk diferenciací pankreatických duktálních progenitorů: vliv demetylace DNA. III. Česko-Slovenský transplantační kongres, Špindlerův Mlýn, 16.-18.9. 2010. O-33 přednáška.

53. Dovolilová E., Girman P., Kříž J., Berková Z., **Zacharovová K.**, Koblas T., Pektorová L., Mindlová M., Vávrová E., Bobek V., Habart D., Saudek F.: Transplantace langerhansových ostrůvků v IKEM. III. Česko-Slovenský transplantační kongres, Špindlerův Mlýn, 16.-18.9. 2010. SO-23 přednáška.

54. Berková Z., Jirák D., **Zacharovová K.**, Dovolilová E., Hájek M., Saudek F.: Nové kontrastní látky pro sledování transplantovaných langerhansových ostrůvků pomocí magnetické rezonance a fluorescenční mikroskopie. III. Česko-Slovenský transplantační kongres, Špindlerův Mlýn, 16.-18.9. 2010. P-2 poster.

55. **Zacharovová K.**, Berková Z., Dovolilová E., Jirák D., Saudek F.: Sledování superparamagnetických částic v průběhu rejekce značených potkaních pankreatických

ostrůvků. III. Česko-Slovenský transplantační kongres, Špindlerův Mlýn, 16.-18.9. 2010.P-34 poster.

56. Tomas Koblas, Ivan Leontovyc, **Klara Zacharovova**, Zuzana Berkova, David Habart, Jan Kriz, Peter Girman, Eva Dovolilova, Frantisek Saudek: Epigenetic regulation of pancreatic progenitor cells differentiation into insulin producing cells. 1st AIDPIT/EPITA Joint Winter Symposium. Innsbruck-Igls, Austria, 23th – 25th January 2011. 21 přednáška.

57. **Klara Zacharovova**, Zuzana Berkova, Eva Dovolilová, Daniel Jirak, Frantisek Saudek: Rejection of islets labelled with supramagnetic nanoparticles (SPIO). 1st AIDPIT/EPITA Joint Winter Symposium. Innsbruck-Igls, Austria, 23th – 25th January 2011. 27 přednáška.

58. Eva Dovolilova, Peter Girman, Jan Kriz, Kvetoslav Lipar, Matej Kocik, **Klara Zacharovova**, Zuzana Berkova, Tomas Koblas, Petr Boucek, Eugenie Cihalova, Vit Bobek, Frantisek Saudek: Pancreas and pancreatic islets transplant activity at the Institute for Clinical and Experimental Medicine (IKEM). 1st AIDPIT/EPITA Joint Winter Symposium. Innsbruck-Igls, Austria, 23th – 25th January 2011. IC6 poster.

59. Zuzana Berkova, Daniel Jirak, **Klara Zacharovova**, Eva Dovolilova, Ivan Lukes, Milan Hajek, Frantisek Saudek: Bimodal contrast agent designed for magnetic resonance imaging and fluorescence microscopy. 1st AIDPIT/EPITA Joint Winter Symposium. Innsbruck-Igls, Austria, 23th – 25th January 2011. IC7 poster.

60. Lenka Pektorova, **Klara Zacharovova**, Eva Dovolilova, Lenka Vojtova, Frantisek Saudek : Anti-Thymocyte Globulin Therapy in a Model of Type 1 Diabetes in NOD Mice. 1st AIDPIT/EPITA Joint Winter Symposium. Innsbruck-Igls, Austria, 23th – 25th January 2011. IE1 poster.

61. Jan Kriz, Daniel Jirak, Peter Girman, **Klara Zacharovova**, Greg Vilk, Milan Hajek, Frantisek Saudek: Vascularisation of an artificial cavity for pancreastic islet transplantataion assessed by magnetic resonance imaging. 1st AIDPIT/EPITA Joint Winter Symposium. Innsbruck-Igls, Austria, 23th – 25th January 2011. IE11 poster.

62. T. Koblas, I. Leontovyc, **K. Zacharovova**, Z. Berkova, P. Girman, J. Kriz, F. Saudek: The effect of epigenetic factors on differentiation of pancreatic progenitor cells into insulin producing cells. 13th World Congress of IPITA, Prague, Czech Republic, 1-4 June 2011. O-026 přednáška.

63. J. Kriz, D. Jirak, P. Girman, **K. Zacharovova**, G. Vilk, M. Hajek, F. Saudek: Dynamic contrast enhanced magnetic resonance imaging of blood supply into the artifi cial cavity for islet transplantation. 13th World Congress of IPITA, Prague, Czech Republic, 1-4 June 2011. O-078 přednáška.

64. E. Dovolilova, P. Girman, J. Kriz, Z. Berkova, **K. Zacharovova**, T. Koblas, L. Pektorova, M. Mindlova, E. Vavrova, I. Leontovyc, D. Habart, E. Cihalova, F. Saudek: Human pancreatic islet isolation and transplantation at the Institute for Clinical and

Experimental Medicine. 13th World Congress of IPITA, Prague, Czech Republic, 1-4 June 2011. P-174 poster.

65. **K. Zacharovova**, L. Pektorova, I. Leontovyc, E. Dovolilova, L. Vojtova, F. Saudek: Low effect of anti-thymocyte globuline monotherapy in non-obese diabetic (NOD) mice treated after the onset of overt diabetes. 13th World Congress of IPITA, Prague, Czech Republic, 1-4 June 2011. P-232 poster.

66. **K. Zacharovova**, Z. Berkova, E. Dovolilova, D. Jirak, F. Saudek: Detection of rat islets labeled with superparamagnetic iron oxide nanoparticles (SPIO) during rejection. 13th World Congress of IPITA, Prague, Czech Republic, 1-4 June 2011. P-283 poster.

67. P. Jezek, L. Plecitá, A. Dlasková, T. Špaček, J. Šantörová, L. Alán, Z. Berková, **K. Zacharovová**, F. Saudek: Super-resolution 3D imaging of mitochondrial network: a new tool for in vitro evaluation of beta-cellmorphology and function. 13th World Congress of IPITA, Prague, Czech Republic, 1-4 June 2011. P-288 poster.

68. Z. Berkova, D. Jirak, **K. Zacharovova**, E. Dovolilova, I. Lukes, M. Hajek, F. Saudek: Comparison of two new effi cient dual MRI/fl uorescence probes for pancreatic islet labeling. 13th World Congress of IPITA, Prague, Czech Republic, 1-4 June 2011. P-289 poster.

69. J. Kriz, D. Jirak, P. Girman, E. Vodraskova, **K. Zacharovova**, E. Dovolilova, M. Hajek, F. Saudek: The effect of mesenchymal stem cells (MSC) on blood supply into artificial cavity can be assessed by DCI MRI. 2nd Joint AIDPIT/EPITA Winter Symposium. Innsbruck-Igls, Austria, 29th – 31st January 2012. PP-16 poster.

70. Z. Berkova, D. Jirak, **K. Zacharovova**, I. Lukes, M. Hajek, F. Saudek: Comparison of magnetic resonance contrast agents used for pancreatic islet labeling. 2nd Joint AIDPIT/EPITA Winter Symposium. Innsbruck-Igls, Austria, 29th – 31st January 2012. PP-24 poster.

71. T. Koblas, I. Leontovyc, **K. Zacharovova**, Z. Berkova, P. Girman, J. Kriz, F. Saudek: Leukemia inhibitory factor stimulates differentiation of non-endocrine pancreatic cels into insulin-producing celss. 2nd Joint AIDPIT/EPITA Winter Symposium. Innsbruck-Igls, Austria, 29th – 31st January 2012. PP-28 poster.

72. **K. Zacharovova**, L. Vargova, I. Leontovyc, E. Dovolilova, L. Vojtova, Z. Cimburek, F. Saudek: Monotherapy with murine ATG or sitagliptin after the onset of diabetes in NOD mice. 2nd Joint AIDPIT/EPITA Winter Symposium. Innsbruck-Igls, Austria, 29th – 31st January 2012. PP-38 poster.

PŘÍLOHY

PŘÍLOHA I.

In vitro assessment of pancreatic islet vitality by oxymetry

K. Zacharovová, Z. Berková, T. Špaček, J. Kříž, E. Dovolilová, P. Girman, T. Koblas, P. Ježek, and F. Saudek

Transplantation Proceedings, 2005. 37(8): p. 3454-6.

In Vitro Assessment of Pancreatic Islet Vitality by Oxymetry

K. Zacharovova, Z. Berkova, T. Spacek, J. Kriz, E. Dovolilova, P. Girman, T. Koblas, P. Jezek, and F. Saudek

ABSTRACT

In order to assess the quality of freshly isolated and cultivated pancreatic islets designed for experimental transplantation in rats we combined the vitality staining test, in vitro measurement of insulin secretion capacity, and assessment of islet respiration. Oxygen consumption was measured using the respirometer Oxygraph 2K equipped with polarographic oxygen sensors. The results of oxymetry demonstrated a linear correlation between islet number and oxygen consumption. Respiration per unit of viable islet tissue was constant. Oxygen consumption tests were in good correlation with the results of insulin release assays, with a correlation coefficient of 0.82. We found no significant differences in all three vitality-testing methods performed with fresh and 24-hour cultivated islets ($P > .05$). We conclude that polarographic oxymetry provides a fast and easy evaluation test of islet quality. After appropriate standardization, the oxymetric technique can be used for routine clinical pretransplant islet quality testing. In addition, cell membrane integrity and mitochondrial function could be assessed after addition of specific respiration inhibitors or stimulators.

ISLET VIABILITY can be affected by many factors, including events occurring during the period of cold ischemia prior to islet isolation, the isolation process itself, and the period of storage before transplantation. Therefore, evaluation of islet viability before transplantation is essential. Several methods are routinely used with some limitations. Membrane integrity tests like fluorescence dye staining[1] or trypan blue exclusion test are rapid but not easily quantifiable. Determination of islet insulin secretion capacity using static incubation[2,3] or dynamic perifusion[4] is important. However, it takes several hours or days to obtain the results. Recently, changes in mitochondrial activities of single cells and tissue samples have been successfully applied as indicators of vitality and functional quality.[5–7] The aim of the present study was to examine the utility of oxymetric evaluation of islet cell function and to compare the results with other routine vitality tests.

MATERIALS AND METHODS

Pancreatic islets were isolated from pancreata of adult male Wistar rats after intraductal collagenase injection, stationary digestion, and purification in a discontinuous Ficoll gradient as previously described.[8] For in vitro quality assessment, three different methods were used and two experimental groups of islets were tested: fresh islets immediately after isolation and islets after a 24-hour culture period.

For culture, the islets were placed in the CMRL-1066 medium (PAN Biotech GmbH, Germany) supplemented with 10% fetal calf serum, 50 mmol/L Hepes, 2 mmol/L L-glutamin, 100 U/mL penicillin and 0.1 mg/mL streptomycin adjusted to pH 7.4 (all reagents from Sigma, St. Louis, USA) in a humidified CO_2 incubator at 37°C and 5% CO_2 atmosphere. Measurement of islet vitality was based on the cell membrane integrity test after staining with propidium iodide and acridine orange. The islets were inspected under fluorescence microscope, and vitality scores of 0%, 25%, 50%, 75%, and 100% were assigned to them according to the percentage of cells stained green (live) versus red (death). A sample of 20 islets from each experimental group was analyzed and the percentage of viable cells per islet was determined.

The in vitro function of the islets was evaluated by static incubation. Samples of 50 islets from each experimental group were incubated at 37°C for 60 minutes in the Krebs' solution, at first with 3 mmol/L glucose (basal solution), subsequently with 22 mmol/L

From the Laboratory of Pancreatic Islets (K.Z., Z.B., J.K., E.D., P.G., T.K., F.S.), Institute for Clinical and Experimental Medicine, Prague, and Physiological Department (T.S., P.J.), the Academy of Sciences of the Czech Republic, Prague, Czech Republic.

This study was supported by grant NR/7917-6/2004 from the IGA of Ministry of Health, Czech Republic.

Address reprint requests to Dr. Frantisek Saudek, Department of Diabetes, Diabetes Center, Institute for Clinical and Experimental Medicine, Videnska 1958/9, 140 21 Prague, Czech Republic. E-mail: frantisek.saudek@medicon.cz

0041-1345/05/$–see front matter
doi:10.1016/j.transproceed.2005.09.053

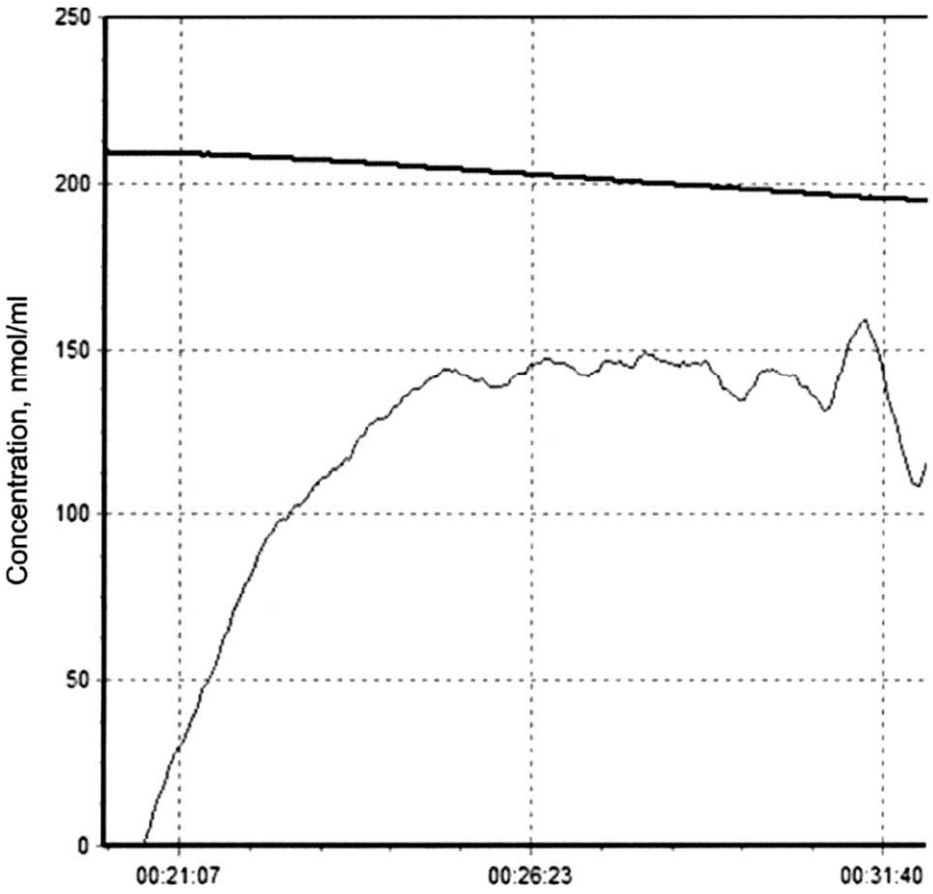

Fig 1. Islet respiration measured with high-resolution respirometry. **Upper line** shows oxygen concentration in the medium (nmol/mL), and **bottom line** represents oxygen consumption (pmol/mL · s) by islets.

glucose containing 0.25 mmol/L IBMX (stimulatory solution), and finally again with 3 mmol/L glucose. At the end of the incubation period, aliquots of the medium were removed for insulin radioimmunoassay (ICN Pharmaceuticals, California, USA). Results were expressed as stimulatory indices (SI, stimulatory to basal insulin release ratio).

A sample of 1000 islets from each experimental group was used for measurement of respiration, which was performed by a polarographic oxygen sensor in a 2-mL glass chamber of the respirometer Oxygraph 2K (Oroboros Instruments, Austria). The amplified signal from the oxygen sensor was recorded on a computer at sampling intervals of 1 second (DatLab acquisition software, Oroboros Instruments, Innsbruck, Austria). The respiration medium was equilibrated with air in the oxygraph chambers at 37°C and stirred until a stable signal was obtained for calibration at air saturation. After calibration the medium was replaced by aerated cell suspensions at a volume of 2.0 mL and the chambers were closed by insertion of stoppers. Respiration rates usually stabilized within 5 to 10 minutes of measurement as indicated by linear depletion of oxygen in the chamber (Fig 1). Oxygen consumption (pmol/mL · s) was counted as a negative time derivative of oxygen concentration (nmol/mL). The influence of islet number on oxygen consumption was tested on 1000 and 2000 islets obtained from the same rate donors (n = 3).

Results were expressed as means ± SD, and the Student *t* test was used for statistical analysis; *P* values < .05 were considered statistically significant. A linear ccorrelation coefficient was calculated to find a relation between glucose-stimulated insulin release and islet respiration rate.

RESULTS

In vitro cell viability, insulin secretion, and oxygen consumption data are summarized in Table 1. Vitality scores of fresh and cultured islets (n = 10) determined by living/death cells ratio were 91.1 ± 2.1% and 92.1 ± 4.4%, respectively ($P > .05$). Stimulation indices were 12.1 ± 8.2 (n = 5) and 10.0 ± 3.7 (n = 8), respectively ($P > .05$). Islet

Table 1. Insulin Secretion Calculated as Stimulation Index and Islet Respiration Expressed as Oxygen Consumption

	Viability (%)	Stimulation Index	Oxygen Consumption (pmol/mL · s)
Fresh islets	91.1 ± 2.1 (n = 10)	12.1 ± 8.2 (n = 5)	18.8 ± 3.3 (n = 5)
Cultured islets	92.1 ± 4.4 (n = 10)	10.0 ± 3.7 (n = 8)	15.2 ± 6.4 (n = 10)

Data are mean value ± SD. Data are not significantly different: $P > .05$.

oxygen consumption of fresh and cultured islets was 18.8 ± 3.3 pmol/mL · s (n = 5) and 15.2 ± 6.4 pmol/mL · s (n = 10), respectively ($P > .05$). Oxygen consumption was proportional to islet number as indicated by a 1.92-fold increase in oxygen consumption after doubling of the islet number (20.7 ± 1.7 vs 39.7 ± 3.9 pmol/mL · s ($n = 3$); $P = .01$). The correlation coefficient between the oxygen consumption rates and insulin secretion (SI) was 0.82 (n = 6).

DISCUSSION

Respirometry represents a very sensitive method for evaluation of tissue or cell metabolic condition.[5,9] For testing of metabolic function of pancreatic islets, it has been used by several investigators so far. Hellerström et al[10] in 1980 used a system called Cartesian divers to observe respiratory changes of beta cells in vitro. Another approach represented the application of an oxygen microsensor in mouse pancreatic islets.[11] The islet flow culture system designed by Sweet et al[12] allows permanent monitoring of oxygen consumption, which could be also eventually used for pretransplant islet evaluation. The system is equipped with an oxygen-sensitive platinum-porphyrine electrode for the detection of oxygen tension between the inflow and outflow medium.

In our study we measured islet oxygen consumption by a high-resolution oxymetry, which fairly correlated with other techniques of islet vitality and function tests. In comparison with other techniques applied so far, it seems to be more simple, fast, reproducible, and economic. The method is simple, rapid, and reproducible. In addition, the method could allow more specific evaluation of islet cell integrity using different inhibitors or stimulators of cellular respiration.[13] After appropriate standardization, the oxymetric technique can be used for routine clinical pretransplant islet quality testing.

REFERENCES

1. Bank HL: Assessment of islet cell viability using fluorescent dyes. Diabetologia 30:812, 1987

2. Gerber PP, Trimble ER, Wollheim CB, et al: Glucose and cyclic AMP as stimulators of somatostatin and insulin secretion from the isolated perfused rat pancreas: a quantitative study. Diabetes 30:40, 1981

3. Kinasiewicz A, Juszczak M, Pachecka J, et al: Pancreatic islets isolation using different protocols with in situ flushing and intraductal collagenase injection. Physiol Res 53:327, 2004

4. Sweet IR, Cook DL, Wiseman RW, et al: Dynamic perifusion to maintain and assess isolated pancreatic islets. Diabetes Technol Ther 4:67, 2002

5. Haller T, Ortner M, Gnaiger E: A respirometer for investigating oxidative cell metabolism: toward optimization of respiratory studies. Anal Biochem 218:338, 1994

6. Kuznetsov AV, Strobl D, Ruttmann E, et al: Evaluation of mitochondrial respiratory function in small biopsies of liver. Anal Biochem 305:186, 2002

7. Hutter E, Renner K, Pfister G, et al: Senescence-associated changes in respiration and oxidative phosphorylation in primary human fibroblasts. Biochem J 380:919, 2004

8. Saudek F, Cihalova E, Karasova L, et al: Increased glucagon-stimulated insulin secretion of cryopreserved rat islets transplanted into nude mice. J Mol Med 77:107, 1999

9. Renner K, Amberger A, Konwalinka G, et al: Changes of mitochondrial respiration, mitochondrial content and cell size after induction of apoptosis in leukemia cells. Biochim Biophys Acta 1642:115, 2003

10. Hellerstrom C, Andersson A, Welsh M: Respiration of the pancreatic B-cell: Effects of glucose and 2-aminonorbornane-2-carboxylic acid. Horm Metab Res (suppl) 10:37, 1980

11. Jung SK, Gorski W, Aspinwall CA, et al: Oxygen microsensor and its application to single cells and mouse pancreatic islets. Anal Chem 71:3642, 1999

12. Sweet IR, Khalil G, Wallen AR, et al: Continuous measurement of oxygen consumption by pancreatic islets. Diabetes Technol Ther 4:661, 2002

13. Jezek P, Engstova H, Zackova M, et al: Fatty acid cycling mechanism and mitochondrial uncoupling proteins. Biochim Biophys Acta 1365:319, 1998

PŘÍLOHA II.

Labeling of pancreatic islets with iron oxide nanoparticles for in vivo detection with magnetic resonance.

Z. Berková, D. Jirák, K. Zacharovová, J. Kříž, A. Lodererová, P. Girman, T. Koblas, E. Dovolilová, M. Vancová, M. Hájek, and F. Saudek

Transplantation, 2008. 85(1): p. 155-9.

Labeling of Pancreatic Islets With Iron Oxide Nanoparticles for In Vivo Detection With Magnetic Resonance

Zuzana Berkova,[1,2] Daniel Jirak,[2,3] Klara Zacharovova,[1,2] Jan Kriz,[1,2] Alena Lodererova,[4] Peter Girman,[1,2] Tomas Koblas,[1,2] Eva Dovolilova,[1,2] Marie Vancova,[5] Milan Hajek,[2,3] and Frantisek Saudek[1,2,6]

In vitro labeling of pancreatic islets with iron nanoparticles enables their direct posttransplant visualization by magnetic resonance; however, there is still a discrepancy in the fate of iron nanoparticles. This study was performed to detail the labeling process, consequently to improve the labeling efficacy and to confirm safety for islet cells. The islets were visible on T_2*-weighted magnetic resonance images as hypointense spots immediately after 1-hr cultivation. Although at this time already the sufficient superparamagnetic effect was achieved, most of the particles were deposed in islet macrophages and only later were they found in endosomes of endocrine islet cells. The iron content depended on length of culture period. The labeled islets showed an intact ultrastructure, responded normally to glucose stimulation in vitro, and were able to treat experimental diabetes. For purpose of subsequent magnetic resonance imaging, a 24-hr culture with ferucarbotran leads to sufficient labeling with no apparent adverse effect on beta cell morphology or function.

Keywords: Pancreatic islets, Islet transplantation, Magnetic resonance, Iron nanoparticles, Iron uptake.

(*Transplantation* 2008;85: 155–159)

Magnetic resonance imaging after previous labeling with superparamagnetic iron oxide (SPIO) nanoparticles currently is the only direct method for the long-term visualization of transplanted islets with sufficient spatial resolution (*1*). Although our method has already been successfully applied in human islet transplantation (*2*), there is still a discrepancy in the fate of iron nanoparticles. We presume that for further improvement of the labeling technique as well as for safety reasons, a more detailed study of iron particle uptake by the islet cells and its functional impact is needed. In the present study, we investigated in detail the time behavior of the labeling process and iron accumulation in different islet cell types, which is important for labeling optimization and for the evaluation of its safety for the islet cells in vitro as well as in vivo.

For islet labeling, a magnetic resonance (MR) contrast agent ferucarbotran (Resovist®; Schering AG, Germany) was used (140 mg Fe/mL of culture medium). The islets were cultivated with ferucarbotran for 1, 4, 8, 12, and 24 hr. From each labeling period, samples of 500 islets were taken for MR imaging and light and electron microscopy. Samples of 2000 islets were used for assessment of iron content and relaxometry.

On T2*-weighted MR images, the labeled islets were clearly demonstrated as hypointense (dark) spots which were visible immediately after a 1-hr culture period, and their number increased with the prolonged labeling time. Both the T1 (spin-lattice) and T2 (spin-spin) relaxation times of labeled islets were shortened after 1 hr and did not change noticeably after extending culture time (Table 1; $P<0.001$).

The mean iron contents after 1, 4, 8, 12, and 24 hr cultures were 4.40 ± 4.07, 2.9 ± 3.13, 6.42 ± 3.47, 3.96 ± 3.63, and 18.08 ± 16.22 ng per islet, respectively. In control islets, the iron concentration was close to the detection limit (0.28 ± 0.14 ng/islet; labeled vs. control islets $P<0.05$). The Pearson correlation coefficient between mean iron islet content and culture time was $r^2=0.7872$.

For iron detection in islet macrophages or beta cells, combined labeling with Prussian blue and anti-ED1 monoclonal antibody or with anti-insulin antibody was used (*3*). Iron was detected in the islets as early as after a 1-hr culture period, initially at the islet periphery and later also inside the islets. Iron was localized in macrophages (stained for CD-68 antigen; Fig. 1) as well in beta cells (stained for insulin) but never in control islets.

Ferucarbotran particles were visualized with electron microscopy as characteristic irregular crystals with an extremely high electrodense core and a less-dense coating (Fig. 2H), even without contrast enhancement. In the control samples, no similar structures were detected. The individual stages of iron incorporation into the islet cells are shown in Fig. 2. After a 1-hr labeling period, ferucarbotran was found adhered on the endocrine cell surface, whereas few particles were already found in the endocytic structures of macrophages. After a 4-hr culture period, the particles were localized also in the beta-cell vesicles. With the prolonged labeling time, the amount of incorporated particles further

This study was supported by grants 2B06175 and LN00A065 from Ministry of Education, Youth and Sports, Czech Republic.

[1] Laboratory of Pancreatic Islets, Institute for Clinical and Experimental Medicine, Videnska 1958/9, 140 21 Prague, Czech Republic.
[2] Center for Cellular Therapy and Tissue Repair, 2nd School of Medicine, Charles University, Prague, Czech Republic.
[3] MR-Unit, Department of Radiodiagnostic and Interventional Radiology, Institute for Clinical and Experimental Medicine, Prague, Czech Republic.
[4] Department of Clinical and Transplantation Pathology, Institute for Clinical and Experimental Medicine, Prague, Czech Republic.
[5] Biology Centre of the ASCR, Institute of Parasitology and University of South Bohemia, Budejovice, Czech Republic.
[6] Address correspondence to Frantisek Saudek, M.D., Department of Diabetes, Diabetes Center, Institute for Clinical and Experimental Medicine, Videnska 1958/9, 140 21 Prague, Czech Republic.
E-mail: frantisek.saudek@medicon.cz

Received 9 July 2007. Revision requested 25 September 2007.
Accepted 8 October 2007.

ISSN 0041-1337/08/8501-155
DOI: 10.1097/01.tp.0000297247.08627.ff

TABLE 1. T1 and T2 relaxation times ($P<0.001$ labeled islets compared with control islets)

	Saline solution	Control islets	Islets labeled with ferucarbotran				
			1 hr	4 hr	8 hr	12 hr	24 hr
T1 (ms)±SD	2400±187	863±110	231.2±34.1	286.7±28.7	260±24.5	302±58.4	165.5±14.9
T2 (ms)±SD	1018±20	251.5±9	23.2±3.4	32.9±10.4	30.7±7.7	32.3±6.5	10.3±4.3

increased and formed huge electrodense clusters. Ultrastructure of the labeled islet cells was not affected; typical cytoplasmatic organelles and cell–cell contacts were observed (Fig. 2G).

After transplantation, 48-hr-labeled islets transplanted into the portal vein of diabetic rats were able to achieve normal blood glucose levels (Fig. 3B) with intravenous glucose-tolerance tests comparable with those in control animals (Fig. 3C; $P>0.05$). Under general anesthesia, standard T2*-weighted gradient echo sequences were applied for MRI examinations. The labeled islets in the liver were visible on MR images as hypointense spots (Fig. 3D–F), and these spots remained detectable with approximately the similar amount throughout the study ($P>0.05$). Using light microscopy, we were able to detect the iron particles in islet cells and islet macrophages (Fig. 3G–H) for as long as 120 days after transplantation into the liver.

For islet labeling, we (as well as other groups) used SPIO nanoparticles containing iron oxides in nonionic crystalline form (*3–6*). Enhancement of tissue contrast for MRI with the use of SPIO nanoparticles enables islet visualization because they produce strong local inhomogeneity in the magnetic field which are visible as hypointense spots on MR images.

Relaxometry was used so that we could observe whether the concentration of the contrast agent in the medium and the culture time are sufficient to achieve the maximal superparamagnetic effect. Relaxivity is a process in which the excited nucleus of hydrogen protons returns to the equilibrium. Contrast agents used in MR sped up these processes and thereby shortened the relaxation times. We found that ferucarbotran concentration of 5 μl/mL is sufficient for achieving the evident superparamagnetic effect. The relaxometry also confirmed that signal loss on MR images resulted from islet labeling and not from any signal perturbation.

Assuming that an average islet is composed of 2000 cells, the mean iron content per 1 islet cell ranged from 2 (after 1-hr) to 9 pg Fe (after 24-hr culture). Our results of iron uptake correlate with data published by Evgenov et al. (*5*) who found that the iron content 1–18 pg Fe per cell depended on iron concentration in the medium during an overnight culture.

Ferucarbotran was originally developed as MR contrast agent for imaging of various liver lesions (*7*, *8*). The iron oxide core of the particles is covered with carboxydextran in order to promote their phagocytosis by liver Kupffer cells (*7*, *9*). Rapid ferucarbotran phagocytosis for potential subsequent in vivo cell tracking was found in vitro by human monocytes (*10*). This probably accounts for intensive SPIO uptake by islet macrophages.

Iron detection at different labeling times, using a combination of immunochemistry and electron microscopy, clarified the discrepancy in our previous findings which indicated a predominant iron localization in beta cells (*4*) or in islet macrophages (*3*). The localization of SPIO particles in both islet cells and macrophages was previously found by other authors (*5*, *6*) who, however, used a different kind of contrast agent.

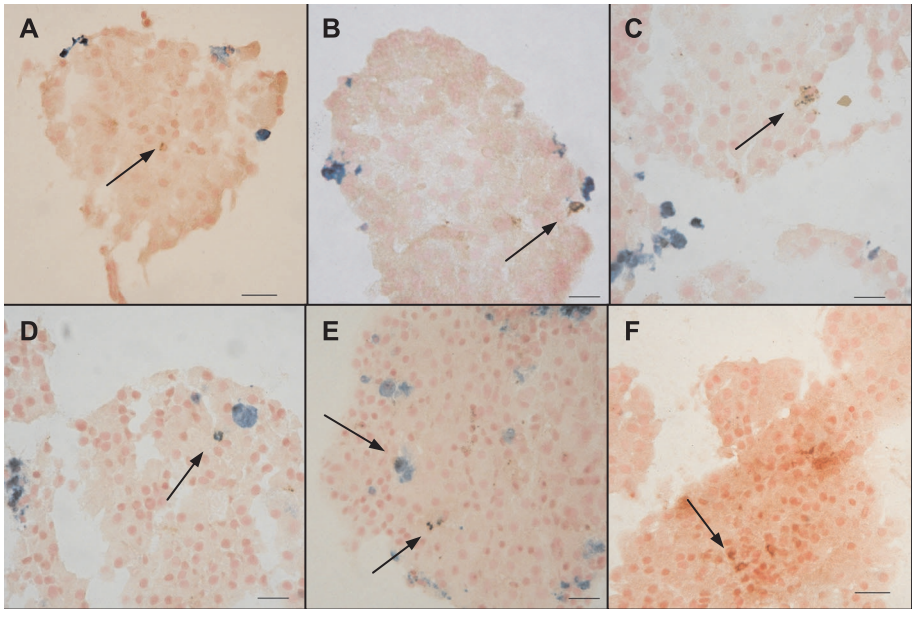

FIGURE 1. Representative images of iron deposits in pancreatic islets in vitro. Immunohistochemistry stain of islets with Prussian blue for iron detection (blue spots) and with anti-ED1 antibody for macrophage detection (black arrows, brown spots). The islets were cultivated for 1 hr (A), 4 hr (B), 8 hr (C), 12 hr (D), and 24 hr (E) with ferucarbotran and as control samples (F) were used islets without labeling. The images show co-localization of iron with macrophages. No iron could be seen in samples of control islets (F). Scale bar is 20 μm.

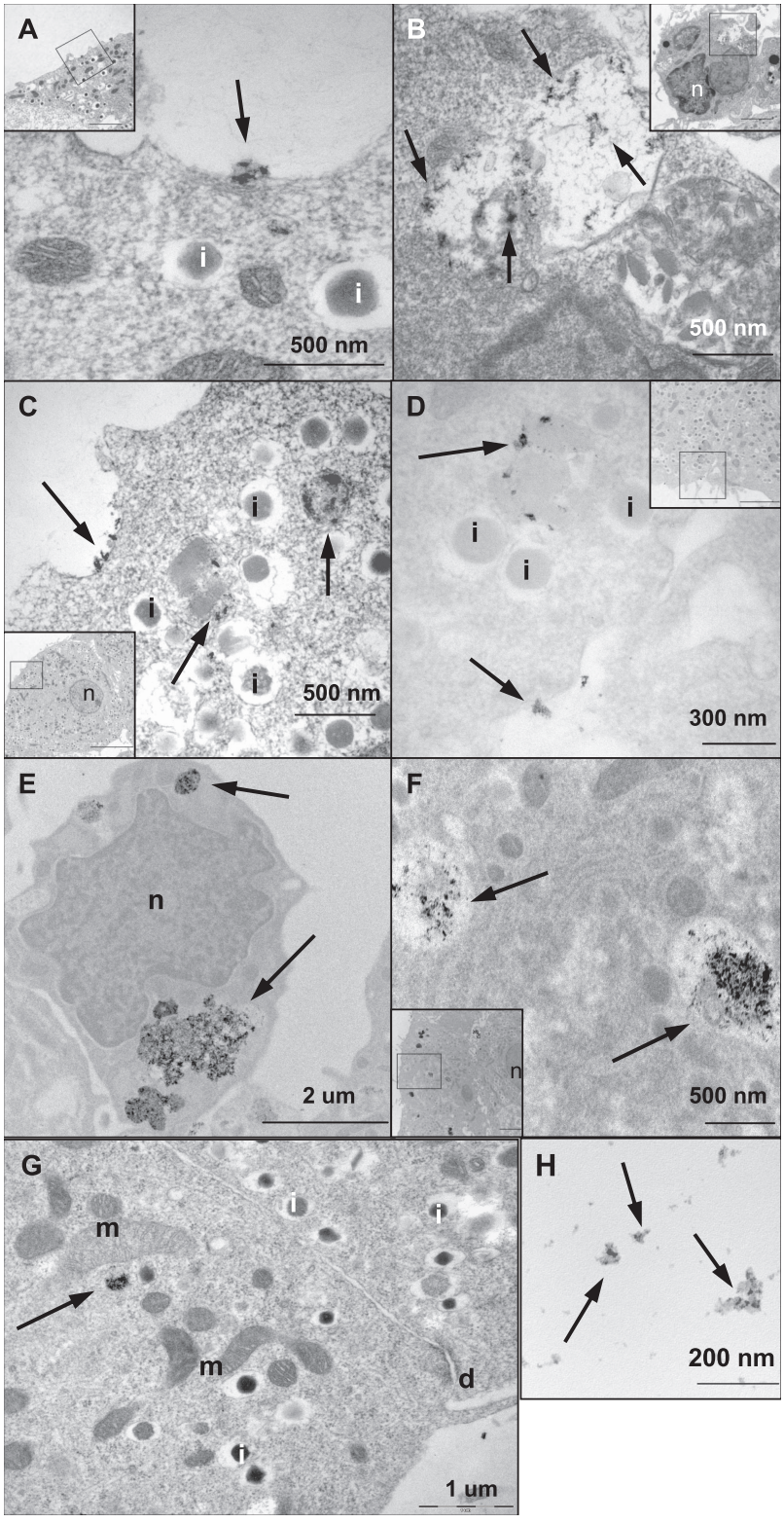

FIGURE 2. Electron microscopy of the labeled islets. After 1-hr labeling iron particles (arrows) are adhered on the cell surface of the endocrine cells (A, beta cell) while few particles are already found in large endocytic structures of macrophages (B). After 4-hr labeling iron particles are localized together with other heterogenous material in beta cell vesicles (C). After 8-hr labeling the amount of incorporated particles further increased and the individual iron containing vesicles in beta cells began to fuse (D, dotted arrow). After 24-hr labeling the iron particles formed huge electrodense clusters in macrophages (E) as well as in beta cells (F). Ultrastructure of the labeled islet cells was not affected (G). Ferucarbotran alone is shown as electrodense elements (H). n = nucleus, I = insulin granules, m = mitochondria, d = desmosome.

As to the optimal labeling period, we determined this as the time when the iron accumulation in the islets allows for their reliable detection on MR images. This requirement was already reached after a 1-hr culture; only the islet macrophages were labeled. After a 4-hr period, SPIO could be detected in the beta, alpha, and delta cells as well. To definitely validate the optimal labeling time, additional in vivo experiments should be performed. We found that a 24-hr labeling time enables detection by MR almost all islets. With regard to our previous reports (*3*, *4*), the labeling time can be shortened from 48 to at least 24 hr.

Although iron uptake during islet labeling is important for detection quality, it could lead to morphological and

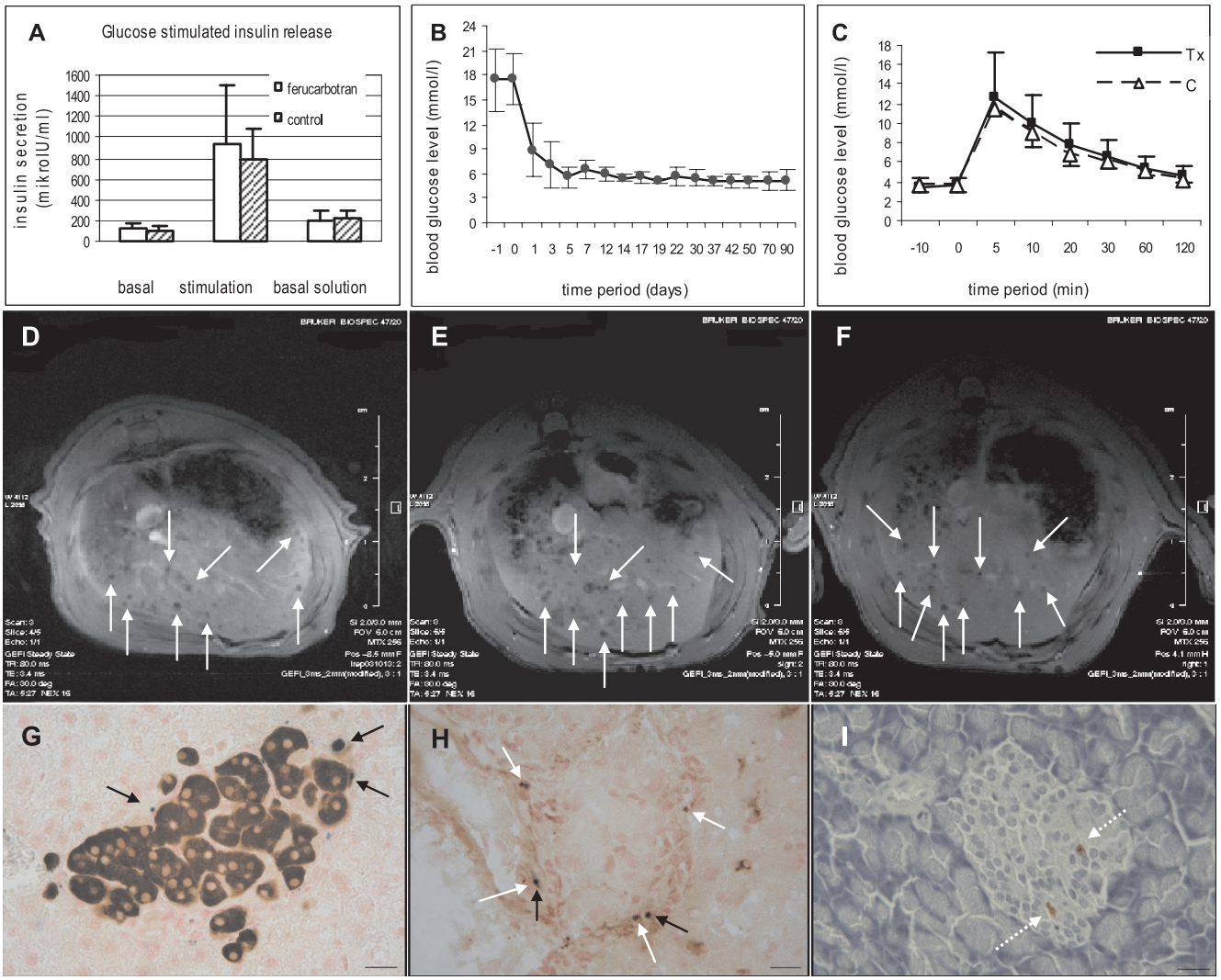

FIGURE 3. (A) Glucose stimulated insulin release in vitro was not affected by labeling with ferucarbotran ($P>0.05$). (B) The labeled pancreatic islets retained their ability to treat diabetes, blood glucose levels significantly decreased on day 1 after transplantation ($P<0.05$), normal conditions were achieved by day 5 and kept up to the end of the experiment. (C) Blood glucose curves of intravenous glucose-tolerance tests did not differ between control healthy (C) and transplanted (Tx) animals ($P>0.05$). (D–F) Representative T_2*-weighted in vivo MR images of intrahepatically transplanted labeled islets 1 week (D), 7 weeks (E), and 13 weeks (F) after transplantation. Islets were visible as dark spots (white arrows) and remained detectable approximately in the same amount throughout the study ($P>0.05$). (G–I) Immunohistochemistry of labeled islets transplanted into the liver. (G) Iron (blue spots, black arrows) was present outside as well as inside the insulin-possitive cells (brown). (I) Iron was also co-localized with macrophages of the transplanted islets (brown, white arrows). (H) In pancreases of transplanted animals (after streptozotocin treatment) were shown only rare insulin-possitive cells (dotted arrows). Scale bar is 20 μm.

functional changes precluding the use of this technique in humans. In our previous studies, a 48-hr culture with ferucarbotran did not impair the insulin stimulation index in vitro (*3*, *11*). We have now confirmed these results in a different rat strain (Fig. 3A; $P>0.05$). In vitro safety after cell labeling with SPIO particles was also reported by other authors (*5*, *6*, *10*, *12*).

Normal iron body stores are 35–45 mg/kg of body weight. Free iron is highly destructive probably because of its ability to catalyze the production of reactive oxygen species that may initiate lipid peroxidation and ultimately damage DNA. Iron overload can contribute to liver, heart, pancreas and joint diseases (*13*). Labeling of islets can cause excess iron in cells, but iron is bound to the counter-ion and in this form should not be available for metabolic pathways and it can be presumed only minimal free iron release.

Arbab et al. (*14*) demonstrated that the release of free iron from SPIO particles was dependent on buffering systems and pH. Some endosomes fused with lysosomes and were degradated, but the majority of particles remained unchanged in endosomes. Searching for intrahepatically transplanted islet cells for ultrastructural investigations has been so far very difficult. Our preliminary findings suggest that SPIO particles remain intact concentrated in endosomes.

Although this technique is sensitive enough to detect a single labeled islet, we were not able to quantify transplanted pancreatic islets in vivo with regard to the fact that magnetic particles appear in MR images much larger than their actual size. However, this technique allows only for following the relative number of islet spots that may change after transplantation, for example, because of rejection (*3*).

Visualization of SPIO labeled transplanted islets using MR is not the only imaging method. An alternative method is labeling with gadolinium chelates showing a positive contrast; however, it seems that this method of imaging is less stable due to the release of the contrast agent from the cells (*15*).

Our method of islet imaging shows high spatial resolution but, as yet, it can be used only for transplanted and not native islets and does not reflect islet function. For a noninvasive assessment of functioning islet mass, the use of positron emission tomography targeted to specific components of islet cells shows promise (*1*).

In conclusion, we have found that islet labeling with SPIO nanoparticles is a time-dependent process. The sufficient superparamagnetic effect was achieved after a 1-hr culture period with the contrast agent. Iron accumulation is most intensive in islet macrophages but, with increased incubation time, the alpha, beta, and delta cells also incorporate iron particles via endocytosis. They gradually concentrate on iron particles in cytoplasmic vesicles distinct from islet cell specific granules without the obvious impairment of ultrastructural morphology. Finally, iron accumulation in beta cells does not cause the immediate reduction of insulin secretion assessed in vitro and does not significantly impair the ability of transplanted islets to treat experimental diabetes. For subsequent in vivo MRI, 24-hr labeling or less is sufficient amount of time. Presently, this method is ready for clinical application.

REFERENCES

1. Souza F, Freeby M, Hultman K, et al. Current progress in non-invasive imaging of beta cell mass of the endocrine pancreas. *Curr Med Chem* 2006; 13: 2761.
2. Toso C, Vallee J-P, Morel P, et al. Clinical magnetic resonance imaging of allogeneic islet grafts after iron-labeling. *Transplantation* 2006; 82 (1 Suppl 3): 452.
3. Kriz J, Jirak D, Girman P, et al. Magnetic resonance imaging of pancreatic islets in tolerance and rejection. *Transplantation* 2005; 80: 1596.
4. Jirak D, Kriz J, Herynek V, et al. MRI of transplanted pancreatic islets. *Magn Reson Med* 2004; 52: 1228.
5. Evgenov NV, Medarova Z, Pratt J, et al. In vivo imaging of immune rejection in transplanted pancreatic islets. *Diabetes* 2006; 55: 2419.
6. Tai JH, Foster P, Rosales A, et al. Imaging islets labeled with magnetic nanoparticles at 1.5 Tesla. *Diabetes* 2006; 55: 2931.
7. Reimer P, Tombach B. Hepatic MRI with SPIO: Detection and characterization of focal liver lesions. *Eur Radiol* 1998; 8: 1198.
8. Vogl TJ, Schwarz W, Blume S, et al. Preoperative evaluation of malignant liver tumors: Comparison of unenhanced and SPIO (Resovist)-enhanced MR imaging with biphasic CTAP and intraoperative US. *Eur Radiol* 2003; 13: 262.
9. Wang Y-X, Hussain S, Krestin G. Superparamagnetic iron oxide contrast agents: Physicochemical characteristics and applications in MR imaging. *Eur Radiol* 2001; 11: 2319.
10. Metz S, Bonaterra G, Rudelius M, Settles M, Rummeny EJ, Daldrup-Link HE. Capacity of human monocytes to phagocytose approved iron oxid MR contrast agents in vitro. *Eur Radiol* 2004; 14: 1851.
11. Berkova Z, Kriz J, Girman P, et al. Vitality of pancreatic islets labeled for magnetic resonance imaging with iron particles. *Transplant Proc* 2005; 37: 3496.
12. Matuszewski L, Persigehl T, Wall A, et al. Cell tagging with clinically approved iron oxides: Feasibility and effect of lipofection, particle size, and surface coating on labeling efficiency. *Radiology* 2005; 235: 155.
13. Lieu PT, Heiskala M, Peterson PA, Yang Y. The roles of iron in health and disease. *Mol Aspects Med* 2001; 22: 1.
14. Arbab AS, Wilson LB, Ashari P, Jordan EK, Lewis BK, Frank JA. A model of lysosomal metabolism of dextran coated superparamagnetic iron oxide (SPIO) nanoparticles: Implications for cellular magnetic resonance imaging. *NMR Biomed* 2005; 18: 383.
15. Biancone L, Crich SG, Cantaluppi V, et al. Magnetic resonance imaging of gadolinium-labeled pancreatic islets for experimental transplantation. *NMR Biomed* 2007; 20: 40.

PŘÍLOHA III.

Processing of superparamagnetic iron contrast agent ferucarbotran in transplanted pancreatic islets

K. Zacharovová, Z. Berková, D. Jirák, V. Herynek, M. Vancová,
E. Dovolilová, and F. Saudek

Manuskript přijat k publikaci 8. května 2012
v časopise Contrast Media & Molecular Imaging

Potvrzení o přijetí článku k publikaci:

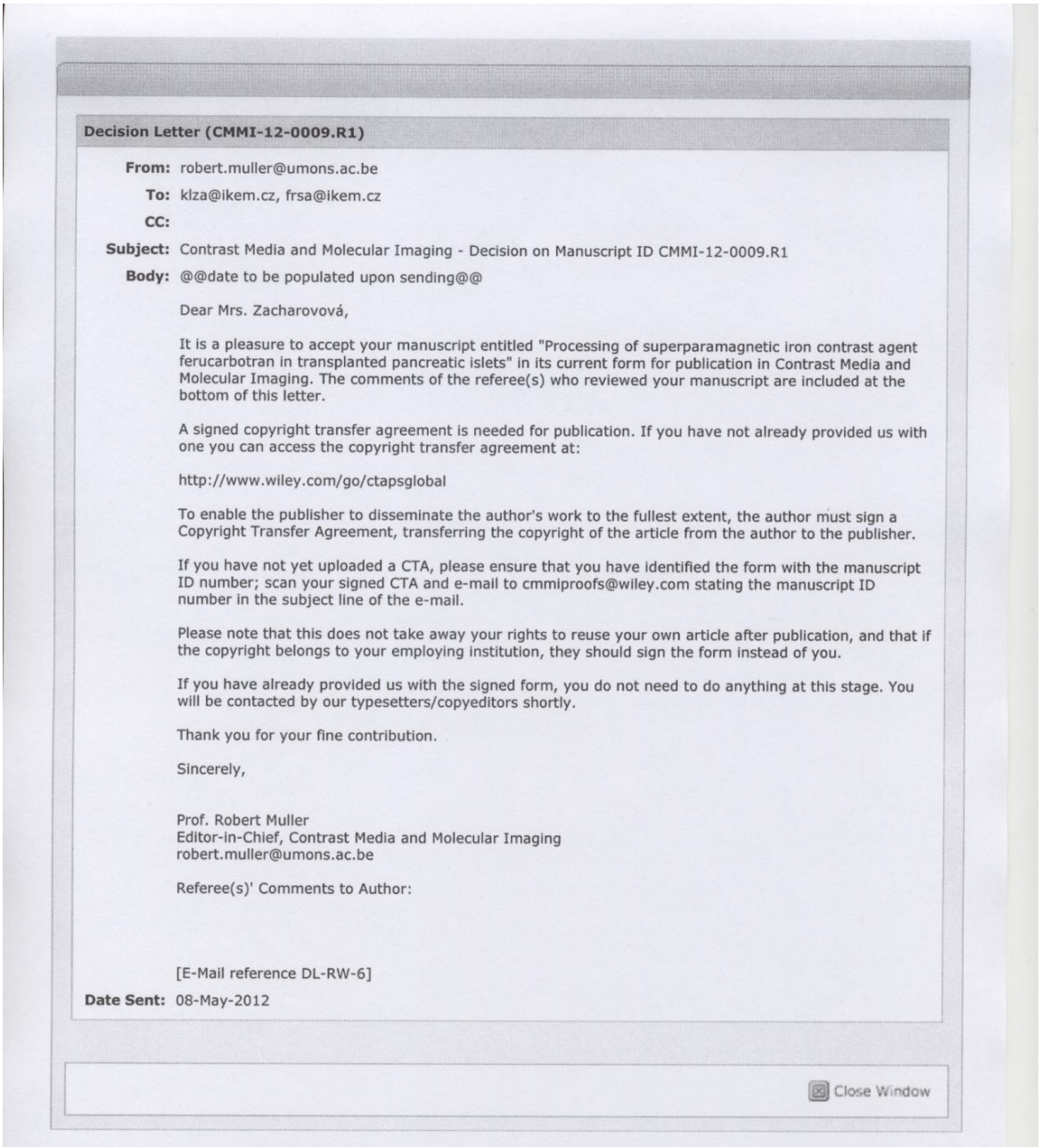

Decision Letter (CMMI-12-0009.R1)

From: robert.muller@umons.ac.be
To: klza@ikem.cz, frsa@ikem.cz
CC:
Subject: Contrast Media and Molecular Imaging - Decision on Manuscript ID CMMI-12-0009.R1
Body: @@date to be populated upon sending@@

Dear Mrs. Zacharovová,

It is a pleasure to accept your manuscript entitled "Processing of superparamagnetic iron contrast agent ferucarbotran in transplanted pancreatic islets" in its current form for publication in Contrast Media and Molecular Imaging. The comments of the referee(s) who reviewed your manuscript are included at the bottom of this letter.

A signed copyright transfer agreement is needed for publication. If you have not already provided us with one you can access the copyright transfer agreement at:

http://www.wiley.com/go/ctapsglobal

To enable the publisher to disseminate the author's work to the fullest extent, the author must sign a Copyright Transfer Agreement, transferring the copyright of the article from the author to the publisher.

If you have not yet uploaded a CTA, please ensure that you have identified the form with the manuscript ID number; scan your signed CTA and e-mail to cmmiproofs@wiley.com stating the manuscript ID number in the subject line of the e-mail.

Please note that this does not take away your rights to reuse your own article after publication, and that if the copyright belongs to your employing institution, they should sign the form instead of you.

If you have already provided us with the signed form, you do not need to do anything at this stage. You will be contacted by our typesetters/copyeditors shortly.

Thank you for your fine contribution.

Sincerely,

Prof. Robert Muller
Editor-in-Chief, Contrast Media and Molecular Imaging
robert.muller@umons.ac.be

Referee(s)' Comments to Author:

[E-Mail reference DL-RW-6]

Date Sent: 08-May-2012

Close Window

SPi | Journal Code: C M M I | Article ID: 1 4 7 7 | Dispatch: 01.06.12 | CE: | No. of Pages: 9 | ME:

Full Paper

CONTRAST MEDIA & MOLECULAR IMAGING

Received: 14 February 2012, Revised: 17 April 2012, Accepted: 08 May 2012, Published online in Wiley Online Library:

(wileyonlinelibrary.com) DOI: 10.1002/cmmi.1477

Processing of superparamagnetic iron contrast agent ferucarbotran in transplanted pancreatic islets

Klára Zacharovová[a]*, Zuzana Berková[a], Daniel Jirák[b], Vít Herynek[b], Marie Vancová[c], Eva Dovolilová[a] and František Saudek[a]

Labeling of pancreatic islets with superparamagnetic iron oxide (SPIO) nanoparticles enables their post-transplant monitoring by magnetic resonance imaging (MRI). Although the nanoparticles are incorporated into islet cells in culture, little is known about their fate *in vivo*. We studied the morphology of labeled islets after transplantation, aiming to identify the MRI contrast particles and their relationship to transplantation outcomes. Rat islets labeled with the ferucarbotran were transplanted into the liver or under the kidney capsule of syngeneic and allogeneic rats. After *in vivo* MRI, morphology was studied by light, fluorescence and transmission electron microscopy. Morphology of syngeneic islets transplanted beneath the kidney capsule vs into the liver was similar. Iron particles were almost completely eliminated from the endocrine cells and remained located in host-derived macrophages surrounding the vital islets for the entire study period. In the allogeneic model, islets lost their function and were completely rejected within nine days following transplantation in both transplant models. However, intercellular transport of the SPIO particles and subsequent MRI findings was different in the liver and kidney. In the liver, the decreasing number of islet-related MRI spots corresponded with clearance of iron particles in rejected islets; in contrast, with renal transplants extensive iron deposits with a high effect on MRI signal persisted in phagocytic cells beneath the capsule. We conclude that MRI detection of the iron contrast agent correlates with islet survival and function in islet transplantation into the liver, while it does not correlate in the case of transplantation beneath the renal capsule.

Keywords: magnetic resonance imaging; pancreatic islets; transplantation; superparamagnetic iron oxide nanoparticles; ferucarbotran; β cells; diabetes; immunohistochemistry; transmission electron microscopy

1. INTRODUCTION

Pancreatic islet transplantation is a promising approach for treatment of selected patients with type I diabetes mellitus. It represents a safer and more convenient alternative for β cell replacement than solid organ pancreas transplantation (1,2). However, transplantation of islets isolated from more than one donor is usually required to achieve insulin independence (3,4). Lower efficiency is due to many factors involving the islet isolation process, immediate islet survival, poor revascularization, local inflammation and immunity, among others (5,6). Currently, the only markers of islet survival are indicators of islet function such as glycemia and C-peptide levels. However, these markers do not reflect early changes in islet mass. To better understand the fate of transplanted islets, a method for *in vivo* imaging of islets is needed. Although several different approaches have been proposed (7–11), only magnetic resonance imaging (MRI) of labeled islets has approached clinical utility thus far (12,13). Transplanted islets labeled *in vitro* with superparamagnetic iron oxide (SPIO) particles can be detected *in vivo* by MRI as hypointense spots (14–16). Their number correlates with the mass of transplanted islets and is reduced during islet rejection (15,17). However, the number of detected negative islet signals does not match exactly the absolute number of the administered islets, probably because a single spot may represent a cluster of islets with an overlapping superparamagnetic effect. Short-term labeling does not significantly impair the vitality and function of islets (18,19). During *in vitro* culture, SPIO particles are incorporated into all major types of islet cells including β, α, and delta cells (16,19,20). However, the particles are preferentially accumulated in islet macrophages (19). Subsequently, SPIO particles can be detected by MRI at the site of transplantation for up to 6 months, in spite of the fact that the hypointense signal decreases gradually over time (21). It is unclear whether the loss of the islet-related hypointense spots is caused only by islet destruction (owing to rejection, ischemia and other factors) or if the iron particles are cleared out of surviving cells by natural mechanisms. Iron particles from necrotic islets may be also incorporated into the surrounding host tissue

* *Correspondence to: Zacharovová, Klára, Institute for Clinical and Experimental Medicine, Vídeňská 1958/9, 140 21 Prague 4, Czech Republic. Email: klza@ikem.cz*

a *K. Zacharovová, Z. Berková, E. Dovolilová, F.š Saudek*
Laboratory of Langerhans Islets, Centre of Experimental Medicine, Institute for Clinical and Experimental Medicine, Prague, Czech Republic

b *D. Jirák, V. Herynek*
MR Unit, Department of Diagnostic and Interventional Radiology, Institute for Clinical and Experimental Medicine, Prague, Czech Republic

c *M. Vancová*
Institute of Parasitology, Biology Centre of the ASCR, Ceske Budejovice, Czech Republic

and may remain detectable despite the loss of the original insulin-producing transplanted tissue, as Marzola *et al.* recently suggested based on experiments with an allogeneic rat model (22).

To determine whether translocation and elimination of the SPIO particles is caused by tissue rejection or represents a natural process, we studied the fate of SPIO particles in labeled pancreatic islets in both syngeneic and allogeneic models. As the process of particle elimination may differ at different transplant sites, islets were implanted into the liver or the renal subcapsular space. While transplantation beneath the kidney capsule is commonly used as a technically easier experimental procedure allowing ultrastructural investigations including those with transplantation of SPIO labeled islets (16,20,23), transplantation into the liver via the portal vein better reflects the current clinical setting of islet transplantation. Islets were labeled with a clinically approved SPIO contrast agent, ferucarbotran–carboxydextran-coated iron oxide nanoparticles (Resovist®, Schering AG, Germany). Localization of SPIO particles within tissue samples was performed using light, fluorescence and transmission electron microscopy (TEM), and the origin of the cells that finally retained the contrast agent was assessed by a specific fluorescence cell tracking method.

2. RESULTS AND DISCUSSION

2.1. Labeled syngeneic islets are easily detected by MRI

Pancreatic islets labeled *in vitro* with SPIO nanoparticles were detected *in vivo* as negative signal voids on T_2*-weighted MRI beginning on the first day following transplantation owing to a strong superparamagnetic effect. This imaging method was originally described by our group (14,15) and subsequently confirmed and modified by others in various islet transplant models (16,20,23,24). In the case of syngeneic transplantation beneath the renal capsule, the labeled islets usually form a confluent hypointense area at the edge of the kidney (Fig. 1A) (16,20,23). However, the renal capsule is not a convenient site for MRI owing to a chemical shift artifact that occurs at the edge of the kidney. This shift in resonance frequency exists between protons in fat and water and results in a low-intensity line at the outer margin of various structures on MRI (25). On the renal interface, it can overlap the islet transplantation site.

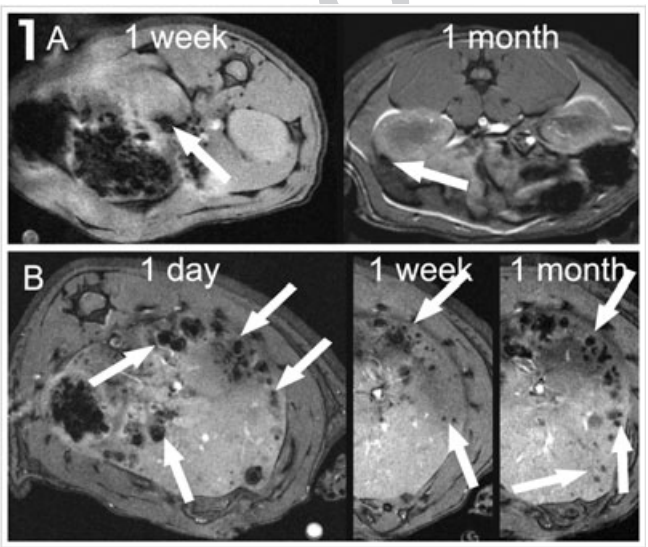

Q2 **Figure 1.** ▪▪

In syngeneic transplantation into the liver, labeled islets were imaged as hypointense spots dispersed in some or all liver lobes (Fig. 1B) during the entire 3 month study period. We did not quantify the time-related changes in MR images, as this was the subject of our previous study (15). A quantitative decrease of hypointense signal intensity over time was described in syngeneic, allogeneic and xenogeneic transplantation models (21,23,26).

2.2. Following syngeneic transplantation, SPIO particles are translocated into peri-islet macrophages

We focused on the location of SPIO nanoparticles in labeled pancreatic islets after transplantation. As we demonstrated previously, during islet labeling the particles travel through the membrane into all cell types, including islet macrophages (19). After transplantation, we observed considerable changes in localization of the SPIO particles.

On the first day after syngeneic transplantation, immunohistochemically detected iron particles were seen in the cytoplasm of β and α cells in both transplantation sites (Fig. 2A). Iron particles in β cells were detected in almost all microphotographs (28/28 in the liver, 15/16 under the kidney capsule). Iron particles were found also in the tissue surrounding the transplanted islets. F2

Beneath the kidney capsule, iron particles were found in the extracellular space within necrotic cellular debris, as confirmed by TEM (Fig. 2B). Other iron particles were detected in myofibroblasts (positive for smooth muscle actin, α-SMA; Fig. 2C) and fibroblasts (positive for S100A4, a Ca^{2+} binding protein belonging to the S100 subfamily; Fig. 2D). These cells are involved in the reparatory process following tissue injury (27). However, most of the free iron particles were taken up by macrophages (Fig. 2E).

In the liver, iron particles were mostly found in cells accumulating around the transplanted islets in vessels, predominantly in macrophages and also in liver fibroblasts and myofibroblasts. Iron particles in macrophages were detected in all microphotographs in both transplantation sites (24/24 in the liver, 15/15 under the kidney capsule).

One week after syngeneic transplantation, iron particles were rarely found in small vesicles of the transplanted endocrine cells (Fig. 3A, B). Most iron particles were stored in macrophages surrounding the islets at both transplantation sites. Electron microscopy showed the iron concentrated in cytoplasmic phagosomes (Fig. 3C). Iron particles were also detected in collagen-producing fibroblasts (Fig. 3D) dispersed over the whole transplantation area in the kidney as well as in the liver. Under the kidney capsule, the myofibroblasts proliferated in the proximity of iron-containing cells (Fig. 3E). In the liver, the iron was also sporadically found in myofibroblasts. Random location of iron particles was detected in endothelial cells (Fig. 3F). F3

One month post syngeneic transplantation, iron particles still persisted in large quantities in macrophages surrounding the syngeneic islets (Fig. 4A) in both transplantation sites. Occasionally, the high iron content prevented reliable immunofluorescence detection of the type of the iron-containing cells. Therefore, the iron was removed from tissue sections by sodium dithionite to uncover the hidden cell antigens (28). Immunofluorescence analysis then identified these cells as tissue macrophages (Fig. 4B). Only a small amount of iron was detected in the transplanted endocrine cells. Iron was detected in some of the fibroblasts surrounding the islets in the liver or beneath the renal capsule. In the renal F4

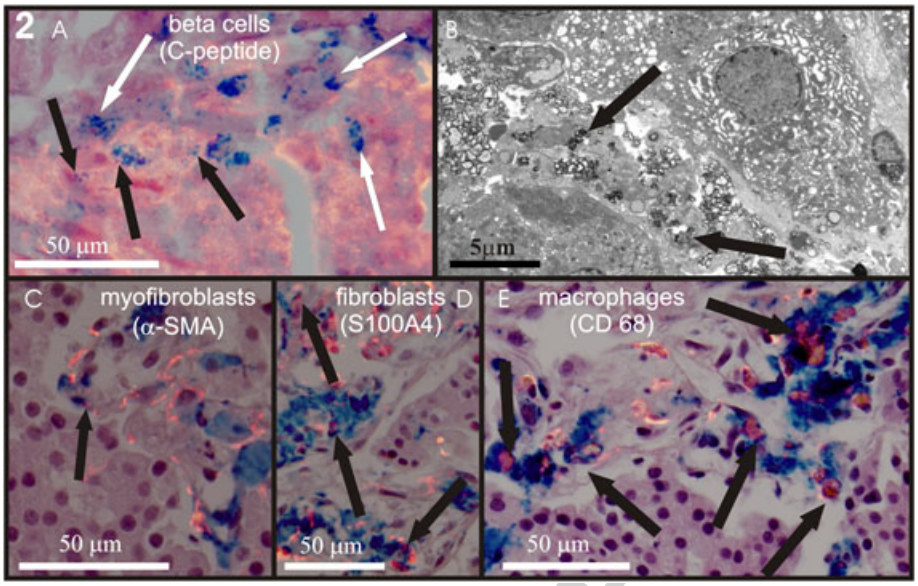

Figure 2. ▪▪

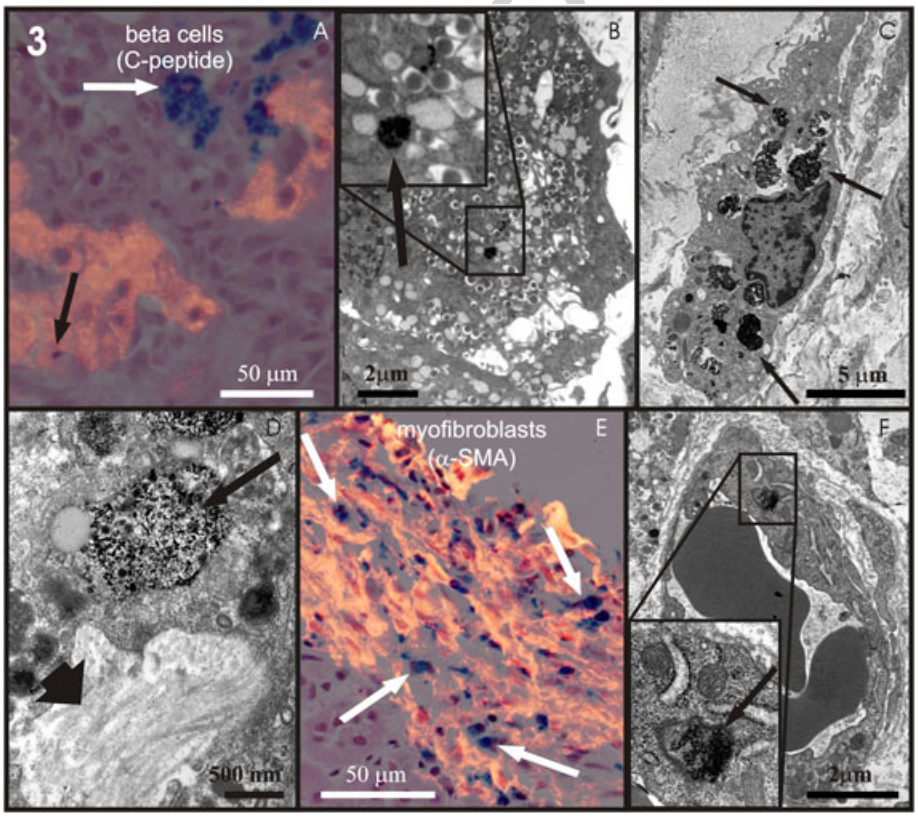

Figure 3. ▪▪

subcapsular area, islet transplantation led to proliferation of numerous myofibroblasts and production of collagen extracellular matrix (Fig. 4C) around the iron containing macrophages.

The localization of iron particles 3 months after syngeneic transplantation did not differ significantly from the location after 1 month. Iron was detected rarely in the endocrine cells. In β cells, it was detected in two out of 15 microphotographs of islets scanned on sections of eight samples dissected from livers of two rats and in seven out of 17 microphotographs of islets under the kidney capsule scanned on sections of two samples dissected from two rats. Again, iron accumulated in large macrophages in the proximity of the transplanted islets (Fig. 5; F5 detected in all microphotographs of all tissue samples).

Translocation of the SPIO particles from labeled islet cells into other cells has been described in several studies (20,23,29). Accumulation of iron particles in cells surrounding the islets was

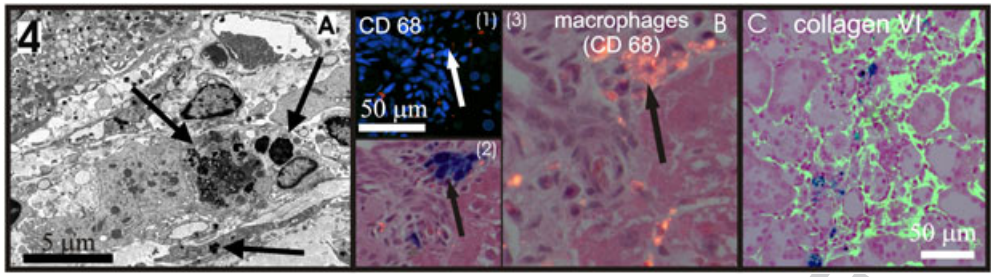

Figure 4. ▪▪

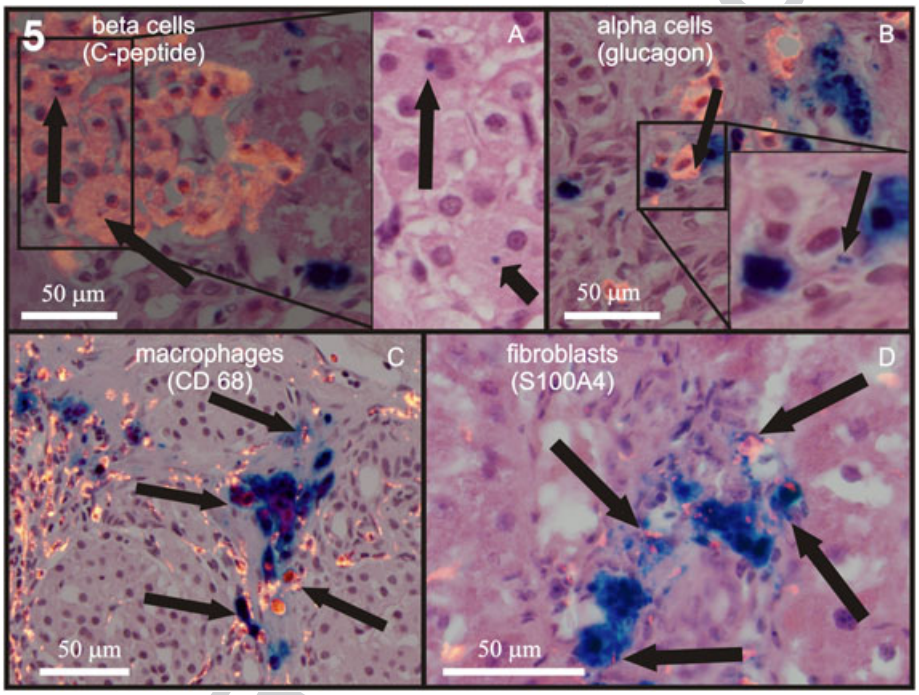

Figure 5. ▪▪

demonstrated by Marzola *et al*. (22). Of note, the authors used an allogeneic model, where the rejection process must be taken into account. Allotransplantation obviously may stimulate local cellular reaction and SPIO particle metabolism and translocation. From our syngeneic model we can conclude that most SPIO particles were readily released from the β cells and some iron might have been metabolized (30,31), but most iron remained in the vicinity of functional islets. In this model, the post-transplant morphology and SPIO localization was similar in both transplantation sites. The stored iron remained at the same location for a long period of time with stable MRI findings.

2.3. Most SPIO particle-containing cells are phagocytic cells of host origin

Persistence of iron particles close to islet cells after transplantation raised the question of the origin of cells retaining the particles. Islets labeled with ferucarbotran were subsequently labeled with the fluorescence dye CellTracker™ Green CMFDA (5-chloromethylfluorescein diacetate; Invitrogen, OR, USA). CMFDA forms insoluble fluorescent conjugate in the cytoplasm of vital cells and enables cell identification shortly after transplantation. CMFDA successfully labeled 55% of islet cells (Fig. 6A). About two-thirds (67%) of the CMFDA-negative cells were identified as dead (propidium iodide positive). CMFDA entered β cells (Fig. 6B) as well as other islet cells, which simultaneously contained iron particles. F6

Secondary labeling with CMFDA did not affect localization of SPIO particles after syngeneic transplantation. Surprisingly, histological examination revealed the particles to be present almost exclusively in CMFDA-negative cells surrounding the islets (Fig. 6C, D). Immunodetection identified the iron containing cells primarily as macrophages (Fig. 6E). Thus iron particles were retained by the host cells, predominantly macrophages. Presumably, the attracted host macrophages phagocytosed the released iron or the entire labeled cells. This finding is analogous to results of other authors who studied transplantation of labeled bone marrow stromal cells (32), neural precursor cells (33) or labeled mesenchymal stem cells (34).

2.4. Beneath the renal capsule, SPIO particles persist despite complete islet rejection

To our knowledge, MRI of islet rejection beneath the renal capsule in immunocompetent animals has not yet been studied. To our surprise, we did not observe any difference between MRI

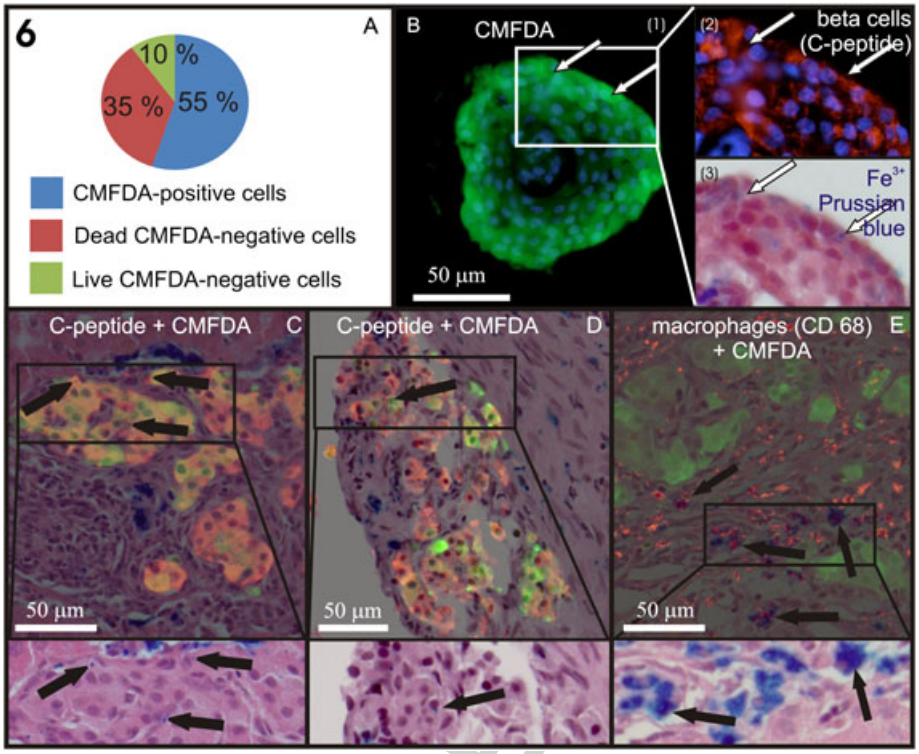

Figure 6. ▪▪

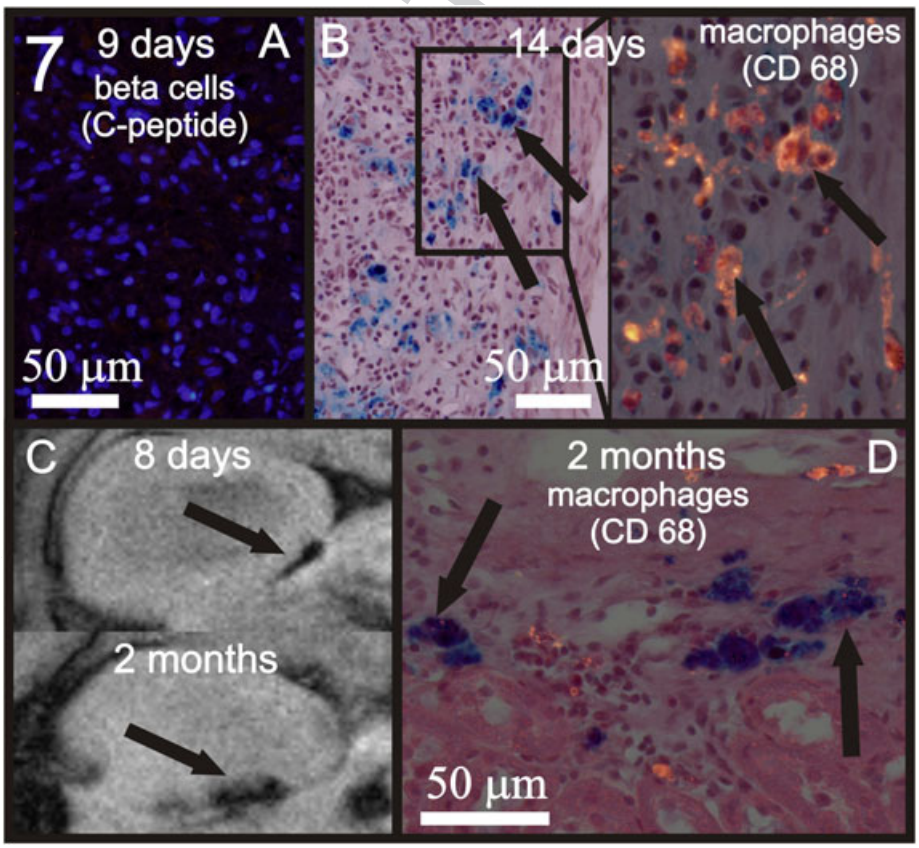

Figure 7. ▪▪

of functioning syngeneic islets and islets which were completely rejected in the allogeneic model as demonstrated by light and fluorescence microscopy. Confluent hypointense signals at the edge of the kidney remained apparent from the first MRI examination 2 days after allogeneic transplantation up to the final MRI 2 months later (Fig. 7C).

Immunofluorescence examination 9 days after allogeneic transplantation revealed numerous macrophages but no C-peptide- or glucagon-positive cells, suggesting their completed rejection (Fig. 7A). In contrast, the concentrated SPIO particles persisted *in situ* in the infiltrating macrophages (Fig. 7B) and were detected up to 2 months after transplantation (Fig. 7D). We thus conclude that MRI of transplanted SPIO-labeled islets beneath the kidney capsule is misleading, as the hypointense signals do not correlate with either islet survival or rejection. In addition, MRI detection itself at the edge of the kidney is especially difficult owing to a chemical shift effect that is typical for the interface of different tissue types (25).

2.5. In portal transplantation, islet rejection results in SPIO particle clearance

Currently, the liver represents the only site for clinical islet transplantation with consistent results, and serial MRI monitoring of labeled islets in the liver area is a promising tool for early diagnosis of rejection. Pilot studies in humans showed that islet-related spots were visible on MRI liver scans for as long as the islets were functioning (12,13), and experimental data suggested that the number of islet-related MRI signals in the liver markedly decreased prior to complete islet rejection after allogeneic transplantation (35). An islet-related hypointense signal could, however, decrease owing to other factors such as spontaneous SPIO particle translocation and metabolization. SPIO particles might also persist *in situ* despite rejection, as we found in the case of islet transplantation beneath the renal capsule and as suggested recently by Marzola *et al*. (22). Our results show, however, that, in contrast to the situation beneath the kidney capsule, in the liver, SPIO particles released from rejected islets do not persist in the transplant area and cannot be detected by the MRI once rejection is complete.

F8 Figure 8(A–C) shows MRI results during consecutive stages of islet rejection. Spots related to the labeled allogeneic islets transplanted into the liver observed on day 2 gradually disappeared (day 8) and were almost absent on day 13. Similar to the kidney capsule model, C-peptide- or glucagon-positive cells were not detected after day 9 (Fig. 8D). An inflammatory infiltrate rich in macrophages was observed in the vicinity of venules. Although some iron particles were still detected in histological sections by Prussian blue staining on day 9, co-localization with immunofluorescence detection revealed that iron was deposited inside macrophages (Fig. 8E). In a few cases iron was also detected in phagocytic cells around the transplant area 14 days after transplantation (Fig. 8F), but only a minimal intensity of Prussian blue staining was observed.

The very low number of iron-positive cells 14 days after allogeneic transplantation is at odds with the findings of Marzola *et al*. (22), who described the presence of the iron particles even during islet rejection. We explain this discrepancy by a different rate of rejection. In the model of Marzola *et al*. (Wistar to Sprague–Dawley rats), rejection was presumably much slower as the endocrine cells were detected even at day 29 after transplantation. Consequently, the iron particles were detected in the liver even at day 42. Also, Kriz *et al*. (35) showed a weak persisting hypointense signal on MRI in a model of a mitigated islet rejection.

In our model (Lewis to Brown Norway rats) with a rather rapid onset of islet rejection, almost all iron was eliminated from the liver after completion of islet rejection. This could be due to emigration of the macrophages from the site of rejection in the resolution-phase of inflammation (36), presumably through the lymphatic system (37–39). We speculate that, under the condition of a slower rejection process, macrophages stay *in situ* for a longer period until the allogeneic antigens are fully eliminated.

3. CONCLUSIONS

MRI allows for the easy detection of transplanted pancreatic islets previously labeled with SPIO particles. Several investigators

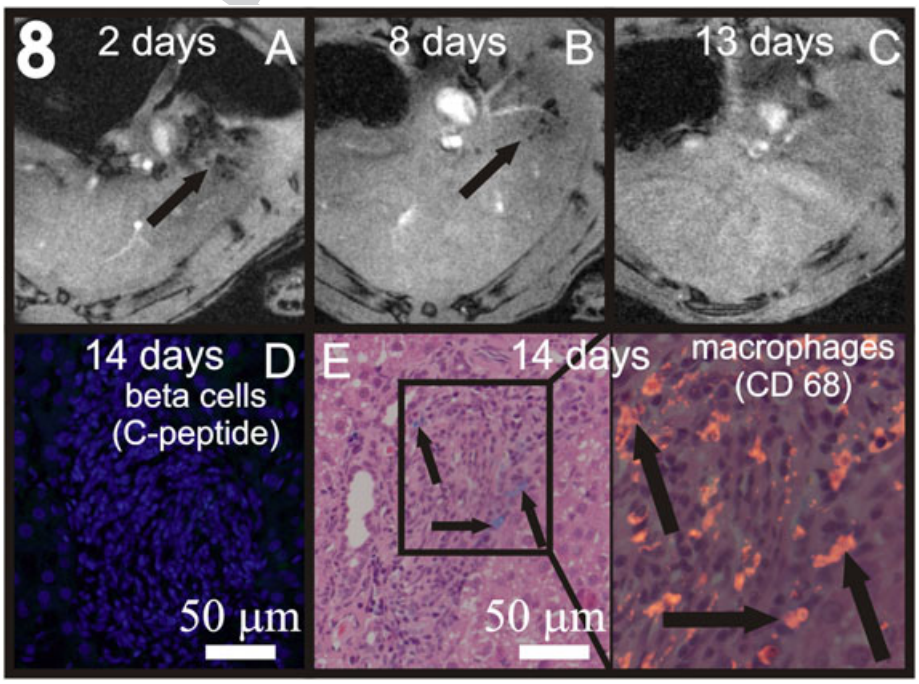

Figure 8. ▪▪

reported that, following transplantation, a portion of the SPIO particles translocate out of the endocrine cells, questioning the importance of their post-transplant monitoring for the diagnosis of rejection. We demonstrated that, by one week after transplantation, almost all iron particles were located outside of islet cells but persisted in their vicinity, mostly in host-derived macrophages. Their persistence had no relation to islet survival in the case of islet transplantation beneath the kidney capsule. MRI is therefore of no value for following their function. On the contrary, if the islets were transplanted into the liver, the SPIO-rich macrophages moved gradually out of the transplant area and were almost absent after completion of rejection. We thus conclude that, for islet transplantation into the liver, MRI monitoring has the potential to provide a timely diagnosis of rejection.

4. EXPERIMENTAL

The Ethics Committee of the Institute for Clinical and Experimental Medicine and the Ministry of Health of Czech Republic approved all animal studies. All animals were kept according to the European Convention on Animal Care.

4.1. Islet isolation and labeling

Pancreatic islets were isolated from male Lewis rats by intraductal infusion of collagenase (1 mg ml^{-1}; Sevapharma, Czech Republic). Islets were separated from exocrine tissue on a discontinuous Ficoll gradient. Isolated islets were cultivated in a humidified incubator at 37 °C and 5% CO_2 atmosphere in CMRL-1066 medium supplemented with 10% fetal calf serum, 1% HEPES and 1% penicillin–streptomycin/L-glutamine (all reagents from Sigma-Aldrich, St Louis, MO, USA).

Islet labeling was performed by 48 h culture in medium supplemented with the SPIO contrast agent ferucarbotran (Schering AG, Germany) at a dose of 5 μL ml^{-1}. Before transplantation, unattached ferucarbotran particles were washed out with Hank's salt solution (Sigma-Aldrich, St Louis, MO, USA).

4.2. Syngeneic islet transplantation

Nondiabetic Lewis rats ($n = 16$) were used as syngeneic recipients. Transplantation was performed under total anesthesia. One thousand hand-picked islets were transplanted under the kidney capsule and 2000 islets were transplanted into the portal vein. The recipients were sacrificed on days 1, 7 and 30 or 3 months after transplantation. The tissue with transplanted islets was dissected and processed for immunohistological examination and for transmission electron microscopy.

4.3. Rejection of transplanted islets

Brown Norway rats ($n = 10$) were utilized as allogeneic recipients of labeled islets. Similar to the syngeneic group, 1000 islets were transplanted under the kidney capsule and 2000 islets were transplanted into the portal vein. Most recipients were sacrificed 9 or 14 days after transplantation; two recipients were kept for 2 months for persistent MRI signal in the kidney.

4.4. Transplantation of double labeled islets

Islets labeled with ferucarbotran were subsequently labeled with CellTracker™ Green CMFDA (5-chloromethylfluorescein diacetate; Invitrogen, OR, USA). Islets were incubated in complete culture medium supplemented with 2.5 mM CMFDA for 30 min at 37 °C and subsequently in CMFDA-free medium for an additional 30 min at 37 °C. Efficiency of cell labeling was calculated by counting the number of fluorescent islet cells dissociated by Accutase (Sigma-Aldrich, St Louis, MO, USA) for 4 min at 37 °C. Live cells were counted; dead cells were differentiated by propidium iodide. Double labeled islets were transplanted into syngeneic recipients ($n = 4$) under the kidney capsule and into the portal vein. Recipients were sacrificed 7 days after transplantation.

4.5. Magnetic resonance imaging

MRI examinations of transplanted animals were performed by 4.7 T spectrometer Biospec equipped with a resonator coil (Bruker, Germany). Standard T_2*-weighted gradient echo sequences were applied (repetition time 100 ms, echo time 3.7 ms, flip angle 30°, resolution 234 × 234 μm × 2 mm, scan time 6 min 49 s). Animals were scanned under general anesthesia (passive inhalation of 1.5–2% isoflurane in air) 1 week after islet transplantation and in the week before sacrifice. Animals with allogeneic islets were examined by MRI on days 2, 8 and 13 after transplantation or after 2 months.

4.6. Histological examination

Animals were sacrificed under total anesthesia. The kidney was removed and one sample of the portion with transplanted islets was dissected and fixed in freshly prepared 4% formaldehyde for 3 h at 4 °C. Three to five representative parts were dissected from the liver with the transplanted islets and fixed in the same manner. The tissue was dehydrated and embedded in paraffin.

4.7. Immunofluorescence antigen detection

Sections of 4 μm were deparaffinized and rehydrated before immunofluorescence antigen detection. Sections were incubated in blocking solution containing 5% normal donkey serum (Jackson Immunoresearch Laboratories, West Grove, PA, USA), 0.05% Triton X-100 and 0.1 M glycine in phosphate-buffered saline (PBS) for 30 min at room temperature to prevent nonspecific binding (all reagents from Sigma-Aldrich, St Louis, MO, USA). Two sections of each tissue sample were incubated with particular primary antibodies in appropriate dilution for 30 min at 37 °C. The primary antibodies diluted in a ready-to-use solution Antibody Diluent® (Dako, Glostrup, Denmark) was used at the following dilutions: rabbit anti-C-peptide, 1:200 (Linco Research, Billerica, MA, USA); mouse anti-human glucagon, 1:200 (R&D Systems, Minneapolis, MN, USA); mouse anti-rat monocytes/macrophages – CD68, 1:100 (Millipore, Hayward, CA, USA); rabbit anti-human S100A4, 1:200 (Dako, Glostrup, Denmark); mouse anti-α smooth muscle actin, 1:1000 (Sigma-Aldrich, St Louis, MO, USA); and goat anti-collagen VI, 1:200 (Santa Cruz Biotechnology, Santa Cruz, CA, USA). After washing in PBS, sections were incubated with the specific secondary antibody diluted in the blocking solution for 30 min at 37 °C. The secondary antibodies were: Alexa Fluor 488 donkey anti-goat IgG, Alexa Fluor 555 donkey anti-mouse IgG, Alexa Fluor 488 donkey anti-mouse IgG or Alexa Fluor 555 donkey anti-rabbit IgG (all from Molecular Probes, Invitrogen, OR, USA). The sections were counterstained with 4,6-diamidino-2-phenylindole (Fluka, Sigma-Aldrich, St Louis, MO, USA) 5 μg ml^{-1} for 5 min at room temperature and mounted in solution of 1,4-diazabicyclo[2.2.2]octane and Poly-vinyl alcohol (Sigma-Aldrich, St Louis, MO, USA) in glycerol. Tissue sections were examined using an Olympus BX41

fluorescence microscope. Each islet detected on the stained sections was recorded using an Olympus DP71 digital camera (Olympus, Japan). Fifteen to 28 micro-images were examined for the particular time period according to number of islets detected on the tissue sections.

4.8. Iron detection

On the same tissue sections, subsequent detection of iron (Fe^{3+}) was performed by Prussian blue staining. The specimens were submerged in freshly prepared Prussian blue solution (2% hydrochloric acid mixed with 2% potassium ferrocyanide) for 30 min. After washing, sections were counterstained with hematoxylin and eosin (all reagents from Sigma-Aldrich, St Louis, MO, USA). The areas of sections matching with previously recorded areas were scanned. Co-localization of iron particles and immunodetected cells was performed by merging of immunofluorescence and Prussian blue staining microphotographs.

4.9. Iron removal

To uncover cell antigens hidden by excessive amount of iron particles, iron was removed from tissue sections by sodium dithionite (Sigma-Aldrich, St Louis, MO, USA). The 1% water solution of sodium dithionite was applied on one of the serial sections for 10 min at room temperature. After washing in phosphate buffer saline, the sections were processed for immunofluorescent detection of macrophages. After iron removal, sections were compared with untreated sections stained with Prussian blue.

4.10. TEM

Only selected samples were processed for TEM owing to difficulty with localization of the transplanted islets in the sample and because of the laboriousness of the method. Samples for electron microscopy were fixed overnight in a mixture of 4% formaldehyde and 2.5% glutaraldehyde in 0.1 M phosphate buffer at 4 °C, post-fixed in 1% OsO_4, dehydrated and embedded in Epon resin (all from Polysciences Inc., Warrington, PA, USA). Ultrathin sections (70–90 nm) were counterstained with uranyl acetate and lead citrate and examined in a Jeol 1010 transmission electron microscope (Jeol Tokyo, Japan) equipped with Mega View III camera (SIS, Muenster, Germany).

Acknowledgments

This study was funded by the Ministry of Health of the Czech Republic, through grant number MZO 00023001 and the research project of the Institute of Parasitology, BC ASCR Z60220518 (M.V.).

REFERENCES

1. Robertson RP. Islet transplantation as a treatment for diabetes–a work in progress. New Engl J Med 2004; 350: 694–705; doi: 10.1056/NEJMra032425
2. Shapiro AM, Lakey JR, Ryan EA, Korbutt GS, Toth E, Warnock GL, Kneteman NM, Rajotte RV. Islet transplantation in seven patients with type 1 diabetes mellitus using a glucocorticoid-free immunosuppressive regimen. New Engl J Med 2000; 343: 230–238; doi: 10.1056/NEJM200007273430401
3. Alejandro R, Barton FB, Hering BJ, Wease S. 2008 Update from the Collaborative Islet Transplant Registry. Transplantation 2008; 86: 1783–1788; doi: 10.1097/TP.0b013e3181913f6a
4. Ryan EA, Paty BW, Senior PA, Bigam D, Alfadhli E, Kneteman NM, Lakey JR, Shapiro AM. Five-year follow-up after clinical islet transplantation. Diabetes 2005; 54: 2060–2069; doi: 10.2337/diabetes.54.7.2060
5. Pileggi A, Ricordi C, Alessiani M, Inverardi L. Factors influencing Islet of Langerhans graft function and monitoring. Clin Chim Acta 2001; 310: 3–16; doi: 10.1016/S0009-8981(01)00503-4
6. Emamaullee JA, Shapiro AM. Factors influencing the loss of beta-cell mass in islet transplantation. Cell Transplant 2007; 16: 1–8.
7. Moore A. Advances in beta-cell imaging. Eur J Radiol 2009; 70: 254–257; doi: 10.1016/j.ejrad.2009.01.044
8. Fujimoto H, Toyoda K, Okitsu T, Liu X, Mukai E, Zhuang X, Uemoto S, Mochizuki N, Inagaki N. Three-dimensional ex vivo imaging and analysis of intraportal islet transplants. Transpl Int 2011; 24: 839–844; doi: 10.1111/j.1432-2277.2011.01271.x
9. Garcia A, Mirbolooki MR, Constantinescu C, Pan ML, Sevrioukov E, Milne N, Wang PH, Lakey J, Chandy KG, Mukherjee J. 18F-Fallypride PET of pancreatic islets: *in vivo* and *in vivo* rodent studies. J Nucl Med 2011; 52: 1125–1132; doi: 10.2967/jnumed.111.088583
10. Pattou F, Kerr-Conte J, Wild D. GLP-1-receptor scanning for imaging of human beta cells transplanted in muscle. New Engl J Med 2010; 363: 1289–1290; doi: 10.1056/NEJMc1004547
11. Cline GW, Zhao X, Jakowski AB, Soeller WC, Treadway JL. Islet-selectivity of G-protein coupled receptor ligands evaluated for PET imaging of pancreatic beta-cell mass. Biochem Biophys Res Commun 2011; 412: 413–418; doi: 10.1016/j.bbrc.2011.07.077
12. Toso C, Vallee JP, Morel P, Ris F, Demuylder-Mischler S, Lepetit-Coiffe M, Marangon N, Saudek F, James Shapiro AM, Bosco D, Berney T. Clinical magnetic resonance imaging of pancreatic islet grafts after iron nanoparticle labeling. Am J Transplant 2008; 8: 701–706; doi: 10.1111/j.1600-6143.2007.02120.x
13. Saudek F, Jirak D, Girman P, Herynek V, Dezortova M, Kriz J, Peregrin J, Berkova Z, Zacharovova K, Hajek M. Magnetic resonance imaging of pancreatic islets transplanted into the liver in humans. Transplantation 2010; 90: 1602–1606; doi: 10.1097/TP.0b013e3181ffba5e
14. Jirak D, Kriz J, Herynek V, Andersson B, Girman P, Burian M, Saudek F, Hajek M. MRI of transplanted pancreatic islets. Magn Reson Med 2004; 52: 1228–1233; doi: 10.1002/mrm.20282
15. Kriz J, Jirak D, Girman P, Berkova Z, Zacharovova K, Honsova E, Lodererova A, Hajek M, Saudek F. Magnetic resonance imaging of pancreatic islets in tolerance and rejection. Transplantation 2005; 80: 1596–1603; doi: 10.1097/01.tp.0000183959.73681.b9
16. Evgenov NV, Medarova Z, Dai G, Bonner-Weir S, Moore A. *In vivo* imaging of islet transplantation. Nat Med 2006; 12: 144–148; doi: 10.1038/nm1316
17. Evgenov NV, Medarova Z, Pratt J, Pantazopoulos P, Leyting S, Bonner-Weir S, Moore A. *In vivo* imaging of immune rejection in transplanted pancreatic islets. Diabetes 2006; 55: 2419–2428; doi: 10.2337/db06-0484
18. Berkova Z, Kriz J, Girman P, Zacharovova K, Koblas T, Dovolilova E, Saudek F. Vitality of pancreatic islets labeled for magnetic resonance imaging with iron particles. Transplant Proc 2005; 37: 3496–3498; doi: 10.1016/j.transproceed.2005.09.052
19. Berkova Z, Jirak D, Zacharovova K, Kriz J, Lodererova A, Girman P, Koblas T, Dovolilova E, Vancova M, Hajek M, Saudek F. Labeling of pancreatic islets with iron oxide nanoparticles for *in vivo* detection with magnetic resonance. Transplantation 2008; 85: 155–159; doi: 10.1097/01.tp.0000297247.08627.ff
20. Tai JH, Foster P, Rosales A, Feng B, Hasilo C, Martinez V, Ramadan S, Snir J, Melling CW, Dhanvantari S, Rutt B, White DJ. Imaging islets labeled with magnetic nanoparticles at 1.5 Tesla. Diabetes 2006; 55: 2931–2938; doi: 10.2337/db06-0393
21. Jirak D, Kriz J, Strzelecki M, Yang J, Hasilo C, White DJ, Foster PJ. Monitoring the survival of islet transplants by MRI using a novel technique for their automated detection and quantification. MAGMA 2009; 22: 257–265; doi: 10.1007/s10334-009-0172-4
22. Marzola P, Longoni B, Szilagyi E, Merigo F, Nicolato E, Fiorini S, Paoli GT, Benati D, Mosca F, Sbarbati A. *In vivo* visualization of transplanted pancreatic islets by MRI: comparison between *in vivo*, histological and electron microscopy findings. Contrast Media Mol Imag 2009; 4: 135–142; doi: 10.1002/cmmi.274
23. Kim HS, Kim H, Park KS, Moon WK. Evaluation of porcine pancreatic islets transplanted in the kidney capsules of diabetic mice using a clinically approved superparamagnetic iron oxide (SPIO) and a 1.5T MR scanner. Korean J Radiol 2010; 11: 673–682; doi: 10.3348/kjr.2010.11.6.673

24. Malosio ML, Esposito A, Poletti A, Chiaretti S, Piemonti L, Melzi R, Nano R, Tedoldi F, Canu T, Santambrogio P, Brigatti C, De Cobelli F, Maffi P, Secchi A, Del Maschio A. Improving the procedure for detection of intrahepatic transplanted islets by magnetic resonance imaging. Am J Transplant 2009; 9: 2372–2382; doi: 10.1111/j.1600-6143.2009.02791.x
25. Weinreb JC, Brateman L, Babcock EE, Maravilla KR, Cohen JM, Horner SD. Chemical shift artifact in clinical magnetic resonance images at 0.35 T. AJR Am J Roentgenol 1985; 145: 183–185.
26. Kriz J, Jirak D, White D, Foster P. Magnetic resonance imaging of pancreatic islets transplanted into the right liver lobes of diabetic mice. Transplant Proc 2008; 40: 444–448; doi: 10.1016/j.transproceed.2008.02.018
27. Desmouliere A, Darby IA, Gabbiani G. Normal and pathologic soft tissue remodeling: role of the myofibroblast, with special emphasis on liver and kidney fibrosis. Lab Invest 2003; 83: 1689–1707; doi: 10.1097/01.LAB.0000101911.53973.90
28. Lillie RD, Geer JC, Gutiérrez A. The removal of histochemically demonstrable iron from tissue sections by brief exposure to sodium dithionite solution. J Histochem Cytochem 1963; 11: 662–664; doi: 10.1177/11.5.662
29. Jiao Y, Peng ZH, Xing TH, Qin J, Zhong CP. Assessment of islet graft survival using a 3.0-Tesla magnetic resonance scanner. Anat Rec (Hoboken) 2008; 291: 1684–1692; doi: 10.1002/ar.20770
30. Weissleder R, Stark DD, Engelstad BL, Bacon BR, Compton CC, White DL, Jacobs P, Lewis J. Superparamagnetic iron oxide: pharmacokinetics and toxicity. AJR Am J Roentgenol 1989; 152: 167–173.
31. Arbab AS, Wilson LB, Ashari P, Jordan EK, Lewis BK, Frank JA. A model of lysosomal metabolism of dextran coated superparamagnetic iron oxide (SPIO) nanoparticles: implications for cellular magnetic resonance imaging. NMR Biomed 2005; 18: 383–389; doi: 10.1002/nbm.970
32. Pawelczyk E, Jordan EK, Balakumaran A, Chaudhry A, Gormley N, Smith M, Lewis BK, Childs R, Robey PG, Frank JA. *In vivo* transfer of intracellular labels from locally implanted bone marrow stromal cells to resident tissue macrophages. PLoS One 2009; 4: e6712; doi: 10.1371/journal.pone.0006712
33. Lepore AC, Walczak P, Rao MS, Fischer I, Bulte JW. MR imaging of lineage-restricted neural precursors following transplantation into the adult spinal cord. Exp Neurol 2006; 201: 49–59; doi: 10.1016/j.expneurol.2006.03.032
34. Terrovitis J, Stuber M, Youssef A, Preece S, Leppo M, Kizana E, Schar M, Gerstenblith G, Weiss RG, Marban E, Abraham MR. Magnetic resonance imaging overestimates ferumoxide-labeled stem cell survival after transplantation in the heart. Circulation 2008; 117: 1555–1562; doi: 10.1161/circulationaha.107.732073
35. Kriz J, Jirak D, Berkova Z, Herynek V, Lodererova A, Girman P, Habart D, Hajek M, Saudek F. Detection of pancreatic islet allograft impairment in advance of functional failure using magnetic resonance imaging. Transpl Int 2012; 25: 250–260; doi: 10.1111/j.1432-2277.2011.01403.x
36. Wyburn KR, Jose MD, Wu H, Atkins RC, Chadban SJ. The role of macrophages in allograft rejection. Transplantation 2005; 80: 1641–1647; doi: 10.1097/01.tp.0000173903.26886.20
37. Bellingan GJ, Xu P, Cooksley H, Cauldwell H, Shock A, Bottoms S, Haslett C, Mutsaers SE, Laurent GJ. Adhesion molecule-dependent mechanisms regulate the rate of macrophage clearance during the resolution of peritoneal inflammation. J Exp Med 2002; 196: 1515–1521; doi: 10.1084/jem.20011794
38. Serhan CN, Savill J. Resolution of inflammation: the beginning programs the end. Nat Immunol 2005; 6: 1191–1197; doi: 10.1038/ni1276
39. Bystrom J, Evans I, Newson J, Stables M, Toor I, van Rooijen N, Crawford M, Colville-Nash P, Farrow S, Gilroy DW. Resolution-phase macrophages possess a unique inflammatory phenotype that is controlled by cAMP. Blood 2008; 112: 4117–4127; doi: 10.1182/blood-2007-12-129767

** Figures legend:

Figure 1. Magnetic resonance images of SPIO-labeled islets transplanted in the syngeneic models A) under the kidney capsule and B) in the liver. White arrows point to hypointense area at the edge of the kidney and dispersed hypointense spots in the liver persisting after syngeneic islet transplantation. The time period of the MRI after transplantation is indicated in the figure.

Figure 2. One day after syngeneic transplantation of labeled islets under the kidney capsule and/or in the liver. A) Iron particles were detected inside (black arrows) and outside (white arrows) beta cells (liver); B) TEM showed iron particles among cell debris (kidney); C) A few iron particle were detected also in myofibroblasts (kidney) and D) fibroblast (kidney); E) The most of the iron was detected in macrophages (kidney). Legend for immunohistological images: red fluorescence - immunodetected antigens indicated in the figure, blue - Prussian blue reaction for detection of Fe^{3+}, counterstained with hematoxylin and eosin.

Figure 3. One week after syngeneic transplantation of labeled islets under the kidney capsule. A) Iron particles were detected rather outside (white arrow) than inside the beta cells (black arrow); B) TEM revealed only small iron deposits in the beta cells (arrow in enlarged area); C) TEM revealed iron (arrow) deposited in macrophages and D) fibroblasts producing collagen (arrowhead); E) immunofluorescence and histological detection showed iron deposits (white arrows) in the proximity of the myofibroblasts; F) Iron particles (arrow in enlarged area) were found also in other cells surrounding the islets as in the endothelial cells at the TEM image. Legend for immunohistological images: red fluorescence - immunodetected antigens indicated in the figure, blue - Prussian blue reaction for detection of Fe^{3+}, counterstained with hematoxylin and eosin.

Figure 4. One month after syngeneic transplantation of labeled islets under the kidney capsule and/or in the liver. A) TEM photo of macrophages storing the iron particles (arrows) (kidney); B) Serial sections of the transplant area with no immunofluorescent signal (1) in the iron storing cells (2) and identification of macrophages after removal of iron by sodium dithionite (3), the arrows show matching area (liver); C) Collagen around the iron containing cells at the transplant site (kidney). Legend for immunohistological images: red fluorescence - immunodetected antigens indicated in the figure, blue fluorescence - nuclei counterstained with DAPI, green fluorescence - immunodetected collagen, blue - Prussian blue reaction for detection of Fe^{3+}, counterstained with hematoxylin and eosin.

Figure 5. Three months after syngeneic transplantation of labeled islets under the kidney capsule and/or in the liver. A) Only few iron particles were detected in beta cells (arrows in enlarged image of the marked area) (kidney); B) Iron was rarely found in the alpha cells (arrows in enlarged image of the marked area) (kidney); C) Iron was still deposited (arrows) in the macrophages (kidney) and D) few particles (arrows) were found in the fibroblasts (liver). Legend: red fluorescence - immunodetected antigens indicated in the figure, blue - Prussian blue reaction for detection of Fe^{3+}, counterstained with hematoxylin and eosin.

Figure 6. Tranpslantation of double labeled syngeneic islets. A) Diagram of the CMFDA labeling efficiency; In vitro - B) isolated islet labeled with SPIO particles and CMFDA - (1) green fluorescence of CMFDA, (2) red fluorescence of C-peptide detecting antibody and (3) Prussian blue staining of iron on hematoxylin-eosin-counterstained section. After islet transplantation the iron particles were rarely detected inside the CMFDA labeled cells. The iron was rather in proximity of CMFDA cells. C) Rare iron particles were detected in C-peptide- and CMFDA- double positive cells in the liver (arrows in marked area and its enlarged image) and D) the same situation was observed in the kidney; E) Iron deposits were detected mainly in the CMFDA negative macrophages (arrows in marked area and its enlarged image) (kidney). Legend: red fluorescence - immunodetected antigens indicated in the figure, green fluorescence - CMFDA, blue fluorescence - nuclei counterstained with DAPI, blue - Prussian blue reaction for detection of Fe^{3+}, counterstained with hematoxylin and eosin.

Figure 7. Transplantation of allogeneic islets labeled with SPIO particles beneath the kidney capsule. A) Beta cells were not detected by immunofluorescence since 9 days after transplantation. B) The iron deposits (arrows in marked area and its enlarged image) were detected in the macrophages even after islet rejection (9 days after transplantation); C) The SPIO particles (arrow) were imaged under the kidney capsule 8 days and even 2 months after allogeneic islet transplantation by MRI as well as D) by histochemical Prussian blue staining (arrows). Legend for immunohistological images: red fluorescence - immunodetected antigens indicated in the figure, blue fluorescence - nuclei counterstained with DAPI, blue - Prussian blue reaction for detection of Fe^{3+}, counterstained with hematoxylin and eosin.

Figure 8. Transplantation of allogeneic islets labeled with SPIO particles in the liver. A) Transplanted islet-related spots (arrows) were detected by MRI in the liver 2 days and B) 8 days but not C) 13 days after transplantation; D) Beta cells were not detected in the liver since day 9 and E) the amount of iron stored in macrophages (arrows in marked area and its enlarged image) was diminished at day 14. Legend for immunohistological images: red fluorescence - immunodetected antigens indicated in the figure, blue fluorescence - nuclei counterstained with DAPI, blue - Prussian blue reaction for detection of Fe^{3+}, counterstained with hematoxylin and eosin.

PŘÍLOHA IV.

Dual imaging probes for magnetic resonance imaging and fluorescence microscopy based on perovskite manganite nanoparticles

M. Kačenka, O. Kaman, J. Kotek, L. Falteisek, J. Černý, D. Jirák, V. Herynek, K. Zacharovová, Z. Berková, P. Jendelová, J. Kupčík, E. Pollert, P. Veverka, and I. Lukeš

Journal of Materials Chemistry, 2011. 21(1): p. 157-164

Journal of Materials Chemistry

Dynamic Article Links

Cite this: J. Mater. Chem., 2011, 21, 157

www.rsc.org/materials

PAPER

Dual imaging probes for magnetic resonance imaging and fluorescence microscopy based on perovskite manganite nanoparticles†

Michal Kačenka,[a] Ondřej Kaman,*[b] Jan Kotek,[a] Lukáš Falteisek,[c] Jan Černý,[c] Daniel Jirák,[d] Vít Herynek,[d] Klára Zacharovová,[d] Zuzana Berková,[d] Pavla Jendelová,[e] Jaroslav Kupčík,[f] Emil Pollert,[b] Pavel Veverka[b] and Ivan Lukeš[a]

Received 29th April 2010, Accepted 4th September 2010
DOI: 10.1039/c0jm01258k

The present study reveals the potential of magnetic nanoparticles based on the $La_{0.75}Sr_{0.25}MnO_3$ perovskite manganite for magnetic resonance imaging (MRI). Moreover, it describes the development of the dual imaging probe where the magnetic cores are combined with a fluorescent moiety while the improved colloidal stability is achieved by a two-ply silica shell. At first, the magnetic cores of $La_{0.75}Sr_{0.25}MnO_3$ are coated with a hybrid silica layer, comprising a covalently attached fluorescein moiety that is subsequently covered by a pure silica layer providing the enhanced stability. The detailed characterization of the intermediate and the final product reveals the importance of the complex two-ply shell. Viability tests show that the complete particles are suitable for biological studies. Internalization of the particles and their presence in intracellular vesicles are observed by fluorescence microscopy in different cell types. Further experiments prove no fatal interference with the vitality and insulin releasing ability of labeled pancreatic islets. Relaxometric measurements confirm high spin–spin relaxivities at magnetic fields of $B_0 = 0.5$–3 T, while visualisation of *in vitro* labeled pancreatic islets by MRI is successfully tested.

1. Introduction

Magnetic resonance imaging (MRI) represents a powerful imaging method commonly utilized in clinical practice. The resolution reached is close to 1 mm^3 with contemporary MRI clinical scanners, and resolution on the cellular level was demonstrated in a laboratory experimental setup.[1] Thus, the method is very suitable not only for examination of human bodies but also for detailed anatomical studies of animal models *in vivo* in biological research.

Although MRI itself is very efficient, the utilization of a contrast agent (CA) can further improve the resolution and informative content of the obtained images. From the physical point of view, there are two major families of CAs classified according to the relaxation process they predominantly accelerate.[2] Whereas T_1-CAs induce a positive contrast, *i.e.* a ^1H NMR signal of the affected tissue increases, compounds affecting the T_2 relaxation cause lowering of a local proton signal and, thus, they show a "negative enhancement" pattern.[3] From the chemical point of view, T_1-CAs are complexes of paramagnetic metal ions, such as Gd(III) or Mn(II), with suitable organic ligands. On the other hand, T_2-CAs, developed slightly later, are based on magnetic nanoparticles, at present predominantly iron oxide nanoparticles. Basically, they consist of magnetite (Fe_3O_4) or maghemite cores (γ-Fe_2O_3) of various sizes ranging from several nanometres to several tens of nanometres covered by *e.g.* dextrans or polysiloxanes. Hence, their overall size reaches several tens to several hundreds of nanometres. In clinical practice, the iron oxides nanoparticles are used as blood-pool and more recently as organ-specific CAs.[4,5]

Even though the clinical use of T_2-CAs is not so wide-spread as the use of T_1-CAs, research in this field has continued because of their exceptional efficiency for high field MRI scanners.[4] This is the reason why other nanomaterials exhibiting tunable magnetic properties and extraordinary relaxometric properties have been introduced.[6] Among these, the most important are the complex oxide nanoparticles (ferrites,[7] manganites[8,9]) and the metallic

[a]*Department of Inorganic Chemistry, Faculty of Science, Charles University, Albertov 6, 128 43 Praha 2, Czech Republic*
[b]*Institute of Physics AS CR, Cukrovarnická 10, 162 53 Praha 6, Czech Republic. E-mail: kamano@seznam.cz; Tel: +420 220 318 418*
[c]*Department of Cell Biology, Faculty of Science, Charles University, Albertov 6, 128 43 Praha 2, Czech Republic*
[d]*Institute of Clinical and Experimental Medicine, Vídeňská 1958, 140 21 Praha 4, Czech Republic*
[e]*Institute of Experimental Medicine AS CR, Vídeňská 1083, 142 40 Praha 4, Czech Republic*
[f]*Institute of Inorganic Chemistry AS CR, Řež u Prahy, 250 68, Czech Republic*

† Electronic supplementary information (ESI) available: Detailed experimental section (description of characterization methods settings, preparation of starting materials, biological experiments), additional figures mentioned within the text. See DOI: 10.1039/c0jm01258k

nanoparticles (Fe,[10] FePt,[11] FeCo[12]) but the utilization of the latter is limited due to their high chemical reactivity.

As mentioned above, MRI shows excellent spatial resolution; on the other hand, the sensitivities of other techniques, such as optical methods, single-photon emission computed tomography (SPECT) or positron emission tomography (PET), are much higher. Thus, the design and synthesis of so called dual or multimodal probes is an important field. The combination of both respective approaches utilizing only one dual probe, *e.g.* magnetic nanoparticles tagged with fluorescent moieties, establishes a very useful method for bioimaging. Such an application enables efficient cellular labeling *in vitro* followed by *in vivo* tracking of the cells implanted into the organism.[13]

Moreover, fluorescent magnetic nanoparticles are promising materials for other medical applications, where the same tool might be used either for diagnostics or for therapy, like for magnetic hyperthermia and optically driven surgery. The positioning of the magnetic cores with the external magnetic field could be used in cell micromanipulation.[14,15]

While bare magnetic nanoparticles exhibit neither sufficient colloidal stability in water nor fluorescent properties, it is necessary to introduce some surface coating able to tag a fluorescent agent and to provide solubilization and biocompatibility of the whole particles. Bifunctional low-molecular compounds possessing strong affinity to the surface of particles and simultaneously a highly hydrophilic moiety (*e.g.* dimercaptosuccinic acid, citric acid) seems to be the simplest way to meet these requirements. However, surface modification by biopolymers (*e.g.* dextran, chitosan), synthetic polymers (*e.g.* polyethyleneglycol, polyvinylalcohol) or a silica layer represents a genuine coating provided that the surface layer is stable and tightly attached. Consequently, such a shell protects the magnetic core from the surrounding biological environment and *vice versa*.[6,16] The fluorescent agents employed in the composite nanoparticle architecture involve mainly organic fluorescent dyes (*e.g.* fluorescein, rhodamine),[17] lanthanide and transition metal complexes covalently attached to the coating material,[18,26] or nanoparticle devices like CdSe quantum dots,[19] carbon nanotubes,[20] *etc*. In spite of the mentioned potential of dual probes, their development is still in the early stages. Only very few publications have been dealing with the preparation of fluorescent magnetic particles, that were tested either *in vitro* or *in vivo*, thus proving they are suitable for biological and biomedical utilization, and simultaneously such particles that are based on other magnetic cores than iron oxides.[14,18]

The present study reports on the preparation and properties of new fluorescent magnetic nanoparticles based on the perovskite manganite $La_{1-x}Sr_xMnO_3$ (LSMO) where $x = 0.25$ that are coated by a double silica layer. The magnetic properties (*i.e.* magnetization and Curie temperature) of LSMO nanoparticles may be efficiently tuned by varying both the compositional parameter x (describing the level of hole doping of the mother phase $LaMnO_3$) and the particle size.[21,22] The LSMO nanoparticles are promising mediators for magnetically induced hyperthermia due to the self-controlled heating efficiency ruling out the risk of local overheating.[22] However, bare LSMO nanoparticles are neither colloidally stable in water nor acceptable for biological applications and thus a surface coating has to be employed. Encapsulation into silica was successfully used to prepare colloidally stable hybrid nanoparticles possessing high magnetization, heating efficiency and low toxicity.[9,23] Bhayani *et al.* reported also low toxicity for LSMO ($x = 0.3$) encapsulated in dextran or coated by bovine serum albumin.[24] More recently, a detailed study of relaxometric properties of silica coated LSMO nanoparticles performed by our group has shown substantial r_2 relaxivity far exceeding the relaxivities of iron oxides.[9]

In order to extend the possible applications of these particles, the present report describes the preparation of LSMO ($x = 0.25$) nanoparticles coated by a double silica layer containing fluorescein moieties covalently attached to the inner layer. The size and morphology of the prepared particles are investigated by transmission electron microscopy (TEM) and photon correlation spectroscopy (PCS). The silica layer is characterized by means of ζ-potential measurements, infrared (IR) and luminescence spectroscopies. The properties important for contrast agents are investigated using relaxometric techniques accompanied by SQUID magnetometry, while the fluorescence microscopy used in biological experiments evaluates the suitability of the nanoparticles for intended applications.

2. Experimental section

The overall preparation of nanoparticles is depicted in Scheme 1.

2.1. Synthesis of starting materials

The LSMO nanoparticles with mean size of crystallites $d_{XRD} =$ 20 nm were prepared according to the previously described procedure[9,22,23] from starting materials with chemically determined contents of cations *via* the sol–gel technique employing citric acid and ethylene glycol. Evaporation, drying, calcination and annealing of the reaction mixture were followed by mechanical treatment of the crude solid product. Fluorescent alkoxysilane (FITC-APS) was prepared by addition reaction of fluorescein isothiocyanate (FITC) and 3-aminopropyltriethoxysilane (APS) in anhydrous ethanol. For a more detailed description see ESI.†

2.2. Primary coating of LSMO nanoparticles with a fluorescent layer (LSMO@siF)

Polyvinylpyrrolidone PVP K25 (3.67 g) was dissolved in water (380 mL) and the solution was placed in an ultrasound bath. Its temperature was stabilized at 25–30 °C. The LSMO particles (200 mg) were dispersed in water (20 mL) and treated with a powerful ultrasound probe for 1 h. This suspension was added dropwise to the PVP solution and the mixture was left in the ultrasound bath for 20 h. Then, the LSMO nanoparticles were separated *via* centrifugation (7500 rpm, 55 min, $r = 10.4$ cm) and washed with ethanol (25 mL) using ultrasound redispersion followed by separation *via* centrifugation (7500 rpm, 65 min, $r =$ 10.4 cm). Finally, the nanoparticles were redispersed in ethanol (400 mL) in a round-bottomed flask equipped with a mechanical stirrer and placed in the ultrasound bath heated at about 40 °C. Tetraethoxysilane (TEOS) (167 μL, 745 μmol) and the FITC-APS product (the whole reaction mixture obtained from 74.5 μmol of the starting APS) were added. After 5 min of stirring ammonia (64 mL) was added. The mixture was further stirred both mechanically and *via* ultrasound in the dark for ≈8 h. The

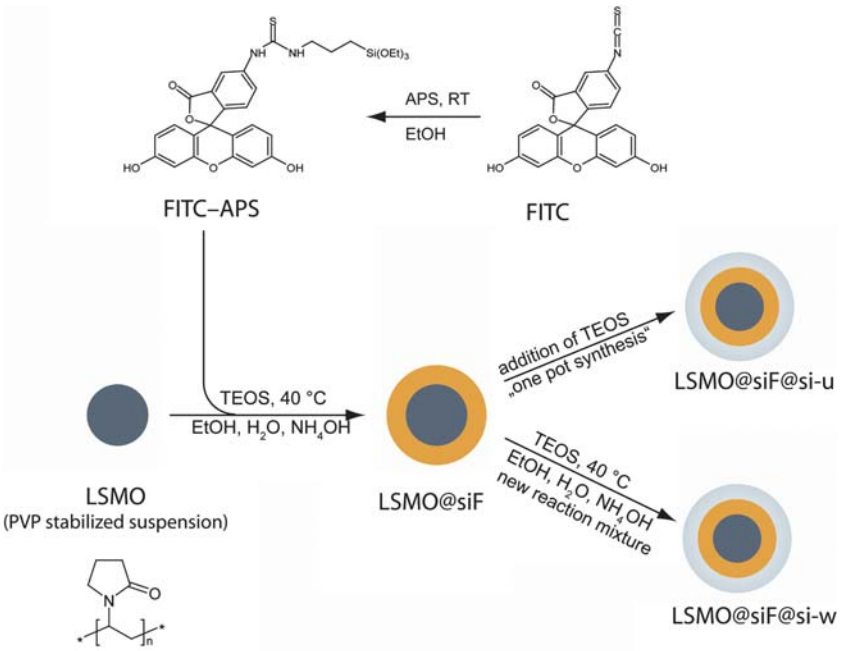

Scheme 1 Preparation scheme of fluorescent nanoparticles.

possible isolation of the LSMO@siF particles involved centrifugation of the mixture, purification of the residue by four washing cycles in ethanol and finally redispersion of the particles in isopropanol.

2.3. Secondary coating of fluorescent nanoparticles (LSMO@siF@si)

Secondary coating immediately followed the fluorescent silica layer formation and two different procedures were applied. The basic procedure (preparation of LSMO@siF@si-u) was effected by the addition of TEOS (167 μl, 745 μmol) directly into the original mixture approximately 8 h after the first step described above and the reaction mixture was kept under the same conditions for the next 12 h.

The other method (preparation of LSMO@siF@si-w) employed gentle separation of LSMO@siF by centrifugation (4000 rpm, 70 min, $r = 10.4$ cm), followed by a washing cycle in ethanol. The solid residue was redispersed in the new reaction mixture (400 mL of ethanol and 64 mL of ammonia) and TEOS (167 μL, 745 μmol) was added. The ultrasound irradiation was terminated after 5 min and then reaction mixture was stirred mechanically for 12 h in the dark at ≈40 °C. Both products were collected *via* centrifugation (6000 rpm, 40 min, $r = 8.5$ cm) and washed three times with ethanol and three times with water. In both cases, the heavy fractions were removed by gentle centrifugation (3000 rpm, 15 min, $r = 8.5$ cm) of their diluted water suspensions, while final products were isolated from the corresponding supernatants and redispersed in water (50 mL). In order to remove residual ethanol, that could negatively affect biological studies, the suspensions were treated in a vacuum drier at 35 °C for 1 h. Thereafter the products were drained from the beakers without the material deposited on the walls. The overall yield of the final fraction was typically 10–15%.

2.4. Biological experiments

HeLa cells, human normal skin fibroblasts and rMSCs were incubated in DMEM based medium containing various concentrations of product. After 48 h, the vitality of tested cells was determined by means of flow cytometry (HeLa cells and fibroblasts) or counting stained cells in a Bürker chamber (rMSCs). The amount of internalized nanoparticles was determined by measuring the fluorescence intensity of the cells in the FITC channel during flow cytometry. Internalization of nanoparticles was investigated by fluorescence microscopy.

Rat pancreatic islets (PIs) were incubated for 24 h in CMRL-1066 medium containing the product at a concentration corresponding to 0.11 mmol(Mn) L^{-1}. The vitality of labeled PIs was determined by counting dead cells under the fluorescence microscope in distinct islets after counterstaining with acridine orange and propidium iodide. The ability to produce insulin was tested using a static incubation technique. The uptake of nanoparticles into PIs was investigated by means of immunofluorescence detection employing fluorescent dye tagged antibodies for distinguishing different cell types within the islet. Gel samples of labeled PIs were prepared for visualization in the 4.7 T MRI device. For a more detailed description see ESI.†

3. Results and discussion

3.1. Synthesis and basic characterizations

The LSMO nanoparticles were prepared employing the described procedure based on the citrate method, followed by annealing at high temperature and mechanical processing necessary for separation of individual nanoparticles.[22] The first coating step represents the modified PVP method that utilizes the adsorption of polyvinylpyrrolidone on the particles providing the colloidal stability and enabling facile growth of silica on the seeds.[25] In

order to select the optimal length of PVP chain, three different PVP of M_r = 10 000, 24 000 and 360 000 were tested. For the selected LSMO particles with the mean size of crystallites d_{XRD} = 20 nm the best colloidal stability was observed in case of PVP with M_r = 24 000.[9] The washing cycle after the LSMO stabilization is crucial for removal of the excess of PVP, otherwise the silica formation could occur not only on LSMO seeds but also directly on free polymer molecules. The actual coating procedure, employing both tetraethoxysilane (TEOS) and the fluorescent alkoxysilane, was carried out similarly to the preparation of functionalized magnetite nanoparticles by Wu *et al.*[26] In our case, the addition reaction of APS and fluorescein isothiocyanate, leading to *N*-1-(3-triethoxysilylpropyl)-*N'*-fluoresceinyl thiourea, did not run completely under the given conditions. Moreover the separation of the prepared alkoxysilane from the reaction mixture would be complicated due to its hydrolytic instability. Therefore, instead of the pure product, the raw reaction mixture was used and thus the particles of LSMO@siF were coated by a hybrid silica shell composed of a silica frame, fluorescein moieties covalently attached *via* thiourea bridges and free 3-aminopropyl groups originating from the unreacted APS. The product do not form colloidally stable suspensions in water in contrast to nanoparticles coated with pure silica, probably mainly due to hydrophobic interactions and low coulombic repulsion of the nanoparticles under neutral pH (see ζ-potential in Fig. 1). The aggregation and sedimentation of LSMO@siF occur in water in a few hours. Finally, fluorescein leaching causes gradual coloration of the supernatant of the dispersion, although extensive washing of the product was carried out before storage and no traces of fluorescein in the supernatant were observed after the original purification.

The preparation of FITC derivatized silica and silica coated nanoparticles is widely reported in the literature, but only a few studies discuss the colloidal stability in detail. Generally, different ratios of fluorescein, APS and TEOS are used, but mostly relatively small amounts of the dye that hardly influences the stability of the suspension. Nevertheless, a similar lack of colloidal stability in the case of the surface layer containing fluorescein was also described.[27]

Therefore the LSMO@siF nanoparticles were subsequently coated in the additional step by a thin secondary silica layer prepared from TEOS. Two different approaches, the first being the formation *in situ* after the first coating step, and the second one involving the separation and purification of LSMO@siF followed by encapsulation in the new reaction mixture, were tested. The single-vessel preparation of the product LSMO@siF@si-u (the intermediate LSMO@siF was not isolated) is facile in comparison to more elaborate work leading to the latter one LSMO@siF@si-w (the intermediate LSMO@siF was washed prior to the next reaction step), but the latter definitely exhibits much higher stability. Simple observation of water suspensions showed that LSMO@siF@si-u is stable in water for approximately one week, after which sedimentation occurs, in contrast to LSMO@siF@si-w providing suspensions which are stable for much longer periods. Furthermore, the fluorescein is partially released to the supernatant of the LSMO@siF@si-u suspension after approximately one week whereas no fluorescein leaching was observed for LSMO@siF@si-w during several weeks of storage. As can be seen in Fig. 1, the ζ-potential dependences on pH differ for these samples, as well. The isoelectric point *IEP* of LSMO@siF@si-w is ≈4.5, whereas the *IEP* of LSMO@siF@si-u, being ≈5.5, is the same as for the intermediate product LSMO@siF. A comparison of the product LSMO@siF@si-u and LSMO@siF indicates similar acidobasic surface properties given by the free amino groups. The *IEP* of LSMO@siF@si-w is still not equal to the value reported for pure silica nanoparticles (*IEP* = 2.9 found for particles prepared by the Stöber process at 40 °C)[28] or pure silica coated LSMO particles (*IEP* = 3.5),[23] but the colloidal behaviour of its suspension is sufficient for the intended studies. The PCS measurement of a fresh LSMO@siF@si-u sample and the LSMO@siF@si-w product evidenced their colloidal stabilities in water and showed reasonable distributions of the hydrodynamic sizes (see Fig. S3 in ESI†) with the mean values d_{hydro} = 147 nm and 153 nm, respectively. The differences between the size distributions of the samples are not significant taking into account the uncertainties and repeatability of determination and sample preparation, but the nanoparticles seem to be larger and exhibit a broader distribution than the silica coated LSMO nanoparticles of the same d_{XRD} covered by an approximately 20 nm thick silica shell, for which $d_{hydro,50}$ = 135 nm was reported in the previous study.[23] Nevertheless, the particles coated with pure silica were measured by Photon Cross Correlation Spectroscopy (PCCS) eliminating the multiple scattering and thus providing lower values than PCS. On the other hand, the more complex preparation of fluorescent magnetic particles LSMO@siF@si could lead to a broader size distribution. Besides the hydrodynamic size, the mean size of manganite crystallites in LSMO@siF@si-u and LSMO@siF@si-w was determined to be almost the same, 26 and 25 nm respectively, which is larger by 5–6 nm than the mean value found for the starting LSMO nanoparticles. Its increase is an expected consequence of the size fractionation that occurred mainly during separation of LSMO particles from the PVP solution, when the exhaustive centrifugation was not carried out thus the lightest fraction of the nanoparticles (the smallest fragments from mechanical processing) was removed with the supernatant.

The morphology of all three products was checked by TEM and HRTEM studies (see Fig. 2). The image analysis of the TEM data employing the spherical approximation provided the silica shell thickness of ≈11 nm for LSMO@siF and revealed its

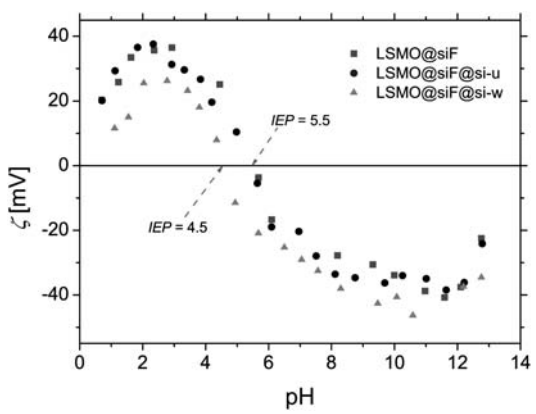

Fig. 1 The pH dependence of ζ-potential for the intermediate and both the final products.

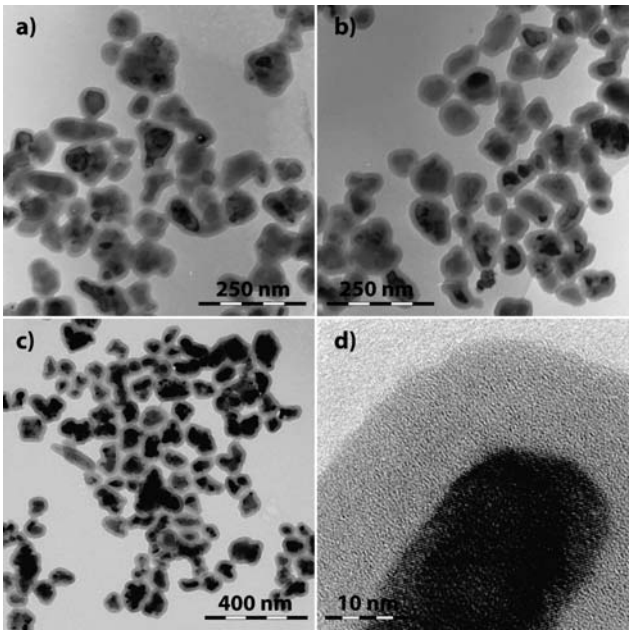

Fig. 2 TEM images of a) the intermediate product LSMO@siF and both the final products: b) LSMO@siF@si-u and c,d) LSMO@siF@si-w.

increase by ≈5 nm during the secondary encapsulation. The overall diameter of LSMO@siF@si-u was estimated to be $d_{TEM} = 89$ (19) nm, while the diameter of the manganite core was found to be 57 (17) nm, *i.e.* it is significantly larger than the d_{XRD} value (see also Fig. 2). It implies that besides the single manganite cores the particles consist of connate crystallites not broken during the mechanical treatment, eventually of physically aggregated crystallites (see Fig. S4 in ESI†). Almost the same results were obtained for LSMO@siF@si-w. The employed spherical approximation remains controversial due to the broad distribution of core shapes and thus the calculated parameters need not describe the actual dimensions precisely. However, for the coated products with the same type of core these results enable a relative comparison of the shell thicknesses and the overall sizes, providing also their rough estimations.

The IR spectra (see Fig. S5 in ESI†) were recorded for both the final and the intermediate products and in addition for the nanoparticles obtained by the encapsulation employing TEOS and APS (LSMO@siA)[9] in order to unambiguously resolve the origin of the bands. The spectra of all these samples show four absorptions bands typical for hydrated silica with silanol groups. The maxima at around 1100, 945, 800 and 470 cm^{-1} are given by the asymmetric stretching vibration of Si–O–Si, the bending of silanol groups, the symmetric stretching vibration of Si–O–Si and its bending vibration, respectively.[29] The band of the asymmetric stretching vibration ν_{as}(Si–O–Si) is more or less divided into two components as a consequence of transverse optical–longitudinal optical (TO–LO) splitting observed for both the crystalline and vitreous SiO_2.[30] The transverse optical vibrational mode occurs at lower energies while the longitudinal optical mode manifests at higher wavenumbers as a shoulder or even a separate maximum. The intermediate product LSMO@siF exhibits other band, not observable in the IR spectra of the final products due to the shielding effect of the whole shell or its top silica layer. Namely the band found at ≈615 cm^{-1} corresponds to MnO_6 octahedra[31] and its wavenumber is characteristic for LSMO nanoparticles.[23] The weak bands at 1480 and 1380 cm^{-1} are connected with the organic moiety of APS, as is obvious from the comparison to the LSMO@siA spectrum. Probably, the first band corresponds to the symmetric deformation mode[32] of NH_3^+ and the latter to the scissoring of CH_2.[33]

3.2. LSMO@siF@si as a dual imaging probe

The relaxometric study of LSMO@siF@si-w at 20 °C carried out at magnetic fields of $B_0 = 0.5$, 1.5 and 3 T provided similar values of r_2 = 580, 540 and 520 s^{-1} $mmol(Mn)^{-1}$ L, respectively, far exceeding the relaxivities reported for clinically used iron oxide nanoparticles.[5] These values belong to the highest ever reported r_2 relaxivities of experimental CAs. The dependence of $r_2(B_0 =$ 0.5 T) on temperature T in Fig. 3 indicates its decrease with increasing T that can be explained by a gradual diminution of the magnetization occurring as T approaches the Curie temperature $T_C = 340$ K, determined on the dry sample of LSMO@siF@si-w. Therefore the relaxivity at human body temperature is $r_2(B_0 =$ 0.5 T, 37 °C) = 420 s^{-1} $mmol(Mn)^{-1}$ L. A comparable, albeit lower, value $r_2(B_0 = 0.5$ T, 37 °C) = 330 s^{-1} $mmol(Mn)^{-1}$ L (measured under the same experimental conditions) and similar dependence on T were already observed for pure silica coated LSMO nanoparticles with the shell thickness of ≈20 nm possessing the same mean size of crystallites.[9] The difference of r_2 relaxivities could originate both from the different nature of the coating layers around the magnetic cores and the distinct size distributions of the magnetic cores in the compared samples (as a consequence of differences in the mechanical processing of the as grown products and different size fractionation connected with the encapsulation procedures). The transverse relaxation rate is strongly and nonlinearly dependent on the diffusional correlation time r^2/D, where r is the particle radius and D designates the self-diffusion constant of water,[34] and thus, even the distribution of the particle size affects significantly the actual r_2 relaxivity. Additionally, the specific magnetization $M_{750kA\ m^{-1}}$ at the magnetic field of $H = 750$ kA m^{-1} found for the dry sample of LSMO@siF@si-w is only 17.0 A m^2 kg^{-1} in comparison to 26.4 A m^2 kg^{-1} determined for the starting LSMO particles since the magnetic phase is diluted by diamagnetic silica.

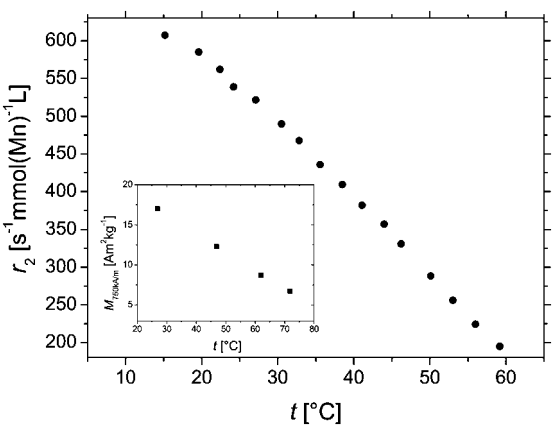

Fig. 3 The r_2 relaxivity dependence on temperature for LSMO@siF@si-w that is related to the decrease of its specific magnetization $M_{750kA\ m^{-1}}$ with increasing temperature depicted in the inset.

The fluorescent properties of the final products were investigated and the corresponding spectra are depicted in Fig. S6 in ESI† together with the spectra of the pure silica coated LSMO nanoparticles LSMO@si that were prepared for comparison.[23] Similarly, the reference spectra of the starting FITC, the reaction mixture of FITC-APS in anhydrous ethanol and the mixture after its hydrolysis in water were recorded (see Fig. S7†). The excitation spectrum of LSMO@siF@si-u shows more complex structure while its broad emission maximum is found at around 514 nm. Namely the main excitation maximum at 492 nm and the mentioned emission maximum correspond well to the maxima reported for fluorescein itself.[35] The reference excitation spectra of pure FITC and its subsequent products exhibit also few maxima that explain together with the scattering of the particles the complex nature of the LSMO@siF@si-u spectrum. The actual scattering contribution should be comparable to the spectrum of pure LSMO@si (Fig. S6†). The excitation spectrum of LSMO@siF@si-w measured at $\lambda_{em} = 514$ nm is similar to the corresponding excitation scan of LSMO@siF@si-u, although the maximum at 492 nm is relatively weaker taking into account the concentration of the nanoparticles that determines the actual amount of scattered light. In the case of LSMO@siF@si-u, the amount of scattered light, forming the background, and consequently the concentration of particles were lower in comparison to those of LSMO@siF@si-w. Furthermore, the differences between the emission spectra ($\lambda_{ex} = 492$ nm) of the two products markedly demonstrate the lower fluorescein content in LSMO@siF@si-w since its band at 514 nm, though well visible in the spectrum of LSMO@siF@si-u, is superimposed by the significant scattering contribution (see also the emission spectrum of LSMO@si). On the other hand, the comparison of the emission spectrum of LSMO@siF@si-w obtained with $\lambda_{ex} =$ 465 nm and the one of LSMO@si better indicates the presence of the fluorescein band in the former spectrum.

3.3. Biological studies

In order to examine the suitability of the final products for labeling purposes and to determine the acceptable concentrations of the agent, the detailed cell viability tests were carried out with HeLa cells and primary skin fibroblasts. Both cell types showed high percentage of viability after 48 h incubation in the whole range of the concentrations tested: 0.011–0.33 mmol(Mn) L^{-1}. Namely the viability of HeLa cells was higher than 90%, compared to fibroblasts where the viability exceeded 80% (see Fig. 4). Generally, fibroblasts as primary cells are more sensitive, even in control experiments which showed viability of 95 and 96% compared to 98 and 99% of HeLa adenocarcinoma derived cell line. The differences between LSMO@siF@si-w and LSMO@siF@si-u are not significant considering the estimated standard deviation of repeatability. The observed viability is comparable to the values reported for various cell lines (human skin carcinoma, neuroepithelioma and mouse neuroblastoma) incubated with dextran and bovine serum albumin coated $La_{0.7}Sr_{0.3}MnO_3$ nanoparticles.[24]

The mean relative fluorescence intensities of the cells, measured by flow cytometry in the FITC channel, are plotted against the concentration of appropriate nanoparticles involved in the incubation in Fig. S8 in ESI.† For HeLa cells the fluorescence intensities are lower for LSMO@siF@si-w in accordance with lower content of fluorescein, but the values could be affected by the different uptake of the distinct products of LSMO@siF@si-w and LSMO@siF@si-u by the cells as well. The fluorescence microscopy confirmed that tested nanoparticles are localized inside the cells and revealed that the particles are present in numerous intracellular vesicles with patterns similar to late endosomes and lysosomes and becoming apparently expanded at higher concentrations. They are visible as perinuclear patches (see Fig. 5) whilst the bulk area of the cell remained clear. At higher concentration of the labeling agents (0.22 and 0.33 mmol(Mn) L^{-1}), the fibroblasts were obviously affected by the nanoparticles and certain morphological changes occurred in contrast to the incubation at lower concentrations (0.011, 0.055 and 0.11 mmol(Mn) L^{-1}) where the cells remained unchanged and the fluorescence intensity was still very high. For all the studied concentrations, the specific fluorescence of the

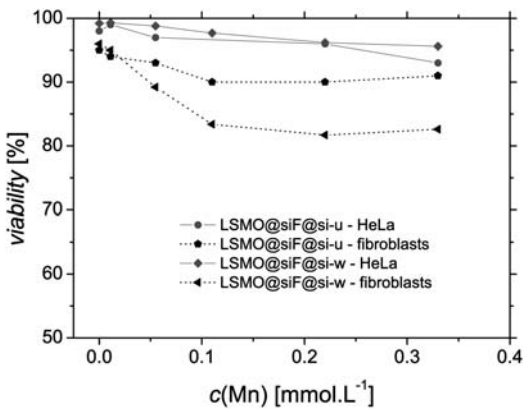

Fig. 4 Viability tests of HeLa cells and fibroblasts exposed to various concentrations of LSMO@siF@si-u and LSMO@siF@si-w particles.

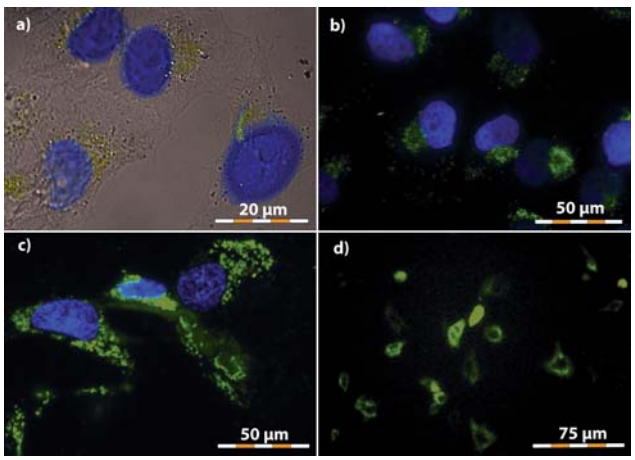

Fig. 5 Fluorescence microscopy images of the cells incubated with nanoparticles at the given concentration and subsequently washed with the PBS buffer: a) HeLa cells – LSMO@siF@si-u, 0.011 mmol(Mn) L^{-1}, overlay image of fluorescence and bright field; b) HeLa cells – LSMO@siF@si-w, 0.33 mmol(Mn) L^{-1}; c) fibroblasts – LSMO@siF@si-w, 0.055 mmol(Mn) L^{-1} and d) rMSCs – LSMO@siF@si-w, 0.13 mmol(Mn) L^{-1}; blue spots – DAPI stained nuclei; green spots – LSMO@siF@si-w.

nanoparticles in the cells was much higher that the autofluorescence of the lysosomes.

Considering the large potential of stem cell transplantation for organ repair and consequent efforts in contemporary biomedicinal research, an efficient dual contrast agent for labeling and tracking these cells would be very useful. As a model for testing the suitability of the studied nanoparticles for cell labeling, rat mesenchymal stem cells (rMSCs) were chosen as an example of adult stem cells, since they are easily derived from bone marrow, they can differentiate into a variety of specialized cell populations, and efficiently proliferate *in vitro*. In addition, they can migrate to tumors and therefore serve in gene therapy as gene carriers. Tests carried out in the similar concentration range of 0.026–0.51 mmol(Mn) L^{-1} for 48 h showed viability higher than 85% in all the experiments with LSMO@siF@si-w and LSMO@siF@si-u. These observations indicated that the particles can be used for rMSCs labeling in spite of the generally higher sensitivity of stem cells. Similar green vesicles to those in HeLa cells and fibroblasts were observed inside the rMSCs using fluorescence microscope (see Fig. 5d) whereas the nuclei remained completely dark due to the absence of the fluorescent particles.

Results obtained with rMSCs are generally comparable with results obtained from labeling experiments with fibroblasts, also adherent primary cell culture. The presence of the nanoparticles obviously affected cell proliferation and adherent properties—after incubation approximately 25% of cells were floating. It is not clear if this is due to changes in surface properties of the culture plastic well (caused by sedimentation of silica particles), or if the cells have partially lost their ability to adhere in the presence of nanoparticles. The cells remained alive, however a type of apoptosis called anoikis can be initiated once the cell adhesion to the matrix is disrupted.[36] No difference in viability in rMSCs labeled with LSMO@siF@si-u or LSMO@siF@si-w was found. However, the percentage of floating cells was lower (10%) in cells labeled with LSMO@siF@si-w and thus the preparation of the dual probe involving the isolation of the intermediate product proved to be more convenient for subsequent stem cell labeling.

Type 1 diabetes mellitus characterized by autoimmune pancreatic islet (PIs) destruction can be treated by transplantation of the PIs into the liver. The success of such transplantation can be efficiently monitored by MRI, but bioimaging of PIs themselves still constitutes an important topic of current biomedical research. The *in vitro* labeling of PIs with LSMO@siF@si-u and LSMO@siF@si-w, carried out at the concentration of 0.11 mmol(Mn) L^{-1} for 24 h, provided promising results. The vitality of PIs exceeded 75% in all experiments, namely vitalities of 75 and 83% were found for LSMO@siF@si-u and vitality of 87% was observed two times for LSMO@siF@si-w. The study of the insulin releasing ability of PIs treated with LSMO@siF@si-u provided stimulation indexes of 2.3 and 4.9 in two experiments, thus showing that their activity is not impaired completely even after incubation with the mentioned product.

Microscopic investigation after immunofluorescent staining of the labeled PIs revealed that the nanoparticles were present inside the peripheral islet cells. They were internalized in various cell types, including insulin producing beta-cells, without any observable differences in the corresponding fluorescence intensity of the particular types (see Fig. 6). Also the contrast agent

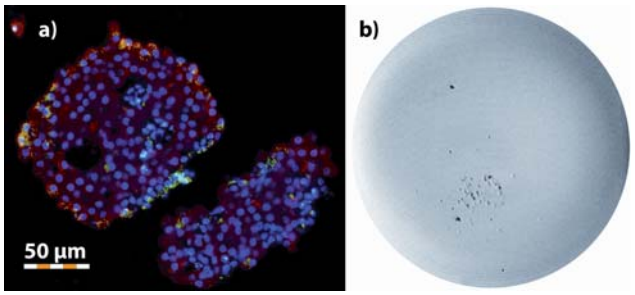

Fig. 6 a) Immunofluorescent staining of the labeled PIs: red spots – immunostained c-peptide indicating beta-cells, green spots – LSMO@siF@si-w, blue spots – DAPI stained cell nuclei; b) T_{2w} MR image of the labeled PIs mounted in agar (4.7 T, well diameter 35 mm).

was not preferentially taken by the rare islet macrophages. The material internalized in the islet cells is, similarly to the above mentioned labeling experiments, present in vesicles of lysosomal/endosomal pattern.

The possibility of visualization of labeled PIs by means of MRI was proved by the T_{2w} MR image measurement (see Fig. 6) of the sample in a gel at $B_0 = 4.7$ T. The corresponding MR signal of the labeled PIs was so strong that they were observable in MR images acquired even with one acquisition, while usually many acquisitions are necessary. Let us mention that until this time only iron oxide based particles have been used for labeling of PIs by T_2 contrast agents.

4. Conclusions

Fluorescent magnetic nanoparticles based on a perovskite manganite $La_{0.75}Sr_{0.25}MnO_3$ core coated with a two-ply silica layer were synthesized and thoroughly characterized in order to prepare a novel dual MRI/fluorescence probe with enhanced colloidal and chemical stability. The inner fluorescent shell of the composite nanoparticles was formed employing a mixture of fluorescent alkoxide and tetraethoxysilane. The outer silica layer synthesized from pure tetraethoxysilane provides the colloidal stability and prevents the leaching process of the dye.

TEM studies showed uniformly coated magnetic cores that do not form larger aggregates in the final product and further it confirmed together with IR spectroscopy the increase of the shell thickness during the two-step procedure. Enhanced colloidal stability was proved by the ζ-potential dependence on pH, while the luminescence spectroscopy demonstrated the presence of fluorescein moieties in the nanoparticles. The relaxometric study at magnetic fields of $B_0 = 0.5$, 1.5 and 3 T at 20 °C revealed extraordinarily high spin–spin relaxivities $r_2 = 580$, 540 and 520 s^{-1} mmol$(Mn)^{-1}$ L, respectively, sharply exceeding the relaxivities of iron oxides. The relaxometric results were also discussed in relation to magnetic characterizations in static field, namely supporting the temperature dependence of r_2.

In vitro experiments performed on HeLa cells, fibroblasts and rMSCs indicated high cell viability, generally exceeding 85%. Simultaneously significant uptake of the nanoparticles and their localization in the intracellular vesicles of late endosomal or lysosomal pattern were observed directly by fluorescence microscopy. Islets of Langerhans exhibited good vitalities during

in vitro labeling whereas their insulin releasing capability was retained. On the other hand the labeled islets provided very strong MR signals due to the uptake of the nanoparticles.

Acknowledgements

This study was carried out under the support of the Academy of Science of the Czech Republic projects KAN201110651 and KAN200200651, the Long-Term Research Plan of the Ministry of Education, Youth and Sports of the Czech Republic No. MSM0021620857 and No. MSM0021620858, the ENCITE – EU FP 201842 project and the Center of Molecular Immunology project No. 1M0506.

References

1 N. Muja and J. W. M. Bulte, *Prog. Nucl. Magn. Reson. Spectrosc.*, 2009, **55**, 61–77; R. Fu, W. W. Brey, K. Shetty, P. Gorkov, S. Saha, J. R. Long, S. C. Grant, E. Y. Chekmenev, J. Hu, Z. Gan, M. Sharma, F. Zhang, T. M. Logan, R. Bruschweller, A. Edison, A. Blue, I. R. Dixon, W. D. Markiewicz and T. A. Cross, *J. Magn. Reson.*, 2005, **117**, 1–8; L. Ciobanu, D. A. Seeber and C. H. Pennington, *J. Magn. Reson.*, 2002, **158**, 178–182; J. M. Tyszka, S. E. Fraser and R. J. Jacobs, *Curr. Opin. Biotechnol.*, 2005, **16**, 93–99.

2 S. Mansson and A. Bjornerud, in *The Chemistry of Contrast Agents in Medical Magnetic Resonance Imaging*, ed.: A. E. Merbach and E. Toth, John Wiley & Sons, Chichester, England, 2001, pp. 1–44.

3 M. T. Vlaardingerbroek and J. A. den Boer, *Magnetic Resonance Imaging: Theory and Practice*, Springer Verlag, Germany, 1996.

4 R. N. Muller, A. Roch, J. M. Colet, A. Ouakssim and P. Gillis, in *The Chemistry of Contrast Agents in Medical Magnetic Resonance Imaging*, ed.: A. E. Merbach and E. Toth, John Wiley & Sons, Chichester, England, 2001, pp. 417–436; Y. W. Jun, J. H. Lee, J. Cheon, in *Nanobiotechnology II*, ed.: C. A. Mirkin and C. M. Niemeyer, Wiley-VCH, Weinheim, 2007, pp. 321–346.

5 Y. X. J. Wang, S. M. Hussain and G. P. Krestin, *Eur. Radiol.*, 2001, **11**, 2319–2331; C. Corot, P. Robert, J. M. Idee and M. Port, *Adv. Drug Delivery Rev.*, 2006, **58**, 1471–1504; M. Rohrer, H. Bauer, J. Mintorovitch, M. Requardt and H. J. Weinmann, *Invest. Radiol.*, 2005, **40**, 715–724.

6 Y. W. Jun, J. H. Lee and J. Cheon, *Angew. Chem., Int. Ed.*, 2008, **47**, 5122–5135; A. H. Lu, E. L. Salabas and F. Schuth, *Angew. Chem., Int. Ed.*, 2007, **46**, 1222–1244.

7 J. Lu, S. L. Ma, J. Y. Sun, C. C. Xia, C. Liu, Z. Y. Wang, X. N. Zhao, F. B. Gao, Q. Y. Gong, B. Song, X. T. Shuai, H. Ai and Z. W. Gu, *Biomaterials*, 2009, **30**, 2919–2928; J. Giri, P. Pradhan, V. Somani, H. Chelawat, S. Chhatre, R. Banerjee and D. Bahadur, *J. Magn. Magn. Mater.*, 2008, **320**, 724–730; J. T. Jang, H. Nah, J. H. Lee, S. H. Moon, M. G. Kim and J. Cheon, *Angew. Chem., Int. Ed.*, 2009, **48**, 1234–1238.

8 O. V. Melnikov, O. Y. Gorbenko, M. N. Markelova, A. R. Kaul, V. A. Atsarkin, V. V. Demidov, C. Soto, E. J. Roy and B. M. Odintsov, *J. Biomed. Mater. Res., Part A*, 2009, **91a**, 1048–1055; J. M. Shin, R. M. Anisur, M. K. Ko, G. H. Im, J. H. Lee and I. S. Lee, *Angew. Chem., Int. Ed.*, 2009, **48**, 321–324.

9 O. Kaman, Ph.D. Thesis: Preparation, structure and properties of hybrid nanoparticles with perovskite and spinel type cores; Dept. of Inorg. Chem., Faculty of Science, Charles Univ., Prague, 2009.

10 S. J. Cho, B. R. Jarrett, A. Y. Louie and S. M. Kauzlarich, *Nanotechnology*, 2006, **17**, 640–644.

11 J. H. Gao, G. L. Liang, J. S. Cheung, Y. Pan, Y. Kuang, F. Zhao, B. Zhang, X. X. Zhang, E. X. Wu and B. Xu, *J. Am. Chem. Soc.*, 2008, **130**, 11828–11833.

12 Y. H. Xu, H. M. Bai and J. P. Wang, *J. Magn. Magn. Mater.*, 2007, **311**, 131–134.

13 M. Hoehn, D. Wiedermann, C. Justicia, P. Ramos-Cabrer, K. Kruttwig, T. Farr and U. Himmelreich, *J. Physiol.*, 2007, **584**, 25–30; J. W. M. Bulte and D. L. Kraitchman, *NMR Biomed.*, 2004, **17**, 484–499.

14 J. Kim, Y. Piao and T. Hyeon, *Chem. Soc. Rev.*, 2009, **38**, 372–390; J. Yang, E. Lim, H. J. Lee, J. Park, S. C. Lee, K. Lee, H. Yoon, J. Suh, Y. Huh and S. Haam, *Biomaterials*, 2008, **29**, 2548–2555.

15 S. A. Corr, Y. P. Rakovich and Y. K. Gun'ko, *Nanoscale Res. Lett.*, 2008, **3**, 87–104.

16 A. K. Gupta and M. Gupta, *Biomaterials*, 2005, **26**, 3995–4021.

17 Y. Lin, S. Wu, Y. Hung, Y. Chou, C. Chang, M. Lin, C. Tsai and C. Mou, *Chem. Mater.*, 2006, **18**, 5170–5172; C. Lu, Y. Hung, J. Hsiao, M. Yao, T. Chung, Y. Lin, S. Wu, S. Hsu, H. Liu, C. Mou, C. Yang, D. Huang and Y. Chen, *Nano Lett.*, 2007, **7**, 149–154; J. Lee, Y. Jun, S. Yeon, J. Shin and J. Cheon, *Angew. Chem., Int. Ed.*, 2006, **45**, 8160–8162.

18 A. T. Heitsch, D. K. Smith, R. N. Patel, D. Ress and B. A. Korgel, *J. Solid State Chem.*, 2008, **181**, 1590–1599.

19 S. T. Selvan, P. K. Patra, C. Y. Ang and J. Y. Ying, *Angew. Chem., Int. Ed.*, 2007, **46**, 2448–2452.

20 J. H. Choi, F. T. Nguyen, P. W. Barone, D. A. Heller, A. E. Moll, D. Patel, S. A. Boppart and M. S. Strano, *Nano Lett.*, 2007, **7**, 861–867.

21 Y. Tokura and Y. Tomioka, *J. Magn. Magn. Mater.*, 1999, **200**, 1–23.

22 E. Pollert, K. Knizek, M. Marysko, P. Kaspar, S. Vasseur and E. Duguet, *J. Magn. Magn. Mater.*, 2007, **316**, 122–125; S. Vasseur, E. Duguet, J. Portier, G. Goglio, S. Mornet, E. Hadova, K. Knizek, M. Marysko, P. Veverka and E. Pollert, *J. Magn. Magn. Mater.*, 2006, **302**, 315–320.

23 O. Kaman, E. Pollert, P. Veverka, M. Veverka, E. Hadova, K. Knizek, M. Marysko, P. Kaspar, M. Klementova, V. Grunwaldova, S. Vasseur, R. Epherre, S. Mornet, G. Goglio and E. Duguet, *Nanotechnology*, 2009, **20**, 275610.

24 K. R. Bhayani, S. N. Kale, S. Arora, R. Rajagopal, H. Mamgain, R. Kaul-Ghanekar, D. C. Kundaliya, S. D. Kulkarni, R. Pasricha, S. D. Dhole, S. B. Ogale and K. M. Paknikar, *Nanotechnology*, 2007, **18**, 345101.

25 C. Graf, D. L. J. Vossen, A. Imhof and A. van Blaaderen, *Langmuir*, 2003, **19**, 6693–6700.

26 J. Wu, Z. Q. Ye, G. L. Wang and J. L. Yuan, *Talanta*, 2007, **72**, 1693–1697.

27 A. Imhof, M. Megens, J. J. Engelberts, D. T. N. de Lang, R. Sprik and W. L. Vos, *J. Phys. Chem. B*, 1999, **103**, 1408–1415; A. Vanblaaderen and A. Vrij, *Langmuir*, 1992, **8**, 2921–2931.

28 M. Ocana, M. Andres-Verges, R. Pozas and C. J. Serna, *J. Colloid Interface Sci.*, 2006, **294**, 355–361.

29 A. Murashkevich, A. Lavitskaya, T. Barannikova and I. Zharskii, *J. Appl. Spectrosc.*, 2008, **75**, 730–734.

30 F. L. Galeener, A. J. Leadbetter and M. W. Stringfellow, *Phys. Rev. B: Condens. Matter*, 1983, **27**, 1052–1078; R. M. Pasternack, S. R. Amy and Y. J. Chabal, *Langmuir*, 2008, **24**, 12963–12971.

31 K. B. Li, R. S. Cheng, S. G. Wang and Y. H. Zhang, *J. Phys.: Condens. Matter*, 1998, **10**, 4315–4322; G. Westin, A. Pohl, M. Ottosson, K. Lashgari and K. Jansson, *J. Sol-Gel Sci. Technol.*, 2008, **48**, 194–202.

32 R. Pena-Alonso, F. Rubio, J. Rubio and J. L. Oteo, *J. Mater. Sci.*, 2007, **42**, 595–603.

33 L. Bistricic, V. Volovsek and V. Dananic, *J. Mol. Struct.*, 2007, **834–836**, 355–363.

34 P. Gillis, F. Moiny and R. A. Brooks, *Magn. Reson. Med.*, 2002, **47**, 257–263; Y. Matsumoto and A. Jasanoff, *Magn. Reson. Imaging*, 2008, **26**, 994–998.

35 P. Siejak and D. Frackowiak, *J. Phys. Chem. B*, 2005, **109**, 14382–14386.

36 J. E. Brinchmann, *J. Neurol. Sci.*, 2008, **265**, 127–130.

PŘÍLOHA V.

Protein microarray analysis as a tool for monitoring cellular autoreactivity in type 1 diabetes patients and their relatives

Z. Vrábelová, S. Kolousková, K. Böhmová, M.K. Faresjö, Z. Šumník, M. Pechová, M. Kverka, D. Chudoba, K. Zacharovová, G. Štádlerová, P. Pithová, M. Hladiková, and K. Štechová

Pediatr Diabetes, 2007. 8(5): p. 252-60

Pediatric Diabetes 2007: 8: 252–260

Pediatric Diabetes

Original Article

Protein microarray analysis as a tool for monitoring cellular autoreactivity in type 1 diabetes patients and their relatives

Vrabelova Z, Kolouskova S, Böhmova K, Faresjö MK, Sumnik Z, Pechova M, Kverka M, Chudoba D, Zacharovova K, Stadlerova G, Pithova P, Hladikova M, Stechova K. Protein microarray analysis as a tool for monitoring cellular autoreactivity in type 1 diabetes patients and their relatives.
Pediatric Diabetes 2007: 8: 252–260.

Background: Autoreactive T cells have a crucial role in type 1 diabetes (T1D) pathogenesis.
Objectives: The aim of our study was to monitor the *in vitro* production of cytokines by peripheral blood mononuclear cells (PBMCs) after stimulation with diabetogenic autoantigens.
Subjects: Ten T1D patients (tested at the time of diagnosis and 6 and 12 months later), 10 first-degree relatives of the T1D patients, and 10 controls underwent the study.
Methods: PBMCs were stimulated with glutamic acid decarboxylase 65 (GAD65) amino acids (a.a.) 247–279, 509–528, and 524–543; proinsulin a.a. 9–23; and tyrosine phosphatase (islet antigen-2)/R2 a.a. 853–872. Interleukin (IL)-2, IL-4, IL-5, IL-6, IL-10, IL-13, interferon (IFN)-γ, tumor necrosis factor β, transforming growth factor β1, and granulocyte colony-stimulating factor (GCSF) were analyzed by protein microarray.
Results: Differences in cytokine(s) poststimulatory and mainly in basal production were observed in all groups. The most prominent findings were in controls, the higher basal levels of IL-2, IL-4, IL-5, IL-13, and GCSF were observed when compared with relatives ($p < 0.05$, for all). After stimulation in controls, there was a significant decrease in IL-2, IL-13, GCSF, and IFN-γ ($p < 0.05$, for all). The group of relatives was the most variable in poststimulatory production. A strong correlation between cytokines production was found but groups differed in this aspect.
Conclusion: By multiplex analysis, it may be possible, for example, to define the risk immunological response pattern among relatives or to monitor the immune response in patients on immune modulation therapy.

Zuzana Vrabelova[a], Stanislava Kolouskova[a], Kristyna Böhmova[a], Maria Karlsson Faresjö[b], Zdenek Sumnik[a], Marta Pechova[c], Miloslav Kverka[d], Daniel Chudoba[e], Klara Zacharovova[f], Gabriela Stadlerova[a], Pavlina Pithova[g], Marie Hladikova[h] and Katerina Stechova[a]

[a]Department of Paediatrics, 2nd Medical Faculty of Charles University, Prague, The Czech Republic; [b]Division of Paediatrics and Diabetes Research Centre, Faculty of Health Sciences, Linköping University, Linkőping, Sweden; [c]Department of Chemistry and Biochemistry, 2nd Medical Faculty of Charles University, Prague, The Czech Republic; [d]Institute of Microbiology, The Czech Academy of Science, Prague, The Czech Republic; [e]Department of Biology and Genetics, 2nd Medical Faculty of Charles University, Prague, The Czech Republic; [f]Department of Diabetology, Institute for Clinical and Experimental Medicine, Prague, The Czech Republic; [g]Department of Internal Medicine, 2nd Medical Faculty of Charles University, Prague, The Czech Republic; and [h]Department of Medical Informatics and Statistics, 2nd Medical Faculty of Charles University, Prague, The Czech Republic

Key words: autoantigen – autoreactive T cells – cytokine – protein microarray – T1D

Corresponding author:
Katerina Stechova, MD, PhD
Laboratory of Autoimmune Diseases
Department of Paediatrics
University Hospital Motol
V Uvalu 84
Prague 5 – Motol, 15006
The Czech Republic.
Tel: +420 224 432 089;
fax: +420 224 432 020;
e-mail: KaterinaStechova@seznam.cz

Submitted 11 January 2007. Accepted for publication 16 July 2007

Type 1 diabetes (T1D) is a chronic disorder that results from the specific destruction of the insulin-producing pancreatic β cells by the immune system. The initial phase of T1D is clinically silent; the real triggers are not really known. The activated immune cells invade the pancreas and slowly destroy β cells until it becomes clinically evident in its consequences (hyperglycemia and ketoacidosis) (1–3).

The destruction of pancreatic β cells is T-cell dependent. The major role is played by the subset of CD4+ autoreactive T lymphocytes (T helper lymphocytes) that can recognize the autoantigens in the context of human leukocyte antigen (HLA) II molecules and then differentiate themselves into the T helper (Th) 1 cells. The production of Th1 cytokines [interferon (IFN)-γ and tumor necrosis factor (TNF)-β] leads to the activation of macrophages and CD8+ cytotoxic lymphocytes, and they then can invade the pancreatic islets and create the toxic environment. The death of β cells amplifies the inflammation.

The presence of antibodies alone is not sufficient to induce the destruction of β cells (1–4). On the contrary, the exceptional humoral immunity associated with the Th2 response after the antigen stimuli of Th0 naive lymphocyte is suppressed in T1D animal models. Thus, the cytokine profile typical of the Th2 response [interleukin (IL)-4, IL-5, and IL-13] seems to have a protective effect (1–5). Current studies also reveal the importance of the failure of regulatory mechanisms represented mainly by T regulatory cells. These cells are able to suppress proliferation and cytokine production from both CD4+ and CD8+ T cells *in vitro* in a cell-contact-dependent manner and by secretion of anti-inflammatory cytokines [for example, IL-10 and transforming growth factor (TGF) β)] (6).

We detected cytokines produced by peripheral blood mononuclear cells (PBMCs) after stimulation with diabetogenic autoantigens using a protein microarray. This method enables semiquantitative multiparameter analysis of one sample. In the case of cytokine detection, primary anticytokine antibodies are attached to the small membrane and visualization is made by secondary anticytokine antibodies, and the whole cytokine spectrum can bee seen at once (7). We tested five groups: the T1D patients at different times (at the diagnosis and 6 and 12 months later), their first-degree relatives, and the healthy controls. We evaluated the secretion of typical Th1, Th2, and Th3 cytokines, and we tested also one inflammatory cytokine (IL-6) and one cytokine from hematopoietic growth factors family (granulocyte colony-stimulating factor, GCSF).

Patients and methods

Subjects

Ten patients with recent onset T1D (mean age 13 yr, age range 3–18 yr, female/male 4/6), treated at the Paediatric Outpatient Departments of the University Hospital Motol, Prague, were included into the study. None of them was in the severe metabolic acidosis at the time of diagnosis or suffered from any other autoimmune disease or inflammation. The samples were collected in the morning within a week after the diagnosis and then the patients were retested 6 and 12 months later (marked as D1, D2, and D3, respectively).

Ten first-degree relatives of the T1D patients and 10 healthy controls (blood donors), with no personal history of any autoimmune disease, underwent this study as well. Informed consent, approved by local ethical committee, was obtained from all the tested subjects.

Subjects' characteristics. The complete HLA-DQA1 and HLA-DQB1 genotypings were carried out by polymerase chain reaction with sequence-specific primers in all subjects (data not shown) (8). Relatives and healthy controls were HLA risk, age, and sex matched.

The sera from all participants were examined by radioimmune assay (Solupharm, Brno, the Czech Republic) for the presence of autoantibodies against the islet antigens glutamic acid decarboxylase 65 (GAD65) and islet antigen-2 (IA-2). Positivity was considered to be above 1 IU/mL for GAD65 (GADA) as well as for IA-2 (IA-2A) (>99th percentile).

None of the relatives as well as the healthy controls was autoantibody(ies) positive.

Assays

PBMCs were prepared by Ficoll gradient centrifugation (Amersham Biosciences, Uppsala, Sweden), and 2×10^6 freshly isolated PBMCs were resuspended in 1 mL of RPMI-1640 medium supplemented with 20% fetal calf serum, L-glutamine (10 μL/mL, 200 mM), and penicillin (1 μL/mL)–streptomycin (1 μg/mL; all Sigma, St.Louis, MO, USA) and cultivated with autoantigens. In all cases, PBMCs were stimulated with a mixture of diabetogenic autoantigens, and if enough cells were available, autoantigens were tested also separately (2×10^6 PBMCs were necessary for each separate autoantigen). The concentration of all autoantigens was 1 μg/10^6 PBMC each. The following autoantigens were used in a mixture and/or separately: GAD65 peptide amino acids (a.a.) 247–279 (NMY-AMMIARFKMFPEVKEKGMAALPRLIAFTSEE-OH), molecular weight 3823.7, marked GAD1; a.a. 509–528 (IPPSLRTLEDNEERMSRLSK-OH), molecular weight 2371.7, GAD2; a.a. 524–543 (SRLSK-VAPVIKARMMEYGTT-OH), molecular weight 2238.7, GAD3 (Department of Medical and Physiological Chemistry, University of Uppsala, Uppsala, Sweden); IA-2 a.a. 853–872 SFYLK(Nleu)VQT-QETRTLTQFHF, molecular weight 2489; and a.a. 9–23 SHLVEALYLVCGERG of β proinsulin chain, molecular weight 1645 (Sigma).

All experiments were completed with positive control [PBMC + 10 μg phytohemagglutinin (Sigma) per 10^6 PBMCs] as well as with a negative control (PBMC in exclusive culture medium). The medium was harvested after 72-h stimulation (37°C, 5% CO_2), frozen (−20°C), and later used for protein microarray analysis that was performed by a custom array kit according to the instructions by the manufacturer (RayBiotech, Norcross, GA, USA). The production of the following cytokines was assessed: IL-2, IL-4, IL-5, IL-6, IL-10, IL-13, IFN-γ, TNF-β, TGF-β1, and GCSF.

Detection was carried out using the Fuji LAS1000 imaging system. Chemiluminescent signals were analyzed using the AIDA software (Advanced Image Data Analyzer, 3.28; Raytest Izotopenmessgeraete, Straubenhardt, Germany). The detection limits according to the manufacturer's Web site (www.raybiotech.com) are displayed in Table 1. The images were edited in the gray-scale 8-bit map. The results are expressed according to the instructions of the manufacturer in percentage of signal intensity. The membranes were compared together, the integral positive controls of each membrane reached the 100% of intensity; no other image transformation was necessary.

Table 1. Detection limits for all tested parameters

Cytokine	Sensitivity (pg/mL)
IL-2	25
IFN-γ	100
TNF-β	1000
IL-4	1
IL-5	1
IL-13	100
IL-10	10
TGF-β1	200
IL-6	1
GCSF	2000

GCSF, granulocyte colony-stimulating factor; IFN, interferon; IL, interleukin; TGF, transforming growth factor; TNF, tumor necrosis factor.

Statistics

The data were processed by SPSS software. For non-parametric data, Kruskal–Wallis test was used for comparison of three or more groups and the Mann–Whitney test was used for comparison of two groups. The Wilcoxon Signed Ranks test was used for comparison of signal intensities in each group (basal × poststimulatory response). For expression of correlation analysis, Spearman's coefficient was used.

Results

Th1 cytokines (IFN-γ and TNF-β)

Significantly higher production of TNF-β was observed in the D2 group in comparison with the relatives ($p < 0.05$).

After stimulation with the autoantigens mixture, we observed a decrease in IFN-γ production in the control group ($p = 0.049$) and in the D3 group ($p = 0.048$). The D3 group also had a decrease in TNF-β poststimulatory production ($p = 0.018$) (Fig. 1).

Th2 cytokines (IL-4, IL-5, and IL-13)

There was a higher basal production of IL-4, IL-5, and IL-13 within the control group when compared with the relatives ($p < 0.05$ for all three cytokines). The D2 group also had a higher IL-13 basal

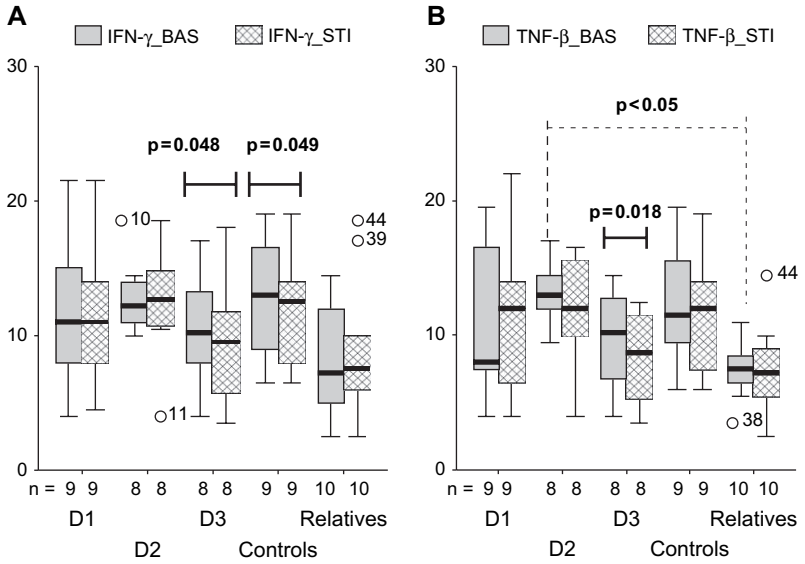

Fig. 1. Th1 cytokines in all groups together. (A) IFN-γ. (B) TNF-β. Results are displayed in percentage of spot intensity (basal and stimulated) and statistical significance is pointed. Data are expressed as median + range. Extreme values are shown. BAS, basal production; D1, type 1 diabetes patients at the time of diagnosis; D2, type 1 diabetes patients at 6 months later; D3, type 1 diabetes patients at 12 months later; IFN, interferon; STI, stimulation with autoantigens mixture; Th1, T helper 1 cells; TNF, tumor necrosis factor.

production when compared with their relatives ($p < 0.05$).

After stimulation, we observed a decrease in the IL-4 production in the D3 group ($p = 0.025$), whereas the production of IL-13 was suppressed in the control group ($p = 0.035$). The production of IL-5 was not significantly changed in all the groups (Fig. 2).

Th3 cytokines (IL-10 and TGF-β)

No difference in the overall basal production of IL-10 within the groups as well as in their poststimulatory response was observed. The controls had a higher basal production of TGF-β in comparison with the relatives ($p < 0.05$), whereas secretion of TGF-β was decreased by autoantigen stimulation in the D3 group ($p = 0.049$) (Fig. 3).

Other tested parameters (IL-2, IL-6, and GCSF)

A higher basal production of IL-2 and GCSF was seen in the group of controls, and it was statistically significant in comparison with the group of relatives ($p < 0.05$). Antigen-induced secretion of IL-2 and GCSF decreased (related to the basal levels) in the group of controls ($p = 0.035$ and 0.03, respectively) and IL-2 also decreased with statistical significance in the D3 group ($p = 0.018$).

Basal and poststimulatory IL-6 production was extremely variable in all groups. The tendency to decrease after stimulation was observed in the groups of controls, relatives, and D3, while an increase was manifested in the D1 and D2 groups. Exclusively in the D3, a decrease was observed ($p = 0.04$) (Fig. 4).

Spearman's correlation analysis

To the section of statistics, when we supposed $p < 0.01$, the r_S should be above 0.8 for the following strong correlations.

In T1D patients, the basal production of IL-2, IL-4, IL-5, IL-13, GCSF, IFN-γ, TNF-β and TGF-β correlated well together ($r_S > 0.8$ for each pair). In this group, only basal TGF-β production did not strongly correlate with IL-13 and IFN-γ ($r_S = 0.74$ and 0.75, respectively), but after stimulation, the situation was slightly changed ($r_S = 0.80$ and 0.82, respectively). IL-6 and IL-10 showed no correlations; they were extremely variable. Situation is displayed in Fig. 5 and is expressed for D1, D2, and D3 all together as correlations did not differ within these groups.

In the control group, the strong correlations between IL-2, IL-4, IL-5, IL13, GCSF, IFN-γ, TNF-β and TGF-β were the same as observed in the group of T1D patients ($r_S > 0.8$ for each pair), and the relations remained even after stimulation. Moreover, basal production of TGF-β correlated with IL-13 and IFN-γ ($r_S = 0.85$ and 0.95, respectively) as well as by stimulation ($r_S = 0.97$ and 0.93, respectively). Furthermore, there was a correlation between basal IL-10 and IL-2, IL-4, IL-5, IL-13, and IL-6 ($r_S > 0.8$ for each pair). After stimulation, IL-10 correlated

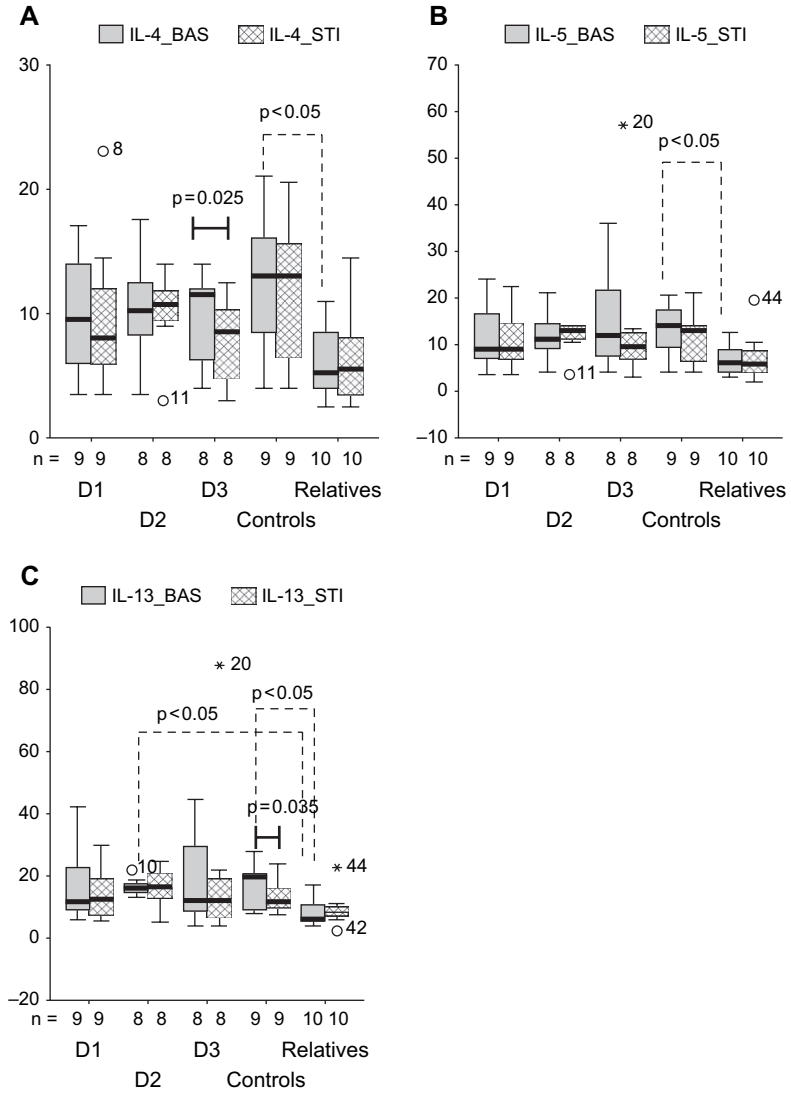

Fig. 2. Th2 cytokines in all groups together. (A) IL-4. (B) IL-5. (C)IL-13. Results are displayed in percentage of spot intensity (basal and stimulated) and statistical significance is pointed. Data are expressed as median + range. Extreme values are shown. BAS, basal production; D1, type 1 diabetes patients at the time of diagnosis; D2, type 1 diabetes patients at 6 months later; D3, type 1 diabetes patients at 12 months later; IL, interleukin; Th2, T helper 2 cells; STI, stimulation with autoantigens mixture. * indicates extreme values.

with IL-5, IL-13, IL-6, and GCSF and even with TGF-β ($r_S > 0.8$ for each pair). IL-6 also had correlations in basal production with IL-5, IL-13, and IL-10, and after stimulation IL-4, GCSF, IFN-γ, TNF-β, and TGF-β were added ($r_S > 0.8$ for each pair). Situation is displayed in Fig. 6.

In the group of relatives, we observed fewer correlations. Basal production of IL-2, IL-4, IL-5, and TGF-β correlated with each other ($r_S > 0.8$ for each pair) and then IFN-γ, TNF-β, GCSF, and IL-13 correlated with each other ($r_S > 0.8$ for each pair) but not together with IL-2, IL-4, IL-5, and TGF-β. After stimulation, the correlation among IL-2, IL-4, IL-5, and TGF-β remained and additional with IL-13 was noticed ($r_S > 0.8$ for each pair). IFN-γ and TNF-β only correlated to each other. The basal production of TGF-β had a correlation only with IL-2, IL-4, and IL-5 ($r_S = 0.87$ and 0.86 and 0.87, respectively) and after stimulation also with IL-13 and GCSF ($r_S = 0.82$ and 0.80, respectively). There was no correlation of TGF-β with IFN-γ or TNF-β in basal or poststimulatory production ($r_S = 0.3$; 0.23, 0.52 and 0.72, respectively) and IL-6 and IL-10 correlated in basal and poststimulated production with each other. Situation is displayed in Fig. 7.

The stimulatory potential of autoantigens

The most potent autoantigen (highest spot intensities) was the GAD65 peptide (a.a. 509–528). In the relatives' group, we observed the strongest reaction

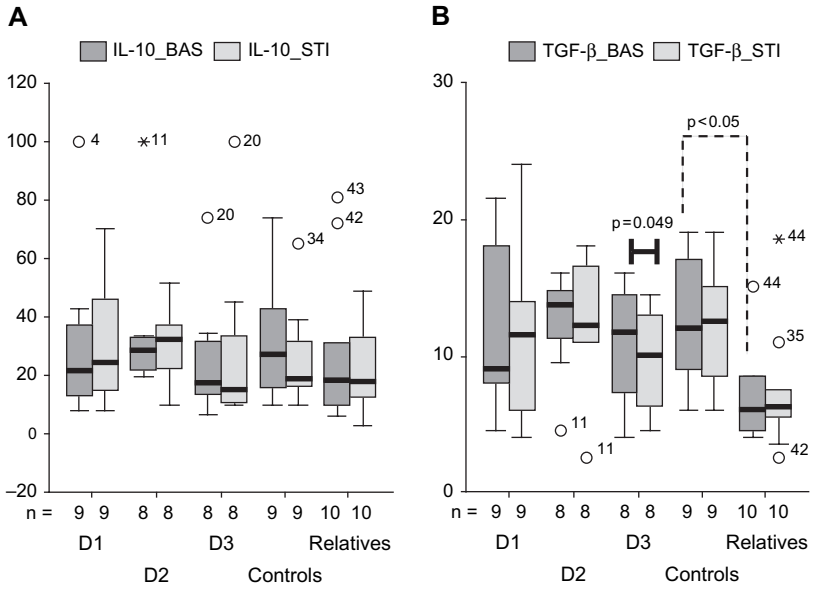

Fig. 3. Th3 cytokines in all groups together. (A) IL-10. (B) TGF-β. Results are displayed in percentage of spot intensity (basal and stimulated) and statistical significance is pointed. Data are expressed as median + range. Extreme values are shown. Bas, basal production; D1, type 1 diabetes patients at the time of diagnosis; D2, type 1 diabetes patients at 6 months later; D3, type 1 diabetes patients at 12 months later; IL, interleukin; STI, stimulation with autoantigens mixture; Th3, T helper 3 cells; TGF, transforming growth factor. * indicates extreme values.

against the IA-2 peptide (5/10 tested). It was not possible to specify the most potential autoantigen in the controls because here the reaction was weak and proportional against single autoantigens (8/10 tested).

Discussion

Over the past two decades, several different systems have been used to study and monitor the autoreactive T cells in T1D patients: T-cell proliferation assay, cytokine-based assays including enzyme-linked immunosorbent spot (ELISPOT), approaches using flow cytometry etc. (9–14). Over the past decade, new genomic and proteomic technologies including protein and gene microarray assays for multiparameter analysis have become available (7, 15, 16). However, the progress and standardization of these autoreactive T-cell assays are quite slow and difficult as the levels of autoreactive T cells in circulation are very low (<1 in 100 000 of the total white blood cell population) (1–4, 9). To study the complex reactivity of PBMCs against diabetogenic autoantigens, we decided to use semi-quantitative detection of cytokines/chemokines by protein microarray. In our previous study, we compared protein microarray data by enzyme-linked immunosorbent assay and ELISPOT with good correlation (data not shown). However, for further exact quantification, we plan to use multiparameter technique (as, for example, Luminex). To avoid artifacts during the freezing, we worked with freshly isolated PBMCs. The selected cultivation media contributed no important test interference. The stimulation by selected concentrations of autoantigens as well as the amount of tested PBMCs were performed according to the previous Immunology of Diabetes Society T-cell Workshops and recommendations and also according to our own experience (9, 17, 18). To adapt this test for clinical praxis, we used a mixture of autoantigens (sometimes not enough PBMCs are available for analysis with all autoantigens), but if it was possible, we also tested autoantigens separately (19).

The real benefit of this method could lie in the possibility to see the whole spectrum of cytokines as a unique combination with typical signs for each group, to observe and to analyze the reaction in the whole complex, and then to define the 'characteristic patterns' for each group and 'risk patterns' for individuals. We believe that for predicting the risk of T1D or for monitoring the efficacy of immunomodulation therapy, it is not so important to determine the levels of individual cytokines as to know how the cytokines cooperate together.

On the basis of our results, we were rather surprised that there were such significant differences even in the basal levels as we expected to see the changes mainly after stimulation. Upon this fact, we suggest that even the basal cytokine production and 'basal cytokine pattern' should be considered. In general, we could see the higher basal levels of all cytokines within the control group when compared with the all groups. In control group after stimulation, IL-2, IL-6, Th2 cytokines, and IFN-γ showed a tendency to decrease,

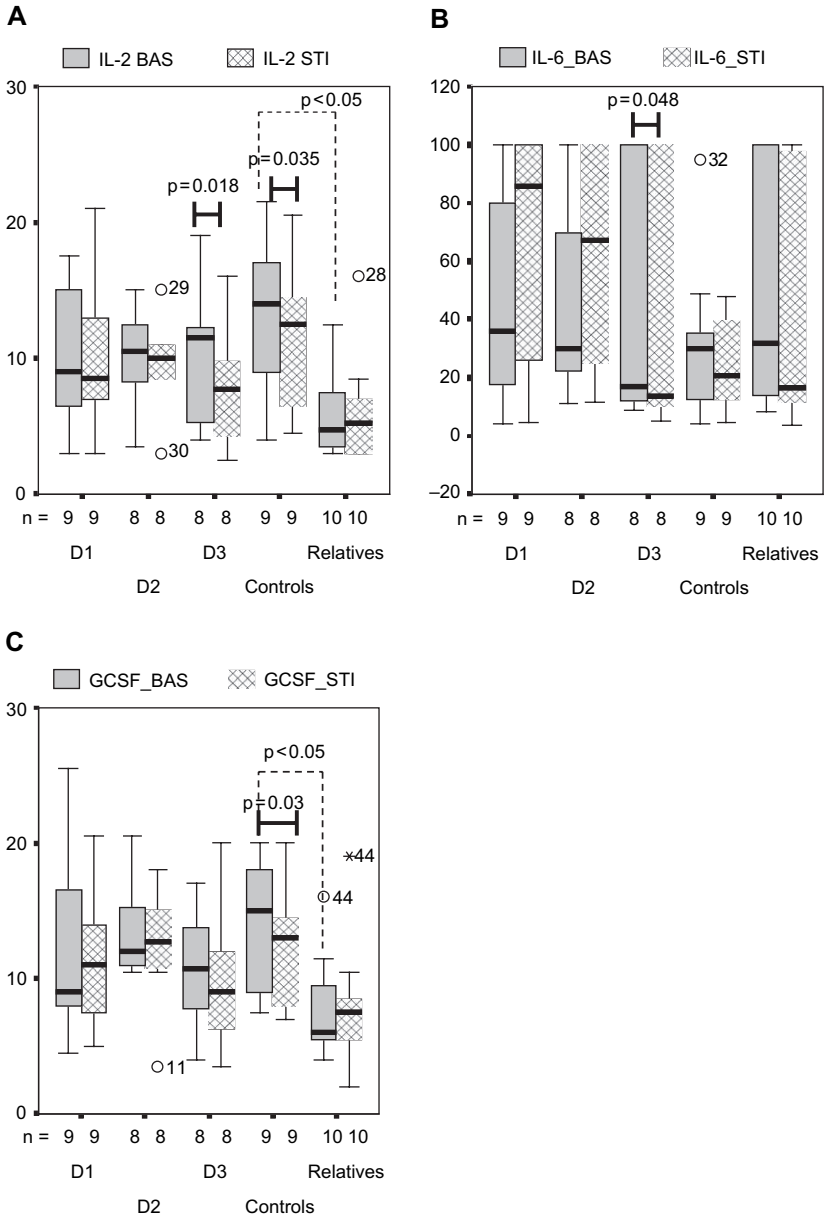

Fig. 4. IL-2, IL-6, and GCSF cytokines in all groups together. (A) IL-2. (B) IL-6. (C) GCSF. Results are displayed in percentage of spot intensity (basal and stimulated) and statistical significance is pointed. Data are expressed as median + range. Extreme values are shown. BAS, basal production; D1, type 1 diabetes patients at the time of diagnosis; D2, type 1 diabetes patients at 6 months later; D3, type 1 diabetes patients at 12 months later; GCSF, granulocyte colony-stimulating factor; IL, interleukin; STI, stimulation with autoantigens mixture. * indicates extreme values.

while the TGF-β showed a tendency to increase. Only some of these findings were significant. The most variable production of cytokines was within the group of relatives. The T1D patient groups at D1, D2 and D3 reacted in different way, however, without any 'specific pattern'. Only in D3, a tendency to decrease the inflammatory response by decrease in IL-6, IL-2, Th1, and Th2 cytokines but even in TGF-β was observed.

Karlsson Faresjo et al. showed that spontaneous and antigen-induced expression and secretion of cytokines (IFN-γ, IL-4, IL-10, and IL-13) is low at the diagnosis of T1D (12). During the first month after diagnosis, one diabetogenic autoantigen (GAD65 a.a. 247–279) caused an increased ratio of IFN-γ/IL-4 messenger RNA expression and increased secretion of IFN-γ (12). The same authors showed that high-risk relatives had a high spontaneous ratio of IFN-γ/IL-4 compared with diabetic children as well as healthy controls. However, this spontaneous production decreased after stimulation with peptides of GAD65 and insulin and in contrast to an increased secretion of IL-4 (13). Arif et al. also showed that the quality of autoreactive T cells in patients with

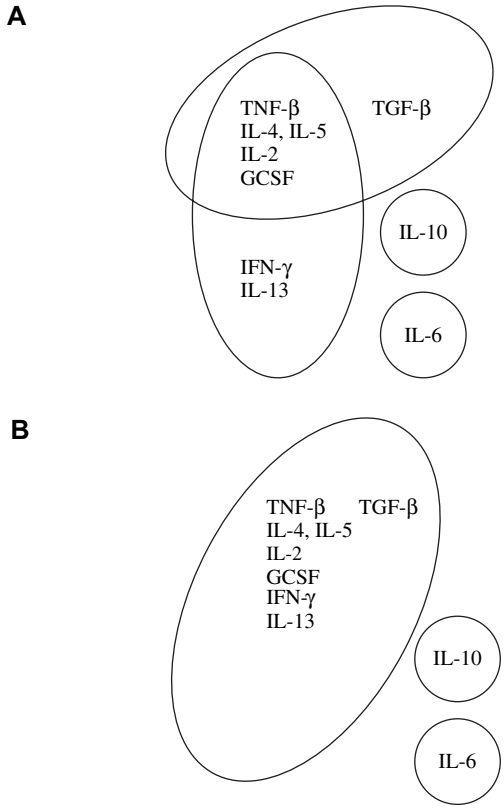

Fig. 5. (A) T1D patients: correlations in cytokine basal production. (B) T1D patients: correlations in stimulated cytokine production. Cytokines that produced was in correlation are displayed. In T1D patients correlations were *de facto* same for basal and for stimulated production within D1, D2 and D3 – so are displayed together as T1D group. GCSF, granulocyte colony-stimulating factor; IFN, interferon; IL, interleukin; T1D, type 1 diabetes; TGF, transforming growth factor; TNF, tumor necrosis factor.

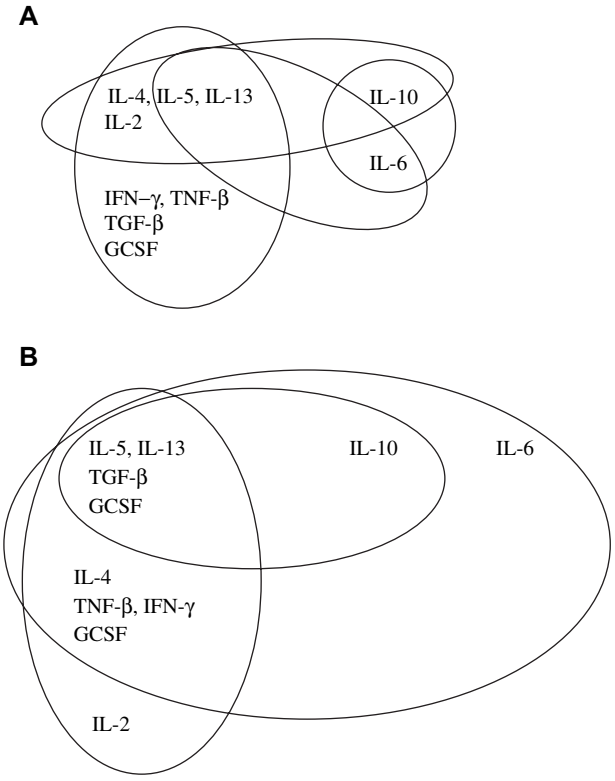

Fig. 6. (A) Controls: correlations in cytokine basal production. (B) Controls: correlations in cytokine-stimulated production. Cytokines that produced was in correlation are displayed. GCSF, granulocyte colony-stimulating factor; IFN, interferon; IL, interleukin; TGF, transforming growth factor; TNF, tumor necrosis factor.

T1D exhibits polarization toward a Th1 response. Furthermore, they demonstrated that the majority of non-diabetic, HLA-matched controls also manifest a response against islet peptides, but one that shows extreme T-regulatory cell bias (IL-10 secreting) (14). In general, these findings are in agreement with our results.

We also used the Spearman's analysis to reveal the relations between cytokines. There, we could see that the basal levels of cytokines in the control group were more or less in balance. The IL-2 and Th2 cytokine spectrum (IL-4, IL-5, and IL-13) strongly correlated with the Th1 cytokine spectrum (IFN-γ and TNF-β) and the Th3 cytokines (mainly TGF-β). The IL-10 production within the controls correlated with the Th2 cytokines and IL-6. The similar pattern could be seen even in the T1D patient's group, but with no correlation for Th3 cytokines with IL-13 and INF-γ (in basal production). In contrast, the situation was very different in the relatives group. The basal IL-2 and Th2 cytokine spectrum correlated with TGF-β, not with IL-10 and Th1 cytokines. The Th1 cytokine production was not correlated with Th3 cytokines at all. After stimulation, the 'patterns' in all the groups remained rather the same. The most variable cytokines were IL-6 and IL-10. IL-6 and IL-10 did not correlate with any cytokine in the T1D group. In the group of controls, IL-6 and IL-10 correlated with the Th2 cytokines in the basal production and after stimulation they also correlated with Th1 and Th3 cytokines. In the relatives group, IL-6 correlated only with IL-10 and *vice versa*.

In the end, some cytokine preferences within the groups as well as some tendency to failure in cooperation of Th3 and Th1/Th2 response in the relatives and T1D groups could be seen. As could be expected, the most variable was the group of relatives. We suppose that there might be a correlation with genotype and antibody status, which however was not performed in this study because of the small numbers. Nevertheless, it would be interesting to focus this group to show all these relations.

We believe that the protein microarray approach and mainly quantitative multiparameter analysis can be very useful methodological tool in T1D research. However, there has to be considered the variety of data for analysis.

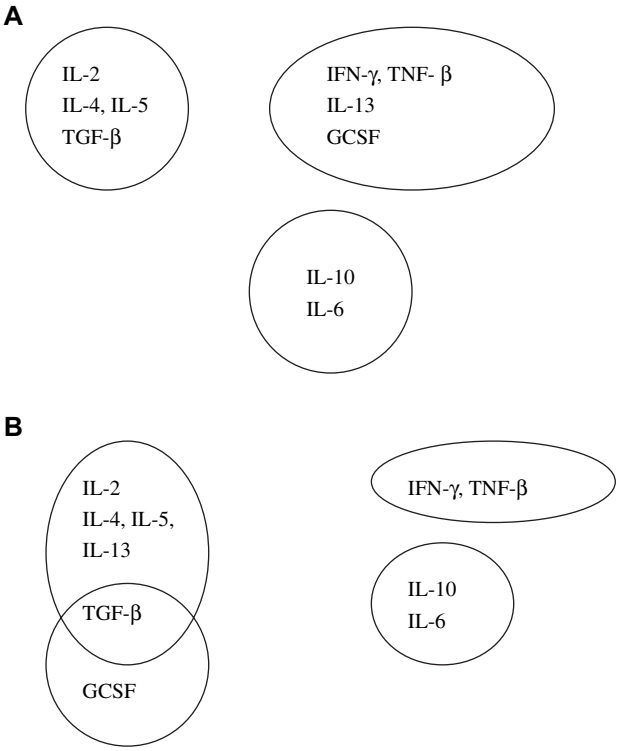

Fig. 7. (A) Relatives: correlations in cytokine basal production. (B) Relatives: correlations in cytokine-stimulated production. Cytokines that produced was in correlation are displayed. GCSF, granulocyte colony-stimulating factor; IFN, interferon; IL, interleukin; TGF, transforming growth factor; TNF, tumor necrosis factor.

Acknowledgements

This project was supported by the research national project of Internal Grant Agency Ministry of Health No. NR/8127-3.

References

1. Atkinson MA, Eisenbarth GS. Type 1 diabetes: new perspectives on disease pathogenesis and treatment. Lancet 2001: 358: 221–229.
2. Saudkova L, Saudek F. Possibilities of preclinical type 1 diabetes diagnostics and methods of detection of autoreactive T cells. Diabetes Metab Endocrinol Nutr 2003: 2: 70–78.
3. Roep BO. The role of T-cells in the pathogenesis of type 1 diabetes: from cause to cure. Diabetologia 2003: 46: 305–321.
4. Tree TI, Peakman M. Autoreactive T cells in human type 1 diabetes. Endocrinol Metab Clin North Am 2004: 33: 113–133.
5. Durinovic-Bello I, Schlosser M, Riedl M et al. Pro- and anti-inflammatory cytokine production by autoimmune T cells against preproinsulin in HLA-DRB1*04, DQ8 type 1 diabetes. Diabetologia 2004: 47: 439–450.
6. Lindley S, Dayan CM, Bishop A, Roep BO, Peakman M, Tree TI. Defective suppressor function in CD4(+)CD25(+) T-cells from patients with type 1 diabetes. Diabetes 2005: 54: 92–99.
7. Utz PJ. Protein arrays for studying blood cells and their secreted products. Immunol Rev 2005: 204: 264–282.
8. Cinek O, Kolouskova S, Pechova M et al. Prediction of insulin-dependent diabetes mellitus in first-degree relatives of diabetic patients. Cas Lek Cesk 2001: 140: 492–496.
9. Schloot NC, Meierhoff G, Karlsson Faresjö M et al. Comparison of cytokine ELISpot assay formats for the detection of islet antigen autoreactive T cells. Report of the third immunology of diabetes society T-cell workshop. J Autoimmun 2003: 21: 365–376.
10. Meierhoff G, Ott PA, Lehmann PV, Schloot NC. Cytokine detection by ELISPOT: relevance for immunological studies in type 1 diabetes. Diabetes Metab Res Rev 2002: 18: 367–380.
11. Naik RG, Beckers C, Wentwoord R et al. Precursor frequencies of T-cells reactive to insulin in recent onset type 1 diabetes mellitus. J Autoimmun 2004: 23: 55–61.
12. Karlsson Faresjo MG, Ernerudh J, Ludvigsson J. Cytokine profile in children during the first 3 months after the diagnosis of type 1 diabetes. Scand J Immunol 2004: 59: 517–526.
13. Karlsson MGE, Sederholm Lawesson S, Ludvigsson J. Th1-like dominance in high-risk first-degree relatives of type I diabetic patients. Diabetologia 2000: 43: 742–749.
14. Arif S, Tree TI, Astill TP et al. Autoreactive T cell responses show proinflammatory polarization in diabetes but a regulatory phenotype in health. J Clin Invest 2004: 113: 451–463.
15. Fathman CG, Soares L, Chan SM, Utz PJ. An array of possibilities for the study of autoimmunity. Nature 2005: 435: 605–611.
16. Krenn V, Petersen I, Haupl T et al. Array technology and proteomics in autoimmune diseases. Pathol Res Pract 2004: 200: 95–103.
17. Peakman M, Tree TI, Endl J, van Endert P, Atkinson MA, Roep BO. Characterization of preparations of GAD65, proinsulin, and the islet tyrosine phosphatase IA-2 for use in detection of autoreactive T-cells in type 1 diabetes: report of phase II of the Second International Immunology of Diabetes Society Workshop for Standardization of T-cell assays in type 1 diabetes. Diabetes 2001: 50: 1749–1754.
18. Narendran P, Mannering SI, Harrison LC. Proinsulin-a pathogenic autoantigen in type 1 diabetes. Autoimmun Rev 2003: 2: 204–210.
19. Stechova K, Kolouskova S, Sumnik Z et al. Anti-GAD65 reactive peripheral blood mononuclear cells in the pathogenesis of cystic fibrosis related diabetes mellitus. Autoimmunity 2005: 38: 319–323.

PŘÍLOHA VI.

High T-helper-1 cytokines but low T-helper-3 cytokines, inflammatory cytokines and chemokines in children with high risk of developing type 1 diabetes

K. Štechová, K. Böhmová, Z. Vrábelová, A. Sepa, G. Štádlerová, K. Zacharovová, and M. Faresjö

Diabetes Metab Res Rev, 2007. 23(6): p. 462-71.

DIABETES/METABOLISM RESEARCH AND REVIEWS
Diabetes Metab Res Rev 2007; **23**: 462–471.
Published online 21 February 2007 in Wiley InterScience (www.interscience.wiley.com) **DOI:** 10.1002/dmrr.718

RESEARCH ARTICLE

High T-helper-1 cytokines but low T-helper-3 cytokines, inflammatory cytokines and chemokines in children with high risk of developing type 1 diabetes

Katerina Stechova[1]
Kristyna Bohmova[1]
Zuzana Vrabelova[1]
Annelie Sepa[2]
Gabriela Stadlerova[1]
Klara Zacharovova[3]
Maria Faresjö[2]*

[1]*Department of Paediatrics, 2nd Medical Faculty of Charles University, University Hospital Motol in Prague, Prague, Czech Republic*

[2]*Division of Paediatrics & Diabetes Research Centre, Department of Molecular & Clinical Medicine, Faculty of Health Sciences, Linköping University, Linköping, Sweden*

[3]*Department of Diabetology, Institute of Clinical and Experimental Medicine, University Hospital Motol in Prague, Prague, Czech Republic*

*Correspondence to: Maria Faresjö, Clinical Experimental Research, Division of Paediatrics, Faculty of Health Sciences, Linköping University, S-581 85 Linköping, Sweden.
E-mail: maria.faresjo@imk.liu.se

Received: 20 June 2006
Revised: 22 November 2006
Accepted: 22 November 2006

Abstract

Background Type 1 diabetes (T1D) is suggested to be of T-helper (Th)1-like origin. However, recent reports indicate a diminished interferon (IFN)-γ secretion at the onset of the disease. We hypothesize that there is a discrepancy in subsets of Th-cells between children with a high risk of developing T1D, children newly diagnosed with T1D and healthy children.

Methods Peripheral blood mononuclear cells (PBMC) were collected from children at high risk for T1D (islet cells antibodies [ICA] $\geq$20 IJDF-U), those newly diagnosed and healthy children carrying the HLA-risk gene *DQB1*0302* or *DQB1*0201* and *DQA1*0501*. Th1- (IFN-γ, tumour necrosis factor [TNF]-β, interleukin [IL]-2), Th2- (IL-4,-5,-13), Th3- (transforming growth factor [TGF-β], IL-10) and inflammatory associated cytokines (TNF-α, IL-1α,-6) and chemokines (monocyte chemoattractant protein [MCP]-1,-2,-3, Monokine unregulated by IFN-γ [MIG], Regulated on Activation, Normal T-cell Expressed and Secreted [RANTES], IL-7,-8,-15) were detected in cell-culture supernatants of PBMC, stimulated with glutamic acid decarboxylase 65 (GAD_{65}) and phytohaemagglutinin (PHA), by protein micro array and enzyme linked immunospot (ELISPOT) technique.

Results The Th1 cytokines IFN-γ and TNF-β, secreted both spontaneously and by GAD_{65}- and mitogen stimulation, were seen to a higher extent in high-risk children than in children newly diagnosed with T1D. In contrast, TNF-α and IL-6, classified as inflammatory cytokines, the chemokines RANTES, MCP-1 and IL-7 as well as the Th3 cytokines TGF-β and IL-10 were elevated in T1D children compared to high-risk children.

Conclusion High Th-1 cytokines were observed in children with high risk of developing TID, whereas in children newly diagnosed with T1D Th3 cytokines, inflammatory cytokines and chemokines were increased. Thus, an inverse relation between Th1-like cells and markers of inflammation was shown between children with high risk and those newly diagnosed with T1D.

Keywords type 1 diabetes; high-risk children; T-helper cells; cytokines; chemokines; protein micro array

Introduction

Type 1 diabetes (T1D) is an autoimmune disease suggested to be of T-helper (Th)1-like origin [1,2]. Cytotoxic actions of Th1-associated cytokines,

interferon (IFN)-α [3–5] and IFN-γ [6], have been observed on human islets *in vivo* in patients with recent-onset T1D. Studies of the peripheral immune system of patients with recent-onset T1D have shown significantly increased levels of interleukin (IL) -1α, -2, IFN-γ and tumour necrosis factor (TNF)-α [7,8]. The T-cell response against β-cell antigens has also shown an association with IFN-γ production in newly diagnosed T1D patients, suggesting a Th1-like phenotype of the T-cell lines [9]. We have previously observed a Th1-like dominated immune profile by high IFN-γ secretion during the pre-diabetic phase [10–12]. However, close to the onset of T1D, when only few β-cells remain, the Th1-like response vanishes and remains suppressed in newly diagnosed T1D patients [10,13–15]. Further, an immune-regulatory defect by reduced function of regulatory/suppressor T (T-reg) cells has been observed at diagnosis of T1D [16].

As part of their different effector capabilities, Th-cells express different sets of chemokine receptors, allowing them to migrate to different tissues. It has been shown that Th1-cells can be distinguished from Th2-cells by differences in chemokine synthesis [17]. Expression of monocyte chemoattractant protein (MCP)-1 in islets has been shown to increase concomitantly with the progression of insulitis in non-obese diabetic mice [18]. Monokine upregulated by IFN-γ (MIG) binds to the receptor CXCR3 on Th1-like cells, and has been found to be induced by IFN-γ in human islets [19]. Expression of Regulated on Activation, Normal T-cell Expressed and Secreted (RANTES) has been observed in pancreatic tissue from normal mice and may serve as protection from possible infectious agents because of the ability of islets to attract CCR5+ lymphocytes [20]. Interleukins such as IL-7, IL-8 and IL-15 are cytokines with a chemoattractant function. Interleukin-7 has a pivotal role in CD4+ T-cell homeostasis and stimulates the expression of CXCR4 on naive CD4+ T cells. IL-15 is a potent growth factor and activator of T cells and NK cells. IL-15 can also act as a T-cell chemoattractant and inducer of IFN-γ production by NK cells [21].

We hypothesize that there is a discrepancy in subsets of Th-cells at different stages of the disease process leading to T1D. The aim of this study was thus to investigate cytokines and chemokines in order to differentiate the subsets of Th-cells in high-risk children, children newly diagnosed with T1D and healthy children.

Materials and methods

Peripheral blood mononuclear cells from high-risk, newly diagnosed T1D and healthy children

The European Nicotinamide Diabetes Intervention Trial (ENDIT) included high-risk first-degree relatives of T1D patients receiving either nicotinamide or placebo [22]. More than 2000 first-degree relatives were screened in Sweden to identify individuals with as much as a 40% risk of developing the disease within 5 years ($\geq$20 islet cells antibodies IJDF units). Eight of 21 high-risk first-degree relatives included in Sweden were children (8–18 years, mean age 13 years, two female (F)/six male (M)) (Table 1). High-risk children were matched for age with eight children 4 days post-diagnosis of T1D (6–16 years, mean age 12 years, 4 F/4 M) and eight healthy children (7–15 years, mean age 11 years, 4 F/4 M) (Table 1). Blood samples from children with TID were taken four days post-diagnosis at the Linköping University hospital, Linköping, Sweden. These T1D children were not participants of the *European Nicotinamide Diabetes Intervention* trial. The healthy children carried the HLA-risk gene *DQB1*0302* or *DQB1*0201* and *DQA1*0501*. None of the healthy children or their first-degree relatives had T1D or any other autoimmune disease and none had increased levels of glutamic acid decarboxylase (GADA) or tyrosinphosphatase (IA–2A) autoantibodies. Blood samples from children with T1D were taken when they visited the diabetes clinic, and blood samples from healthy children were taken at school, when possible during the morning hours to avoid time-of-day differences. Peripheral blood mononuclear cells (PBMC) were isolated by Ficoll-Paque density-gradient centrifugation (Pharmacia Biotech, Sollentuna, Sweden) from sodium-heparinized venous blood samples. PBMC were cryopreserved in liquid nitrogen until use [10].

Table 1. Characteristics of high-risk, newly diagnosed T1D and healthy children

High-risk children							Newly diagnosed T1D children					Healthy children	
Age	Gender	N/P	Dev. T1D	C-peptide	GADA	IA-2A	Age	Gender	C-peptide	GADA	IA-2A	Age	Gender
8	F	N	Yes (6 mon)	0.57	183	1940	6	M	0.09	305	100	7	F
10	M	P	No	0.54	0	0	9	M	0.02	431	31	7	M
12	F	P	No	0.43	4120	6920	11	F	0.16	n.a.	n.a.	9	F
12	M	N	Yes (4 yrs)	0.46	860	3950	11	F	0.27	n.a.	n.a.	10	F
14	M	N	Yes (1 yr)	0.56	0	237	12	F	0.10	1650	1780	11	M
15	M	N	No	0.40	30 480	74	14	M	0.15	127	1010	13	M
15	M	P	No	0.05	139 440	0	16	F	0.38	n.a.	n.a.	14	M
18	M	P	No	0.98	13 560	3340	16	M	0.13	93	0	15	F

The individual characteristics of high-risk children, newly diagnosed T1D children and healthy children – age (years), gender (F = female/M = male), C-peptide (nmol/L), GAD_{65} autoantibodies (GADA, RA units/mL) and tyrosinphosphatase autoantibodies (IA-2A, RA units/mL) – plus for high-risk children treatment (N = nicotinamide/P = placebo) and development of T1D (Dev. T1D; months/years) after blood sampling.
n.a. = not analysed

DOI: 10.1002/dmrr

In vitro stimulation of PBMC

PBMC (1.5×10^6) (viability approximately 90% or more for each population) were diluted in 1500 μL AIM V research-grade serum-free medium (Gibco, Täby, Sweden) supplemented with 2 mM L-glutamine, 50 μg/L streptomycin sulphate, 10 μg/L gentamicin sulphate and 2×10^{-5} M 2-mercaptoethanol (Sigma, Stockholm, Sweden). PBMC were incubated in medium alone (spontaneous secretion) or with glutamic acid decarboxylase 65 ([GAD_{65}], DiamydTM, Diamyd Therapeutics AB, Stockholm, Sweden) and phytohaemagglutinin ([PHA], Sigma, Stockholm, Sweden) at a concentration of 5 μg/mL [15,23] at 37 °C, in a humidified atmosphere with 5% CO_2. The medium was harvested after 48 h stimulation and used for detection of cytokines and chemokines by protein micro array.

Protein micro array

Protein micro array was performed with a commercially available kit according to the manufacturer's instructions (RayBiotech, GA, USA), as previously shown [24]. Production of the following cytokines and chemokines was assessed: Granulocyte Colony Stimulating Factor (GCSF), Granulocyte Macrophage-Colony Stimulating Factor (GM-CSF), Growth-Related Oncogene (GRO), GRO-α, IL-1α, -2, -3, -5, -6, -7, -8, -10, -13, -15, IFN-γ, MCP-1, -2, -3, MIG, RANTES, TGF-β1, TNF-α and TNF-β (kit no. H0108001). Detection was carried out using the Fuji LAS1000 imaging system. Chemiluminescent signals were analysed using the AIDA software (Advanced Image Data Analyzer 3.28, Raytest Izotopenmessgeraete, Straubenhardt, Germany). The intensity of spots (%) was calculated. Sensitivity for cytokines and chemokines (manufacturer's figures) are displayed in Table 2.

Table 2. Cytokines & chemokines

Th1-ass. cytokines	Sensitivity (pg/mL)
IL-2	25
IFN-γ	100
TNF-β	1000
Th2-ass. cytokines	**Sensitivity (pg/mL)**
IL-5	1
IL-13	100
Th3-ass. cytokines	**Sensitivity (pg/mL)**
IL-10	10
TGF-β1	200
Chemokines	**Sensitivity (pg/mL)**
RANTES	2000
MCP-1	3
MCP-2	100
MCP-3	1000
MIG	1
IL-7	100
IL-8	1
IL-15	100
GRO	1000
GRO-α	1000
Inflammatory ass. cytokines	**Sensitivity (pg/mL)**
IL-1α	1000
IL-6	1
TNF-α	100

Sensitivity (pg/mL) of cytokines and chemokines, grouped according to association with subgroups of Th-cells.

Stimulation of lymphocytes and enumeration of IL-4-secreting cells by enzyme linked immunospot (ELISPOT)

The enzyme linked immunospot (ELISPOT) technique was used for detection of low numbers of Th2-cytokine (IL-4)-secreting PBMC at the single cell level [10,11]. Aliquots of 100 000 PBMC/well were incubated in quadruplicate in medium alone (spontaneous secretion) or stimulated with GAD_{65} (Diamyd), the synthetic peptide of GAD_{65} a.a. 247–279 (NMYAMMIARFK MFPEVKEKGMAALPRLIAFTSE-OH) molecular weight 3823.7 (Dept of Medical and Physiological Chemistry, University of Uppsala, Sweden) and tyrosine phosphatase (IA-2, produced in *E. coli*, Åbo Akademi, Turku, Finland), all at the optimized concentration of 100 pg/mL, 10 mg/mL of ovalbumin (OVA, Sigma) and PHA at a concentration of 20 μg/mL [10]. In samples with a limited number of cells, the order of priority for stimulation with antigens was PHA, GAD_{65}, the GAD_{65} peptide (a.a. 247–279), IA–2 and OVA.

Plates were blinded for identity to avoid any influence on the outcome of the observation. Plates were counted automatically, under manual supervision, using the AID ELISPOT Reader System (AID, Strasbourg, France). The median value of the quadruplicates was calculated for each stimulation and for spontaneous secretion. As a negative control, some wells on each plate were incubated exclusively with culture medium, without cells but otherwise treated as the other wells, whereas stimulation with PHA was used as a positive control. The laboratory of Faresjö participated in the first ELISPOT workshop as one of the core laboratories, and our Mabtech assay was judged to be sensitive and reproducible [25].

Autoantibodies

GADA and IA–2A were detected by radio immune assay, using *in vitro* transcribed and translated human ^{35}S–GAD_{65} or ^{35}S–IA–2 as label [26]. For T1D and healthy children, the cut-off for positivity at the 98th percentile of 1-year-old Swedish children from the general population was >104 relative units/mL for GADA (N = 4400) and >36 relative units/mL for IA–2A (N = 4400). For high-risk children, the cut-off for positivity at the 98th percentile of 2–3-year-old Swedish children from the general population was >105.1 RA units/mL,

corresponding to 36.6 WHO units, for GADA and >30 RA units/mL (N = 4258), corresponding to 28.5 WHO units, for IA–2A (N = 4461).

C-peptide

C-peptide was determined with a radioimmunoassay technique based on the original assay developed by Heding [27]. The detection limit for the assay is 0.03 nmol/L, and the reference value among fasting healthy children and adolescents is 0.18–0.63 nmol/L.

Statistics

As the expression and secretion of immunological markers was not normally distributed (even after logarithmic transformation), two groups were compared by Mann–Whitney U-test and three or more groups using the Kruskal–Wallis test for unpaired observations. Post hoc comparisons of grouped immunological parameters (e.g. sum scores were calculated) were analysed with Wilcoxon signed-ranks test, with adjusted degrees of freedom to compensate for multiple comparisons. Spearman's rank correlation was used when comparing paired non-parametric variables. A probability level of <0.05 was considered to be statistically significant. Calculations were performed using the statistical package StatView 5.0.1 for Macintosh (Abacus Concepts Inc., Berkeley, CA, USA).

Ethics

The study was approved by the Research Ethics Committee of the Faculty of Health Sciences, Linköping University.

Results

Th1-associated cytokines (IFN-γ, TNF-β, IL-2)

The typical Th1-like cytokine IFN-γ was seen to a higher extent spontaneously in high-risk children than in either diabetic ($p < 0.05$) or healthy ($p < 0.05$) children (Figure 1(a)). Furthermore, spontaneous secretion of TNF-β was found to be higher in high-risk ($p = 0.1$) and diabetic ($p < 0.05$) children than in healthy children (Figure 1(b)) and correlated to spontaneous secretion of IFN-γ ($r = 0.56$, $p < 0.01$).

GAD_{65}-induced IFN-γ was higher in the group of high-risk children than in diabetic ($p = 0.06$) or healthy ($p = 0.01$) children (Figure 1(a)). Further, TNF-β induced by GAD_{65} was found to a higher extent in high-risk ($p < 0.05$) and T1D ($p < 0.01$) children than in healthy children (Figure 1(b)) and correlated positively with GAD_{65}-induced secretion of IFN-γ ($r = 0.63$, $p < 0.05$).

High-risk children showed a very high IFN-γ response by stimulation with PHA compared to T1D children ($p < 0.01$). Further, T1D children had a lower PHA-induced IFN-γ response than healthy children ($p = 0.09$).

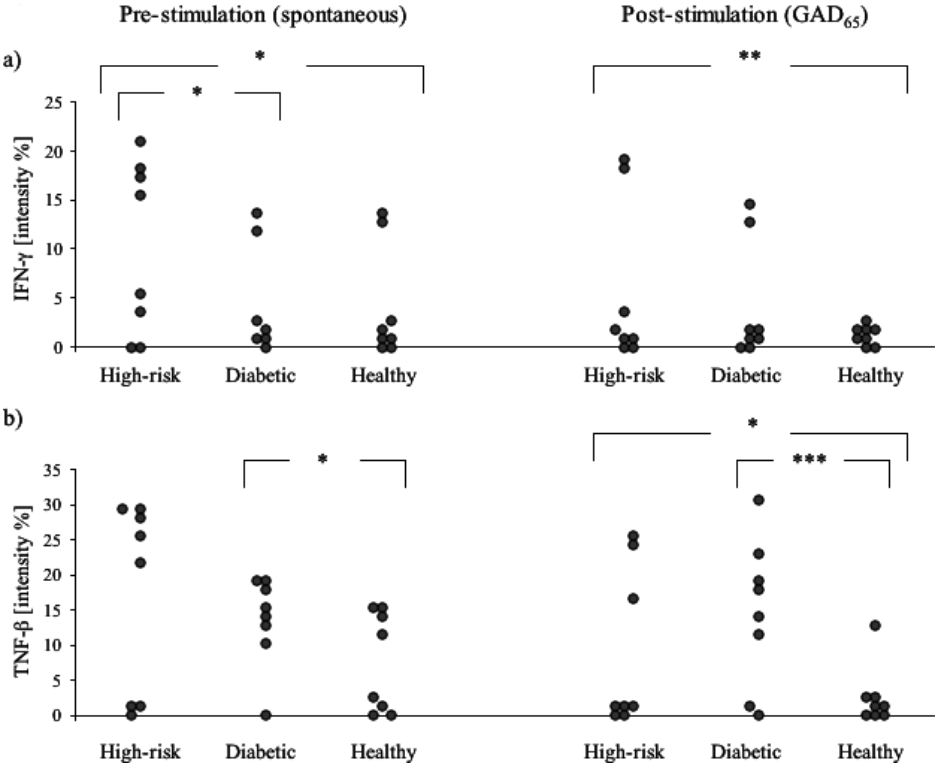

Figure 1. Secretion of the Th1-associated cytokines IFN-γ (a) and TNF-β (b) pre-stimulation (spontaneous) as well as post-stimulation (GAD65-induced). * $p < 0.05$, ** $p = 0.01$, *** $p < 0.01$

PHA induced secretion of TNF-β in all children without any differences between groups.

IL-2 was rarely detected in any of the studied children.

Th2-associated cytokines (IL-4, -5, -13)

High-risk children secreted higher levels of IL-5 by PHA stimulation compared to both diabetic ($p < 0.01$) and healthy children ($p < 0.01$), whereas PHA-induced IL-4 secretion was correlated to IL-13 in all children ($r = 0.49$, $p < 0.05$).

Th3-associated cytokines (TGF-β IL-10)

Spontaneous and GAD_{65}-induced TGF-β was significantly higher in newly diagnosed T1D children compared to high-risk ($p = 0.05$ and $p < 0.05$ respectively) and healthy children ($p < 0.05$ and $p < 0.01$ respectively) (Figure 2). High-risk children secreted less IL-10 both spontaneously compared to T1D children ($p = 0.06$) and by stimulation with PHA compared to healthy children ($p < 0.05$).

Chemokines (RANTES, MCP-1, -2, -3, MIG, IL-7, -8, -15, GRO, GRO-α)

The levels of both spontaneously secreted (Figure 3) and GAD_{65}-induced RANTES were significantly lower among high-risk children than healthy children ($p < 0.05$ and $p = 0.05$ respectively) and tended to compare with diabetic children ($p = 0.09$ and $p = 0.1$ respectively). Further, PHA-induced secretion of RANTES was significantly lower in high-risk children compared to diabetic ($p < 0.001$) and healthy ($p < 0.01$) children (Figure 3).

GAD_{65}-induced MCP-1 secretion was significantly higher in diabetic children than in high-risk ($p < 0.05$) or healthy ($p < 0.05$) children (Figure 4). Further, both diabetic ($p = 0.01$) and healthy ($p = 0.01$) children secreted higher levels of MCP-1 induced by PHA than high-risk children. Thus, spontaneous ($r = 0.78$, $p < 0.05$) as well as GAD_{65} ($p = 0.51$, $p = 0.06$) or PHA ($r = 0.55$, $p = 0.01$)-induced MCP-1 was positively correlated to RANTES. No significant differences in secretion of MCP-2 and MCP-3 were observed between the groups of children studied.

MIG, induced by PHA, tended to be higher among high-risk children than in either diabetic or healthy children ($p = 0.06$ and $p = 0.06$ respectively) and was positively

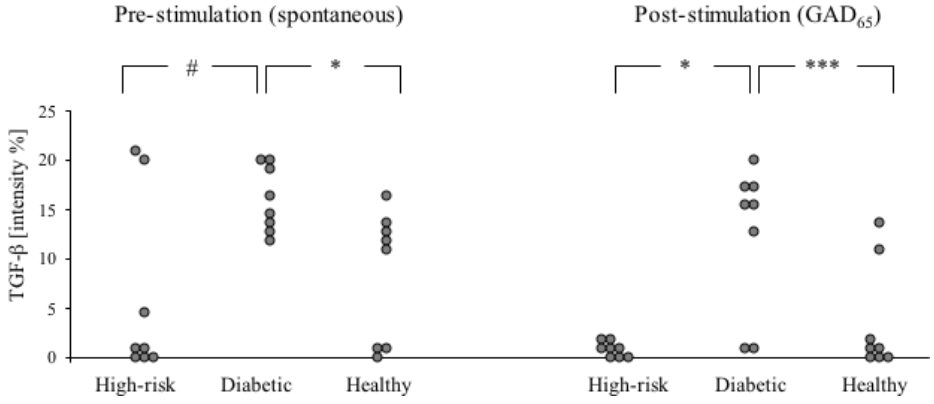

Figure 2. Secretion of the Th3-associated cytokine TGF-β pre-stimulation (spontaneous) and post-stimulation (GAD65-induced). # $p = 0.05$, * $p < 0.05$, *** $p < 0.01$

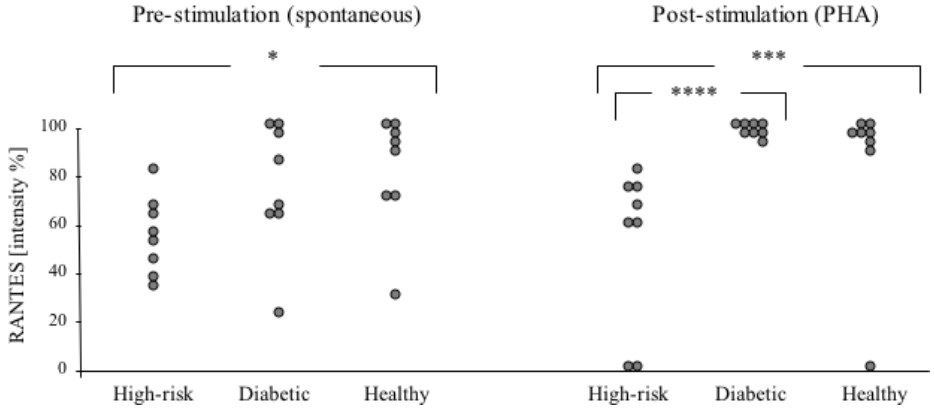

Figure 3. Secretion of the chemokine RANTES pre-stimulation (spontaneous) and post-stimulation (PHA-induced). * $p < 0.05$, *** $p < 0.01$, **** $p < 0.001$

DOI: 10.1002/dmrr

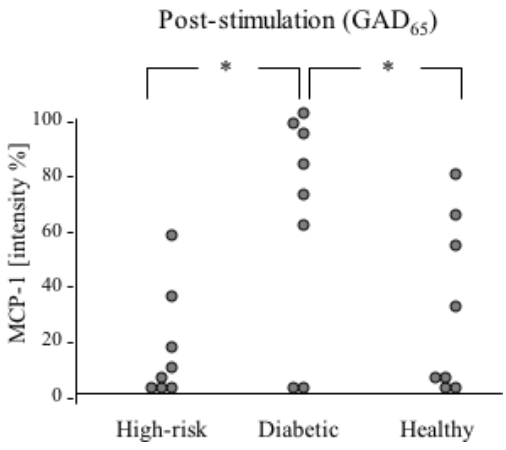

Figure 4. Secretion of the chemokine MCP-1 induced by GAD65. * $p < 0.05$

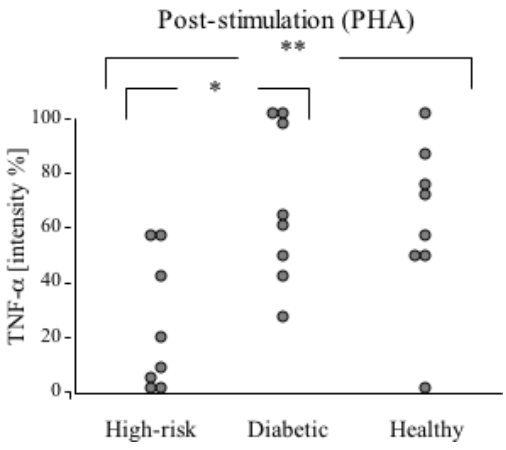

Figure 5. Secretion of the inflammatory cytokine TNF-α induced by PHA. * $p < 0.05$, ** $p = 0.01$

correlated to PHA-induced secretion of IFN-γ in diabetic children ($r = 0.85$, $p < 0.05$).

PHA-induced secretion of IL-7 tended to be higher in T1D children than high-risk children ($p = 0.06$). Spontaneously secreted RANTES was correlated to IL-7 among high-risk children ($r = 0.73$, $p = 0.05$), whereas both GAD_{65}- ($r = 0.44$, $p = 0.1$) and PHA-induced ($r = 0.41$, $p = 0.06$) IL-7 secretion was correlated to RANTES in all children. Spontaneous IL-7 secretion was inversely correlated to secretion of IL-4 in both high-risk and diabetic children ($r = -0.45$, $p < 0.05$).

A high level of IL-8 was detected in all children without differences between groups (data not shown), in contrast to IL-15, which was secreted only to a low extent in a few samples, equally between the groups.

Stimulation with PHA induced lower secretion of GRO in diabetic children compared to healthy children ($p < 0.05$), whereas spontaneously secreted GRO-α tended to be higher in children with T1D compared to healthy children ($p = 0.06$). GAD_{65} induced equal secretion of GRO and GRO-α in all studied subjects.

Inflammatory associated cytokines (TNF-α, IL-1α, -6)

Spontaneous secretion of TNF-α ($p < 0.05$) as well as GAD_{65}- ($p = 0.09$) or PHA-induced TNF-α ($p < 0.05$) (Figure 5) was found to a higher extent in T1D children than in high-risk children. PHA-induced TNF-α was also found to a higher extent in healthy children than in high-risk children ($p = 0.01$) (Figure 5).

GAD_{65}-induced IL-6 tended to be higher in T1D children than in healthy children ($p = 0.08$). Secretion of IL-6 was correlated to TNF-α after stimulation with either GAD_{65} ($r = 0.53$, $p = 0.06$) or PHA ($r = 0.55$, $p = 0.01$). No discrepancy was observed in secretion of IL-1α between the three studied groups.

Post hoc comparisons of grouped immunological parameters

Spontaneous secretion of following immunological parameters differed significantly between high-risk, T1D and healthy children: Th1 cytokines (IFN-γ, TNF-β), Th3 cytokine (TGF-β), inflammatory cytokine (TNF-α) and chemokine (RANTES). These Th1 cytokines were significantly lower in T1D ($p < 0.05$) and higher in high-risk children ($p < 0.05$), compared to the Th3 cytokine, inflammatory cytokine and chemokine (Figure 6(a)). Comparing all detectable immunological parameters still showed that Th1 cytokines (IFN-γ, TNF-β) were significantly lower among T1D children compared to Th3 cytokines (TGF-β, IL-10), inflammatory cytokines (TNF-α, IL-6) and chemokines (RANTES, MCP-1, MIG) ($p = 0.01$, data not shown).

GAD_{65}-induced secretion of the following immunological parameters differed significantly between high-risk, T1D and healthy children: Th1 cytokines (IFN-γ, TNF-β), Th3 cytokine (TGF-β), inflammatory cytokine (TNF-α) and chemokines (RANTES, MCP-1). These Th1 cytokines were significantly lower in T1D compared to the Th3 cytokine, inflammatory cytokine and chemokines ($p < 0.05$, Figure 6(b)).

PHA-induced secretion of the following immunological parameters differed significantly between high-risk, T1D and healthy children: Th1 cytokine (IFN-γ), Th3 cytokine (IL-10), inflammatory cytokine (TNF-α) and chemokines (RANTES, MCP-1). The Th1 cytokine was significantly lower in T1D ($p < 0.05$) and higher in high-risk children ($p < 0.05$), compared to the Th3 cytokine, inflammatory cytokine and chemokines. Comparing all detectable immunological parameters still showed that Th1 cytokines (IFN-γ, TNF-β) were significantly lower among T1D children ($p < 0.05$) and higher in high-risk children ($p < 0.05$), compared to the Th3 cytokines (TGF-β, IL-10), inflammatory cytokines (TNF-α, IL-6) and chemokines (RANTES, MCP-1, MIG) (data not shown).

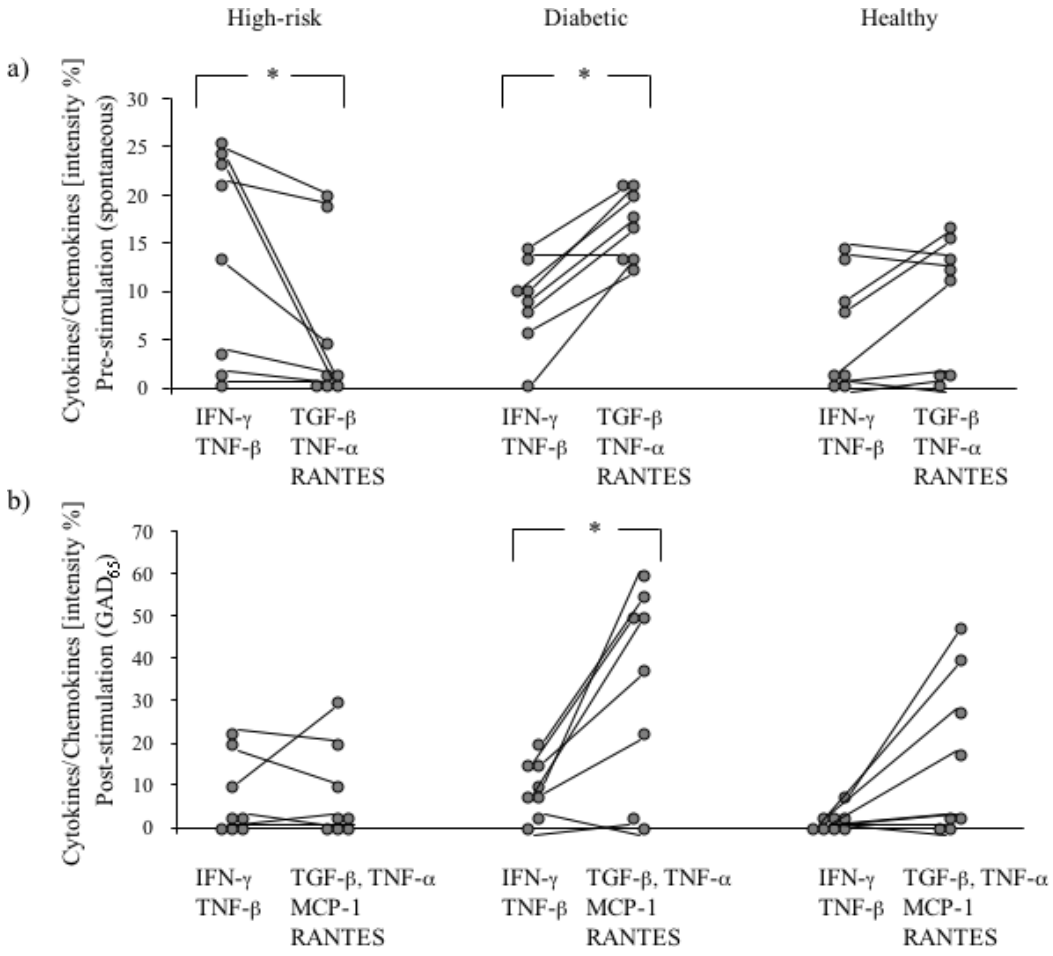

Figure 6. Post hoc comparison of spontaneous secretion of Th1 (IFN-γ, TNF-β) *versus* Th3 (TGF-β)/inflammatory marker (TNF-α)/chemokine (RANTES) (a) and GAD_{65}-induced comparison of Th1 (IFN-γ, TNF-β) *versus* Th3 (TGF-β)/inflammatory marker (TNF-α)/chemokines (MCP-1, RANTES) (b) on individual basis in high-risk, T1D and healthy children. * $p < 0.05$

Immunological markers in relation to C-peptide

The Th1-associated cytokines IFN-γ ($r = 0.66$, $p = 0.01$) and TNF-β ($r = 0.47$, $p = 0.07$), secreted spontaneously, correlated to C-peptide in both high-risk and T1D children, whereas the Th2-associated cytokine IL-13 correlated to C-peptide only in the high-risk children ($r = 0.59$, $p = 0.1$). Exclusively in newly diagnosed T1D children, spontaneously secreted IL-7 ($r = 0.73$, $p = 0.05$) (Figure 7) and IL-6 ($r = 0.67$, $p = 0.08$) tended to correlate with secretion of C-peptide.

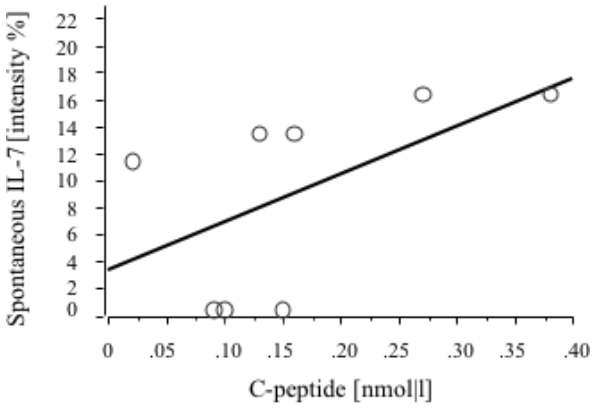

Figure 7. Relation between C-peptide and spontaneous secretion of IL-7 ($r = 0.73$, $p = 0.05$)

Immunological markers not detected

GCSF, GM-CSF and IL-3 were not found in any child in the three studied groups.

Discussion

T1D has been associated with increased concentrations of Th1 cytokines, for example, IFN-α, IFN-γ, IL-2 and TNF-β. Therefore, it has been suggested that T1D is a Th1-associated autoimmune disease. We found a high spontaneous secretion of IFN-γ and TNF-β in children with a high risk of developing T1D. The Th1-like profile was significantly higher in high-risk children than in newly diagnosed T1D children. This agrees with our previous observation of a Th1-like dominated immune profile by high IFN-γ secretion during the pre-diabetic

phase [10–12]. In high-risk individuals, the autoantigens GAD_{65}, IA–2 and heat shock protein as well as mitogen stimulation are found to induce prominent IFN-γ secretion [12]. Here, we observed that newly diagnosed T1D children secreted less autoantigen- and mitogen-induced IFN-γ and TNF-β than high-risk children. We and others have previously shown that close to the onset of T1D, when only few β-cells remain, the Th1-like response vanishes and remains suppressed in newly diagnosed T1D patients [12–15,28,29]. This observation agrees with previous investigations where T-cell reactivity to GAD_{65} (a.a. 247–266 and 260–279) is shown to decrease at diabetes onset [30–32]. Diminished secretion of IFN-γ in newly diagnosed T1D patients has also been observed from *in vitro* mitogen stimulation [33,34]. Further, a disrupted ability to suppress T-cell proliferation during *in vitro* co-cultures of CD4 + CD25 + T cells in patients with recent-onset adult T1D has been found despite normal levels of this cell population [16]. This result is in line with our observation of a decreased secretion of the Th3-associated cytokines TGF-β and IL-10 in high-risk children, some of whom later developed T1D.

Compared to newly diagnosed T1D children, high-risk individuals responded with high secretion of IL-5 from mitogen stimulation. We have previously shown that healthy high-risk individuals seem to have an ability to change a Th1-like immune deviation into a more protective Th2-like response in the presence of diabetes-associated autoantigens [10,12]. Further, Th2 cytokines, for example, IL-5 and IL-13, show no relationship to multiple autoantibodies (GADA, IA–2A and islet cells antibodies [35].

There is increasing evidence that chemokines can play a role in the pathogenesis of T1D. It has been shown that Th1 cells can be distinguished from Th2 cells by their differences in chemokine synthesis [17]. Th1 cells have been associated with CCR5 and CXCR3, receptors for the chemokines RANTES and MIG, respectively. Delayed-type hypersensitivity-containing granulomas contain high levels of TNF-α and IFN-γ, and the ability of these cytokines to induce RANTES has been demonstrated in endothelial cells [36]. At diagnosis of T1D, but before insulin treatment, a reduced expression of the receptors CCR5 and CXCR3 has been observed [14]. We found that high-risk children, some of whom later developed T1D, secreted lower RANTES, both spontaneously and by GAD_{65}- and PHA stimulation compared to already diagnosed T1D children receiving insulin treatment. Recently, it has also been observed that two functional polymorphisms in the *CCR5* gene cause decreased expression of the RANTES receptor on immunocompetent cells and are associated with increased risk of diabetic nephropathy in T1D [37].

Interleukin-7 has a pivotal role in CD4 T-cell homeostasis stimulating the expression of CXCR4 on naive CD4 T cells. We and others [38] have found a correlation between IL-7 and RANTES. This can possibly be explained by the fact that RANTES increase co-localization of surface molecules CD4 and CXCR4 on CD4 T cells [39].

The chemokine MCP-1 plays an important role in the development of local inflammation by attracting monocytes and lymphocytes [40], and expression of MCP-1 in islets has been shown to increase concomitantly with the progression of insulitis in non-obese diabetic mice [18]. We found MCP-1 induced by the autoantigen GAD_{65} to a higher extent in newly diagnosed T1D children than in either high-risk or healthy children. Even though MCP-1 serum levels tend only to be higher in patients compared to control subjects [14], a high basal MCP-1 production by human islets is shown to correlate with poor clinical outcome following islet transplantation in T1D patients [41].

Both IFN-γ and MIG were high among high-risk children. MIG that binds to the receptor CXCR3 has been found to be induced by IFN-γ in human islets [19], explaining the positive correlation observed between MIG and IFN-γ in our cohort of newly diagnosed T1D children. MIG attracts monocytes and activated Th1- and NK cells. Thus, production of MIG by human islet cells can contribute to mononuclear, NK- and Th1 cell homing in early insulitis [19]. Human islet cells exposed to IFN-γ and also IL-1β show secretion of MIG and IL-15 [19]. In line with previous studies of human islets and other cell types, we found a low concentration of IL-15 from peripheral mononuclear cells [19,42]. However, picomolar amounts of IL-15 have been shown to be effective in maintaining NK cell survival, suggesting that even very low concentrations of this chemokine can be physiologically relevant.

TNF-α, classified as an inflammatory cytokine, is shown to induce IL-6. In type 2 diabetes (T2D), IL-6 is argued to be an important regulator of the acute phase response associated with insulin-resistant states [43], even though an independent role of IL-6 in T1D is still not proven [44]. Recently, it was shown that monocyte IL-6 in the resting state and IL-1β in activated monocytes were elevated in T1D patients (duration longer than one year) compared with control subjects [45]. In our cohort, both TNF-α and IL-6 were found to a higher extent in T1D children than in either high-risk or healthy children. Involvement of TNF-α in the damage of the insulin-producing cells has been observed in mice infected with coxsackie B4 and A7 viruses, indicating an immunity-related inflammatory process [46]. Further, it has been suggested that TNF-α plays a direct role in the metabolic syndrome, since T2D patients show a high concentration of TNF-α in plasma [47]. TNF-α, shown to impair insulin-stimulated rates of glucose storage in cultured human muscle cells, may indicate an effect on insulin signalling [48]. We speculate that the correlation between C-peptide and IL-6 as well as IL-7, observed only in children with recent-onset T1D, is a sign of an ongoing destruction of the remaining insulin-producing β-cells. This finding is in contrast to the correlation observed between C-peptide and the Th2 cytokine IL-13 seen exclusively in still healthy high-risk children. In fact, our previous finding of a diminished IFN-γ secretion associated with fasting C-peptide levels in T1D children suggests that factors related to β-cell function in T1D may modify T-cell function [28]. Thus,

T-cell responses detected at or after diagnosis may not reflect the pathogenic process leading to TID.

Taken together, these findings show that protein micro array can be used for screening of possible immunological markers involved in the autoimmune process against the insulin-producing β-cells. This technique does not deliver exact concentrations but indicates higher or lower concentrations of secreted cytokines and chemokines. However, low secreted cytokines, especially IL-4, is better detected at low antigen concentration stimulation at the single level with the sensitive ELISPOT technique [10]. Thus, protein micro array is useful for screening and comparisons between, for example, children with high risk and those already diagnosed with T1D.

In conclusion, cytokines secreted by Th1-like cells (IFN-γ and TNF-β) were more pronounced in high-risk children, whereas in newly diagnosed T1D children, markers of inflammation (TNF-α and IL-6), chemokines associated with destructive insulitis (RANTES, MCP-1 and IL-7) and Th3 cytokines (TGF-β and IL-10) were elevated. Thus, an inverse relation observed between Th1-like cells and markers of inflammation was shown between children with high risk and those newly diagnosed with T1D. We speculate that the immunological process led by Th1-like cells precedes the clinical onset, followed by an increased activation of inflammatory cytokines and chemokines involved in the destruction of the remaining insulin-producing β-cells, but this needs to be confirmed in larger longitudinal cohorts before any conclusion can be drawn.

Acknowledgement

This study was generously supported by the Schelins Foundation, the Swedish Child Diabetes Foundation (*Barndiabetesfonden*) and the Internal Grant Agency of the Czech Ministry of Health (no. NR/8127-3).

References

1. Castano L, Eisenbarth GS. Type-I diabetes: a chronic autoimmune disease of human, mouse, and rat. *Annu Rev Immunol* 1990; **8**: 647–679.
2. Atkinson MA, Kaufman DL, Campbell L, *et al*. Response of peripheral-blood mononuclear cells to glutamate decarboxylase in insulin-dependent diabetes. *Lancet* 1992; **339**: 458–459.
3. Foulis AK, Farquharson MA, Meager A. Immunoreactive a-interferon in insulin-secreting b cells in type 1 diabetes mellitus. *Lancet* 1987; **2**: 1423–1427.
4. Somoza N, Vargas F, Roura-Mir C, *et al*. Pancreas in recent onset insulin-dependent diabetes mellitus: Changes in HLA, adhesion molecules and autoantigens, restricted T cell receptor Vb usage, and cytokine profile. *J Immunol* 1994; **153**: 1360–1377.
5. Huang X, Yuan J, Goddard A, *et al*. Interferon expression on the pancreases of patients with type I diabetes. *Diabetes* 1995; **44**: 658–664.
6. Foulis AK, McGill M, Farquharson MA. Insulitis in type 1 (insulin-dependent) diabetes mellitus in man – macrophages, lymphocytes, and interferon-g containing cells. *J Pathol* 1991; **165**: 97–103.
7. Hussain MJ, Peakman M, Gallati H, *et al*. Elevated serum levels of macrophage-derived cytokines precede and accompany the onset of IDDM. *Diabetologia* 1996; **39**: 60–69.
8. Kallmann BA, Hüther M, Tubes M, *et al*. Systemic bias of cytokine production toward cell-mediated immune regulation in IDDM and toward humoral immunity in Graves'disease. *Diabetes* 1997; **46**: 237–243.
9. Kallan AA, Duinkerken G, de Jong R, *et al*. Th1-like cytokine production profile and individual specific alterations in TCRBV-gene usage of T cells from newly diagnosed type 1 diabetes patients after stimulation with b-cell antigens. *J Autoimmun* 1997; **10**: 589–598.
10. Karlsson MGE, Sederholm Lawesson S, Ludvigsson J. Th1-like dominance in high-risk first-degree relatives of type 1 diabetic patients. *Diabetologia* 2000; **43**: 742–749.
11. Karlsson Faresjö MGE, Ludvigsson J. Diminished Th1-like response to autoantigens in children with a high risk of developing type 1 diabetes. *Scand J Immunol* 2005; **61**: 173–179.
12. Hedman M, Ludvigsson J, Karlsson Faresjö MGE. Nicotinamide reduces high secretion of IFN-g in high-risk relatives even though it does not prevent type 1 diabetes. *J Interferon Cytokine Res* 2006; **26**: 207–213.
13. Halminen M, Simell O, Knip M, Ilonen J. Cytokine expression in unstimulated PBMC of children with type 1 diabetes and subjects positive for diabetes-associated antibodies. *Scand J Immunol* 2001; **53**: 510–513.
14. Lohmann T, Laue S, Nietzschmann U, *et al*. Reduced expression of Th1-associated chemokine receptors on peripheral blood lymphocytes at diagnosis of type 1 diabetes. *Diabetes* 2002; **51**: 2474–2480.
15. Karlsson Faresjö M, Ernerudh E, Ludvigsson J. Cytokine profile in children during the first 3 months after the diagnosis of type 1 diabetes. *Scand J Immunol* 2004; **59**: 517–526.
16. Lindley S, Dayan CM, Bishop A, Roep BO, Peakman M, Tree TIM. Defective suppressor function in CD4+CD25+ T-cells from patients with type 1 diabetes. *Diabetes* 2005; **54**: 92–99.
17. Bradley LM, Asensio VC, Schioetz LK, *et al*. Islet-specific Th1, but not Th2, cells secrete multiple chemokines and promote rapid induction of autoimmune diabetes. *J Immunol* 1999; **162**: 2511–2520.
18. Chen MC, Proost P, Gysemans C, Mathieu C, Eizirik DL. Monocyte chemoattractant protein-1 is expressed in pancreatic islets from prediabetic NOD mice and in interleukin-1 beta-exposed human and rat islet cells. *Diabetologia* 2001; **44**: 325–332.
19. Cardozo AK, Proost P, Gysemans C, Chen MC, Mathieu C, Eizirik DL. IL-1b and IFN-g induce the expression of diverse chemokines and IL-15 in human and rat pancreatic islet cells, and in islets from pre-diabetic NOD mice. *Diabetologia* 2003; **46**: 255–266.
20. Carvalho-Pinto C, Garcia MI, HGomez L, *et al*. Leukocyte attraction through the CCR 5 receptor controls progress from insulitis to diabetes in non-obese diabetic mice. *Eur J Immunol* 2004; **34**: 548–557.
21. Kirman I, Vainer B, Nielsen OH. Interleukin-15 and its role in chronic inflammatory diseases. *Inflamm Res* 1998; **47**: 285–289.
22. Group E.N.D.I.S.E. European Nicotinamide Diabetes Intervention Trial (ENDIT): a randomised controlled trail of intervention before the onset of type 1 diabetes. *Lancet* 2004; **363**: 925–931.
23. Karlsson MGE, Garcia J, Ludvigsson J. Cow's milk proteins cause similar Th1- and Th2-like immune response in diabetic and healthy children. *Diabetologia* 2001; **44**: 1140–1147.
24. Stechova K, Kolouskova S, Sumnik Z, *et al*. Anti-GAD65 reactive peripheral blood mononuclear cells in the pathogenesis of cystic fibrosis diabetes mellitus. *Autoimmunity* 2005; **38**: 319–323.
25. Schloot NC, Meierhoff G, Karlsson Faresjö M, *et al*. Comparison of cytokine ELISpot assay formats for the detection of islet antigen autoreactive T cells. Report of the Third Immunology of Diabetes Society T-cell Workshop. *J Autoimmun* 2003; **21**: 365–376.
26. Wahlberg J, Fredriksson J, Vaarala O, Ludvigsson J, Group F.T.A.s. Vaccinations may induce diabetes-related autoantibodies in one-year-old children. *Ann N Y Acad Sci* 2003; **1005**: 404–408.
27. Heding LG. Radioimmunological determination of human C-peptide in serum. *Diabetologia* 1975; **11**: 541–548.
28. Karlsson Faresjö MGE, Vaarala O, Thuswaldner S, Ilonen J, Hinkkanen A, Ludvigsson J. Diminished IFN-gamma response in children with type 1 diabetes. *Diabetes Metab Res Rev* 2006; **22**: 462–470.

29. Avanzini MA, Ciardelli L, Lenta E, *et al*. IFN-gamma low production capacity in type 1 diabetes mellitus patients at onset of disease. *Exp Clin Endocrinol Diabetes* 2005; **113**: 313–317.
30. Kaufman DL, Clare-Salzler M, Tian J, *et al*. Spontaneous loss of T-cell tolerance to glutamic acid decarboxylase in murine insulin-dependent diabetes. *Nature* 1993; **366**: 69–72.
31. Atkinson MA, Bowman MA, Campbell L, Darrow BL, Kaufman DL, Maclaren NK. Cellular immunity to a determinant common to glutamate decarboxylase and coxsackie virus in insulin-dependent diabetes. *J Clin Invest* 1994; **94**: 2125–2129.
32. Schloot NC, Roep BO, Wegmann DR, Yu L, Wang TB, Eisenbarth GS. T-cell reactivity to GAD65 peptide sequences shared with coxsackie virus protein in recent-onset IDDM, post-onset IDDM patients and control subjects. *Diabetologia* 1997; **40**: 332–338.
33. Mayer AF, Rharbaoui C, Thivolet J, Orgiazzi J, Madec AM. The relationship between peripheral T cell reactivity to insulin, clinical remissions and cytokine production in type 1 (insulin-dependent) diabetes mellitus. *J Endocrinol Metab* 1999; **84**: 2419–2424.
34. Kukreja A, Cost G, Marker J, *et al*. Multiple immuno-regulatory defects in type-1 diabetes. *J Clin Invest* 2002; **1**: 131–140.
35. Hanifi-Maghaddam P, Schloot NC, Kappler S, Seissler J, Kolb H. An association of autoantibody status and serum cytokine levels in type 1 diabetes. *Diabetes* 2003; **52**: 1137–1142.
36. Marfaing-Koka A, Devergne O, Gorgone G, *et al*. Regulation of the production of the RANTES chemokine by endothelial cells. *J Immunol* 1995; **154**: 1870–1878.
37. Mlynarski WM, Placha GP, Wolkow PP, Bochenski JP, Warram JH, Krolewski AS. Risk of diabetic nephropathy in type 1 diabetes is associated with functional polymorphisms in RANTES receptor gene (CCR5). *Diabetes* 2005; **54**: 3331–3335.
38. Boulassel MR, Smith GHR, Edwardes MD, *et al*. Influence of RANTES, SDF-1 and TGF-b levels on the value of interleukin-7 as a predictor of virological response in HIV-1-infected patients receiving double boosted protease inhibitor-based therapy. *HIV Med* 2005; **6**: 268–277.
39. Kinter A, Catanzaro A, Monaco J. CC-chemokines enhance the replication of t-tropic strains of HIV-1 in CD4(+) T cells: Role of signal transduction. *Proc Natl Acad Sci U S A* 1998; **95**: 11880–11885.
40. Gunn MD, Nelken NA, Liao X, Williams LT. Monocyte chemoattractant protein-1 is sufficient for the chemotaxis of monocytes and lymphocytes in transgenic mice but requires an additional stimulus for inflammatory activation. *J Immunol* 1997; **158**: 376–383.
41. Piemonti L, Leone BE, Nano R. Human pancreatic islets produce and secrete MCP-1/CCL2: relevance in human islet transplantation. *Diabetes* 2002; **51**: 55–65.
42. Fehniger TA, Caligiuri MA. Interleukin 15: biology and relevance to human disease. *Blood* 2001; **97**: 14–32.
43. Kern PA, Ranganathan S, Li C, Wood L, Ranganathan G. Adipose tissue tumor necrosis factor and interleukin-6 expression in human obesity and insulin resistance. *Am J Physiol Endocrinol Metab* 2001; **280**: E745–E751.
44. Kristiansen OP, Mandrup-Poulsen T. Interleukin-6 and diabetes: the good, the bad, or the indifferent? *Diabetes* 2005; **54**: S114–S124.
45. Devaraj S, Glaser N, Griffen S, Wang-Polagruto J, Miguelino E, Jialal I. Increased monocytic activity and biomarkers of inflammation in patients with type 1 diabetes. *Diabetes* 2006; **55**: 774–779.
46. Bopegamage SA, Petrovicova A. Tumor necrosis factor alfa and glucose levels in sera of mice infected with coxscakie B4 and A7 viruses. *Acta Virol* 1998; **42**: 409–411.
47. Mishima Y, Kuyama A, Tada A, Takahashi K, Ishioka T, Kibata M. Relationship between serum tumor necrosis factor-alpha and insulin resistance in obese men with Type 2 diabetes mellitus. *Diabetes Res Clin Pract* 2001; **52**: 119–123.
48. Halse R, Pearson SL, McCormack JG, Yeaman SJ, Taylor R. Effects of tumor necrosis factor-alpha on insulin action in cultured human muscle cells. *Diabetes* 2001; **50**: 1102–1109.

PŘÍLOHA VII.

Immunoregulatory effect of anti-thymocyte globulin monotherapy on peripheral lymphoid tissues of non-obese diabetic mice

L. Vargová, K. Zacharovová, E. Dovolilová, L. Vojtová, and F. Saudek

Transplant Proc, 2011. 43(9): p. 3277-80.

Immunoregulatory Effect of Anti-thymocyte Globulin Monotherapy on Peripheral Lymphoid Tissues of Non-obese Diabetic Mice

L. Vargova, K. Zacharovova, E. Dovolilova, L. Vojtova, and F. Saudek

ABSTRACT

Objective. Experimental and clinical studies have shown that autoimmunity-causing diabetes may be abrogated by immune intervention. Several anti–T-lymphocyte antibodies focus on distinct T-cell targets. We tested the effect of murine anti-thymocyte globulin (ATG; Genzyme, Framingham, MA) in peripheral lymphoid organs of non-obese diabetic (NOD) mice after the onset of hyperglycemia.

Methods. Diabetic NOD mice were treated with two doses of ATG (1 mg totally) or maintained without treatment as controls. Blood glucose levels were monitored twice a week. The mice were terminated at day 0, 7, 14, or 28 after the initiation of the study. Subpopulations of T-lymphocytes and FoxP3+ (forkhead box P3 positive) regulatory T-cells were analyzed among elements isolated from the spleen and pancreatic lymph nodes.

Results. Mice with blood glucose levels greater than 13 mmol/L were included in the study. Diabetes remission occurred in 16% (3/19) of mice treated with ATG. Only one case of remission was observed in the control group (6%; 1/16). ATG therapy a significantly decreased the CD8+/CD4+ T-lymphocyte ratio. Among splenocytes, a significant difference was detected only on day 7 (0.069 versus 0.198 T-lymphocyte ratio); in lymph nodes, a decrease was observed on day 28 (0.21 versus 0.51 T-lymphocytes ratio). The regulatory T-cells population increased after ATG administration compared with the control group at day 7 (16.2% versus 10.8% in CD4+ splenocytes; 20.7% versus 10.3% in CD4+ lymph node cells). However, the increased FoxP3+ cell population was not durable.

Conclusions. ATG treatment of diabetic NOD mice showed an immunoregulatory effect in peripheral lymphoid tissue with a significantly deceased CD8+/CD4+ ratio, which, however, did not normalize the metabolic parameters in a short period after the onset of overt diabetes.

SEVERAL groups have reported positive effects of anti-thymocyte globulin (ATG),[1] anti-lymphocyte serum,[2] or anti-CD3 antibody[3] therapies to treat newly established autoimmune diabetes in experimental models as well as in humans.[4,5] Anti-lymphocyte therapy has been shown to retard the progression of β-cell loss maintaining or improving insulin production. Responses were also associated with a change in the ratio of CD4+ T cells to CD8+ T cells.[6] Recently this treatment has been reported to rapidly expand CD4+ CD25+ FOXP3+ T cells.[7] According to ClinicalTrials.gov, several randomized prospective studies with the use of humanized anti-CD3 antibodies or ATG in type 1 diabetes of recent onset are currently in progress.[8] At present, our group has performed a randomized prospective clinical study using polyclonal anti–T-cell globulin.[9] Only a few experimental studies have been performed in diabetic mouse models. As they are more relevant to clinical studies in humans with recent onset of

From the Diabetes Department (L.V., F.S.), and the Department of Experimental Medicine (K.Z., E.D., L.V.), Institute for Clinical and Experimental Medicine, Prague, Czech Republic.

Supported by Grant number GA P304/10/0762 from the Czech Sience Foundation.

Address reprint requests to Lenka Vargova, Diabetes Department, Institute for Clinical and Experimental Medicine, Videnska 1958/9, 140 21 Prague 4, Czech Republic. E-mail: lept@medicon.cz

0041-1345/–see front matter
doi:10.1016/j.transproceed.2011.09.057

diabetes, we sought to examine the efficacy to cure diabetes of murine anti-thymocyte globulin (mATG) in diabetic non-obese diabetic (NOD) mice. In contrast to previous studies, we investigated the effects of therapy on peripheral lymphoid tissues, which may be important to re-establish immune tolerance in diabetes.

METHODS

Mice and Monitoring for Diabetes

Female NOD mice (strain NOD/ShiLtJ) were housed in specialized ventilated breeding boxes equipped with air filtration, and provided with autoclaved water and food ad libitum. Blood glucose levels were measured from the tip of the tail. Mice with glycemia levels greater than 13 mmol/L after two consecutive measurements were included in the study groups. Treatment was initiated within 1 week from the diabetic manifestations (blood glucose level $>$ 13 mmol/L). The age of the mice included in the study was 12 to 30 weeks. Diabetic mice were randomized into four groups with termination at days 0, 7, 14, and 28 after the initiation of the study. Blood glucose levels were monitored twice a week throughout the study period. No exogenous insulin was administered. This study was approved by the local Committee for the Protection of Animals Against Cruelty.

ATG Administration

Diabetic NOD mice were treated with two doses of intraperitoneally administrated mATG (Genzyme, Framingham, MA) at days 0 and 4 (1 mg totally) or maintained without treatment as controls.

Intraperitoneal Glucose Tolerance Test

Intraperitoneal glucose tolerance testing (IPGTT) was performed on day 24. After overnight fasting, glucose (1 mg/g body weight) was provided by intraperitoneal injection of 10% glucose solution. Blood glucose values were obtained at 0, 10, 20, 30, 40, 50, and 60 minutes using a Performa Nano (Roche, Basel, Switzerland) meter. We determined the coefficient of glucose assimilation.

Flow Cytometry

On the day of termination, the mice were sacrificed to remove the spleen and pancreatic lymph nodes. Splenocytes isolated by mild dissociation in Iscove's modified Dulbeco's medium were separated by gradient centrifugation in Ficoll-Paque PLUS (GE Healthcare, Uppsala, Sweden). Lymph node cells were isolated by dissociation of nodes through 60-μm mesh. Isolated cells were labelled for flow cytometric analysis. We used fluorescent antibodies against surface antigens CD3, CD4, CD8, CD25 (A488 anti-CD3, eBioscience, San Diego, USA; Qdot605 anti.CD4, Invitrogen, Eugene, USA; PerCP-Cy5.5 anti-CD8, eBioscience; APC anti-CD25, produced in Institute of Microbiology ASCR, Prague, Czech Republic). Subsequently, the fixed cells were permeabilized (FoxP3 Staining Buffer Set, eBioscience) with the intracellular antigen FoxP3 labelled using a PE-conjugated antibody (eBioscience) for comparison with staining using appropriate PE-conjugated isotype controls (eBioscience). The labelled cells were analyzed using the flow cytometer LSR II with FACSDiva software (BD, San Jose, USA).

Subpopulations and CD4+ and CD8+ T-lymphocyte ratios were determined as well as FoxP3+ regulatory T-cells analyzed among the CD3+ CD4+ CD25+ cell population.

Statistical Analysis

Statistical analysis was performed using the Student t test. All data are presented as mean values $\pm$ standard deviation. P values $<$ .05 were deemed significant.

RESULTS

Mice with blood glucose levels higher than 13 mmol/L after two consecutive measurements were included in the study. Diabetes remission (sustained glycemia at levels less than 13 mmol/L) occurred in 16% (3/19) of mice treated with ATG. In all of them, the pre-treatment blood glucose was 15.6 mmol/L and less. Only one case of remission was observed in the control group (6%; 1/16; Fig 1). Mice were maintained without exogenous insulin administration. Although the IPGTT was out of normal range in all diabetic animals, the coefficient of glucose assimilation was significantly higher among the ATG group (0.36 versus 0.12 mmol/L/min; $P < .05$).

We observed the effect of polyclonal anti-lymphocyte antibodies on the ratio of cytotoxic and helper T-cells populations. ATG therapy lead to a significant decrease in CD8+/CD4+ T-lymphocyte ratio compared with the control group. Among splenocytes, a significant difference was detected only on day 7 (0.069 in mATG group versus 0.198 in control group, $P = .001$); whereas lymph node cells showed a decrease even on day 28 (0.21 in mATG group versus 0.51 in control group, $P = .003$) Similarly, the

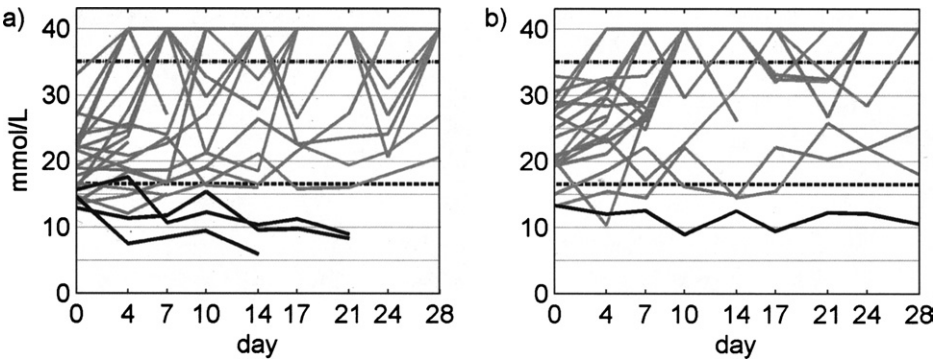

Fig 1. Glycemia **(A)** after mATG administration, **(B)** control group. Data represent blood glucose values from individual animals. *Bottom line* represents our threshold of initial glucose level crucial for remission. *Upper line* represents glucose levels up to 35 mmol/L. All the animals did not receive any exogenous insulin.

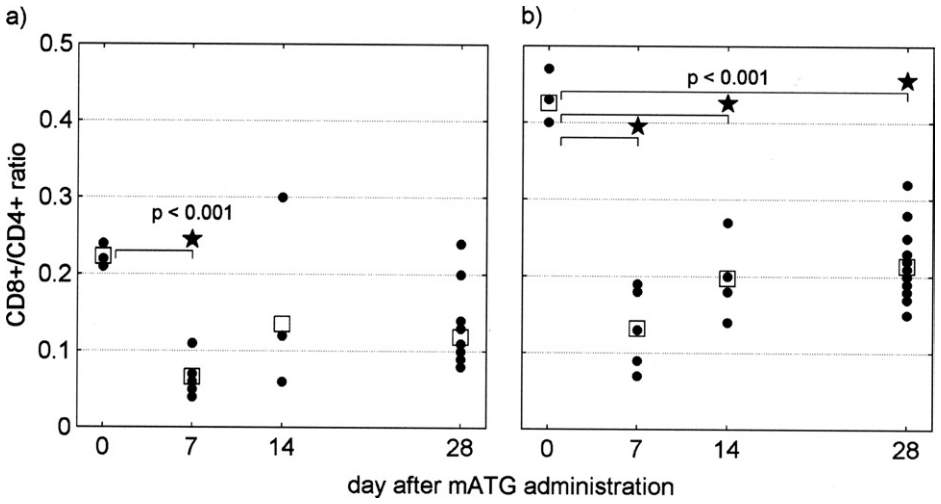

Fig 2. CD8+/CD4+ T-lyphocyte ratio after mATG administration. ATG therapy lead to a significant decrease of CD8+/CD4+ T-lymphocyte ratio within the mATG group in comparison to pre-administration values. **(A)** In splenocytes, a significant difference was detected only on day 7 (0.22 at day 0 versus 0.069 at day 7; $P < .001$) **(B)** In lymph nodes, a decrease was found even on day 28 (0.43 at day 0 versus 0.21 at day 28; $P < .001$). □ represents mean value, ★ represents P value $< .05$.

differences were detected within the mATG group compared with pre- administration values (Fig 2).

The regulatory T-cell population (Treg, % of FoxP3+ cells among the CD4+ cells) was significantly increased after ATG administration among splenocytes, namely, from 9.1% at day 0 to 16.2% at day 7 ($P = .03$). On day 14, the FoxP3+ population was still increased (15.8%, $P = .02$) but at day 28 they had decreased to 12.2%. Among control group the Treg population among splenocytes was constant; namely, 9.6% at day 0, 10.8% at day 7, 9.7% at day 14, and 10.3% at day 28. However, the difference between the mATG and the control group was significant only on day 14 ($P = .02$). Among lymph node cells, the Treg population was also increased after mATG administration from 8.1% to 20.7% at day 7 ($P = .0008$). The gradual decrease in the Treg population during this time was lower than among splenocytes and Treg population kept higher from day 0 to day 28; 14.6% at day 14 ($P = .008$), and 13.5% at day 28 ($P = .03$; Fig 3). However, because the mild increase in the Treg population among the control group, a significant difference between groups was only detected at day 7 ($P = .001$) The Treg population in controls was 8.2% at day 0, 10.3% at day 7, 11.2% at day 14, and 12.1% at day 28.

DISCUSSION

ATG treatment of diabetic NOD mice showed only partial metabolic improvement among already hyperglycemic NOD mice. Most of the successful studies were performed previously on pre- diabetic mice. Of the 463 agents evalu-

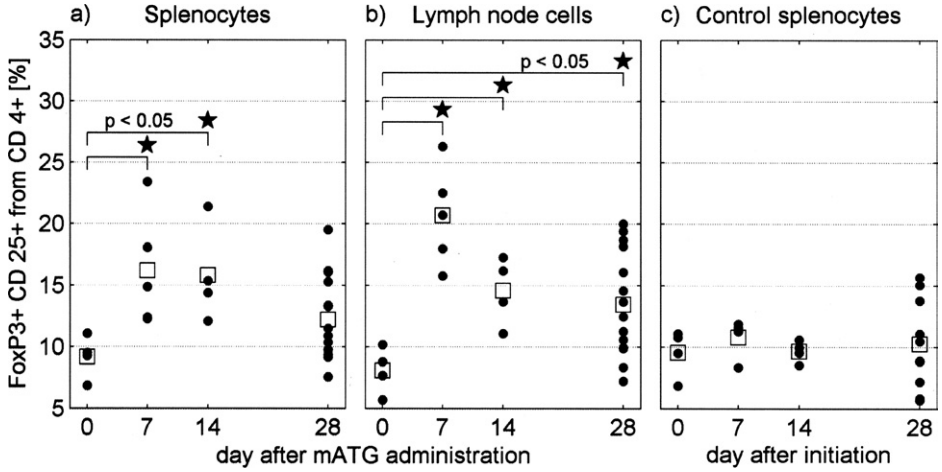

Fig 3. Regulatory T-cell population after mATG administration in splenocytes **(A)**, in lymph node cells **(B)** and in splenocytes **(C)** of control group. Population of the regulatory T-cells was increased after mATG administration in comparison to the control group and within the mATG group in comparison to pre-administration values as well. In splenocytes, the increase of regulatory T-cells was significant only 2 weeks after mATG administration (9.1% at day 0 versus 15.8% at day 14; $P = .02$). In lymph node cells, the increase was significant until the end of the experiment (8.1% at day 0 versus 13.5% at day 28; $P = .03$). In the control group, the FoxP3+ population did not change. □ represents mean value, ★ represents P value $< .05$.

ated in the intervention diabetic studies, only 23 protocols were initiated in diabetic NOD mice with 16 considered successful.[10] Also, a failure of ATG treatment to reverse overt diabetes was recently published, Our results are consistent with recently published data using ATG treatment of acute virally induced rat insulin promoter–lymphocytic choriomeningitis virus (RIP-LCMV). In this study, mATG did not reverse diabetes among newly diabetic RIP-LCMV mice.[11] Although ATG treatment alone did not cure diabetes, there were metabolic effects.

We have experience with a clinical immunointervention study using polyclonal rabbit anti-T-cell globulin administered to new onset type 1 diabetes patients. The pilot study comprised 25 subjects followed for 2 years who showed considerable preservation of residual C-peptide production and lower insulin requirements compared with a control group. In addition, a sustained conversion of CD4+/CD8+ cell ratio in peripheral blood cells suggested an immunoregulatory effect. The effect seemed to be comparable to that reported with the use of humanized monoclonal anti-CD3 antibodies. Recently, we observed a significant increase in FoxP3+ population for 9 months after ATG administration (data not published). The Treg population was assessed by flow cytometry on frozen samples of lymphocytes obtained during the study. In clinical terms, this was a unique result.[9]

In the NOD mouse model, an effect of mATG was shown by a greater rate of diabetes remission which was dependent on the blood glucose levels at the time of the mATG administration namely initial glycemia less than 15.6 mmol/L. mATG produced a significant difference in glucose assimilation rates. The efficiency of treatment depended on the level of initial glycemia. A further relevant aspect for treatment efficiency is the time between manifestation of diabetes and treatment initiation.[2,12]

The main effect of mATG treatment was evident in T-lymphocyte subpopulations. We observed that mATG administration decreased the CD8+/CD4+ T-lymphocyte ratio in splenocytes and pancreatic lymph node cells, favoring Tregs. We confirmed an increase in the regulatory T-cell population after mATG administration in splenocytes as well as in lymph node cells. The influence of anti T-cell therapy on the regulatory T-cell population has been shown in clinical and experimental studies in vitro and in vivo.[7,13] Compared with data published by another group,[1] we observed a significant increase in Tregs among pancreatic lymph node cells up to the end of our study (day 28). However, the regulatory T-cell increase was transient, and over time the population apparently decreased. Better results may be obtained with more prolonged mATG treatment.[14]

To conclude, mATG treatment alone produced an immunoregulatory effect in peripheral lymphoid tissue, although it was not sufficient to cure NOD mice with established overt diabetes. Better results in NOD mice were achieved in studies using a pre- diabetic model or with a longer study period combined with insulin therapy.

REFERENCES

1. Simon G, Parker M, Ramiya V, et al: Murine antithymocyte globulin therapy alters disease progression in NOD mice by a time-dependent induction of immunoregulation. Diabetes 57:405, 2008

2. Maki T, Ichikawa T, Blanco R, et al: Long-term abrogation of autoimmune diabetes in nonobese diabetic mice by immunotherapy with anti-lymphocyte serum. Proc Natl Acad Sci U S A 89:3434, 1992

3. Chatenoud L, Primo J, Bach JF: CD3 antibody-induced dominant self tolerance in overtly diabetic NOD mice. J Immunol 158:2947, 1997

4. Herold KC, Gitelman SE, Masharani U, et al: A single course of anti-CD3 monoclonal antibody hOKT3gamma1(Ala-Ala) results in improvement in C-peptide responses and clinical parameters for at least 2 years after onset of type 1 diabetes. Diabetes 54:1763, 2005

5. Keymeulen B, Vandemeulebroucke E, Ziegler AG, et al: Insulin needs after CD3-antibody therapy in new-onset type 1 diabetes. N Engl J Med 352:2598, 2005

6. Herold KC, Hagopian W, Auger JA, et al: Anti-CD3 monoclonal antibody in new-onset type 1 diabetes mellitus. N Engl J Med 346:1692, 2002

7. Feng X, Kajigaya S, Solomou EE, et al: Rabbit ATG but not horse ATG promotes expansion of functional CD4+CD25highFOXP3+ regulatory T cells in vitro. Blood 111:3675, 2008

8. ClinicalTrials.gov [web site]. Available at: http://clinicaltrials.gov. Accessed: 2006, NCT00378508; 2007, NCT00515099

9. Saudek F, Havrdova T, Boucek P, et al: Polyclonal anti-T-cell therapy for type 1 diabetes mellitus of recent onset. Rev Diabet Stud 1:80, 2004

10. Shoda LK, Young DL, Ramanujan S, et al: A comprehensive review of interventions in the NOD mouse and implications for translation. Immunity 23:115, 2005

11. Bresson D, von Herrath MG: Anti-thymoglobulin (ATG) treatment does not reverse type 1 diabetes in the acute virally induced rat insulin promoter-lymphocytic choriomeningitis virus (RIP-LCMV) model. Clin Exp Immunol 163:375, 2011

12. Mottram PL, Murray-Segal LJ, Han W, et al: Remission and pancreas isograft survival in recent onset diabetic NOD mice after treatment with low-dose anti-CD3 monoclonal antibodies. Transpl Immunol 10:63, 2002

13. Lopez M, Clarkson MR, Albin M, et al: A novel mechanism of action for anti-thymocyte globulin: induction of CD4+CD25+Foxp3+ regulatory T cells. J Am Soc Nephrol 17:2844, 2006

14. Vergani A, D'Addio F, Jurewicz M, et al: A novel clinically relevant strategy to abrogate autoimmunity and regulate alloimmunity in NOD mice. Diabetes 59:2253, 2010